UNIVERSITÉ DE MONTRÉAL

FLUID-ELASTIC INSTABILITY OF A TUBE BUNDLE IN TWO-PHASE CROSS-FLOW USING MEASURED QUASI-STATIC FORCES

SOROUSH SHAHRIARY
DÉPARTEMENT DE GÉNIE MÉCANIQUE
ÉCOLE POLYTECHNIQUE DE MONTRÉAL

MÉMOIRE PRÉSENTÉ EN VUE DE L'OBTENTION
DU DIPLÔME DE MAÎTRISE ÈS SCIENCES APPLIQUÉES
(GÉNIE MÉCANIQUE)
NOVEMBRE 2007

Your file Votre référence
ISBN: 978-0-494-36939-5
Our file Notre référence
ISBN: 978-0-494-36939-5

UNIVERSITÉ DE MONTRÉAL

ÉCOLE POLYTECHNIQUE DE MONTRÉAL

Ce mémoire intitulé :

FLUIDELASTIC INSTABILITY OF A TUBE BUNDLE IN TWO-PHASE CROSS-FLOW USING MEASURED QUASI-STATIC FORCES

présenté par : SHAHRIARY Soroush

en vue de l'obtention du diplôme de : Maîtrise ès sciences appliquées

a été dûment accepté par le jury d'examen constitué de :

M. CAMARERO Ricardo, Ph.D., président

M. MUREITHI Njuki W., Ph.D., membre et directeur de recherche

M. PETTIGREW Michel J., Post.Grad.Dipl., membre et codirecteur de recherche

M. PRICE Stuart J., Ph.D., membre

Dedicated to:

My father who is my first teacher,
to my wife who acompanied me
and to my daughter who made us keep going.

ACKNOWLEDGEMENTS

I am deeply indebted to my advisors, Professor Njuki Mureithi and Professor Michel Pettigrew for their constant support and encouragement. Without their help, this work would not have been possible. I would also like to thank the members of my committee Professor Stuart J. Price and Professor Ricardo Camarero who reviewed the work in a short time and honored me their presence at my defense.

I would like to acknowledge that the constant support of the CRSNG/EACL/BWC industrial research chair of fluid-structure interaction has made this work possible. The members of the fluid-structure interaction chair helped me with their valuable suggestions and support for the past two and a half years.

I am grateful to Christine Monnette who designed the two-phase flow test section, Emmanuelle Sommiere who designed the force balance and to Remi Violette who provided me with the necessary dynamic tests data. Thanks to Thierry Lafrance and Bénédict Besner for their assistance with many aspects of data acquisition and instrumentation. Nour Aimène's expertise with strain gauges made it possible to have a high precision measurement system.

At last, I am grateful to Romain Watteaux who helped me with the verification of the complex calculations and correction of the French contents along with Abdelhak Oulmane and as well to Dr. Navid Arjmand for helping me with the initial correction of the English contents of the present work.

RÉSUMÉ

Bien qu'un grand nombre d'échangeurs de chaleur opèrent en écoulement diphasique, la nature complexe de l'écoulement rend la prédiction du domaine d'instabilité fluide-élastique un défi encore à relever. Dans un générateur de vapeur, en raison de la vitesse élevée du mélange diphasique, la région du coude en U est très sensible au phénomène d'instabilité. Dans le travail rapporté ici, cette région est modelée par un faisceau de tubes triangulaires parallèles.

L'instabilité fluide-élastique en écoulement diphasique est par convention étudiée en utilisant des mélanges air-eau. Puisque la production et le contrôle des mélanges air-eau sont plus simples et moins coûteux par rapport aux autres types, ce mélange est choisi pour notre étude. Ce choix nous a permit d'utiliser la boucle expérimentale existante ainsi que les résultats expérimentaux déjà obtenus.

La boucle diphasique en écoulement air-eau du laboratoire d'interactions Fluide-Structure à l'École Polytechnique de Montréal a été employée pour les mesures de forces quasi-statiques. La section d'essai étant composée de trois colonnes de cylindres et une colonne de demi-cylindres de chaque côté. Le champ de forces quasi-statiques a été mesuré dans un faisceau de tubes triangle-tournés (P/D=1.5 et D=30mm) pour différents taux de vide et vitesses d'écoulement. Les forces se sont avérées fortement dépendantes au taux de vide, au débit ainsi qu'aux positions relatives des tubes.

Les variations des forces fluides obtenues sur cette section d'essai diffèrent de celles mesurées dans la même configuration de cylindres pour un écoulement d'air avec cependant un rapport pas-diamètre différent. Bien que les résultats trouvés en écoulement diphasique à de hauts taux de vide soient semblables à ceux rapportés pour un écoulement d'air pur, les changements pour le coefficient de portance dans la direction de l'écoulement sont absents dans cette configuration de cylindre. On remarque cependant que pour les taux de vide inférieur à 40%, la variation du coefficient de portance du cylindre central dans la direction de l'écoulement est l'inverse de celle pour un écoulement air pur. Ceci signifie que pour de bas taux de vide, l'instabilité en

écoulement diphasique peut être régie par la variation des coefficients de force tandis que pour de plus hauts taux de vide, l'instabilité fluide-élastique est la plupart du temps régie par des effets avec temps de latente.

Le champ de force fluide a alors été utilisé avec le modèle quasi-stationnaire, à l'origine développé pour des écoulements monophasiques, pour modeler le problème en écoulement diphasique. Puisque le faisceau de tubes étudiés n'est pas vraiment infini, la présence de petites modifications dans la formulation originelle, pour prendre en compte les différents angles de phase, était inévitable.

La variation des coefficients de force les plus importants en fonction du nombre de Reynolds a été mis en avant dans cette analyse. Prenant en compte ces variations lors de l'évaluation de l'instabilité à vitesse réduite (ou a faible nombres de Reynolds), la prévision « prématurée » de l'instabilité dans le modèle quasi-statique est expliquée (par opposition aux changements de la vitesse interstitielle à l'origine utilisée pour expliquer les régions instables déraisonnablement étroites).

Avec un essai dynamique, il est possible d'aller au delà du modèle quasi-stationnaire et de trouver le premier ordre de la fonction d'affaiblissement en utilisant le modèle quasi-instable. En utilisant la formule approximative de cette fonction ainsi que les données de cet essai dynamique et les coefficients de force obtenus expérimentalement, le premier ordre de la fonction d'affaiblissement a été calculé pour différentes taux de vide.

Le travail présenté met en avant certaines des complexités du champ de force fluide pour un écoulement diphasique. Les données sont de valeur inestimable puisqu'elles sont les données expérimentales nécessaires à la classe des modèles théoriques d'instabilité fluide-élastique quasi-statique, quasi-stationnaire et quasi-instationnaire. Cette base de données ouvre ainsi une nouvelle porte sur la faisabilité des modèles quasi-stationnaires en écoulement diphasique.

ABSTRACT

Although a great number of the process heat exchangers operate in two-phase flow, the complex nature of the flow makes the prediction of fluidelastic instability a challenging problem yet to be fully solved. In the nuclear steam generator, because of the high velocity of the two-phase mixture, the U-bend region is very susceptible to fluidelastic instability. In the work reported here, the U-bend region is modeled by a parallel triangular tube bundle.

Fluidelastic instability in two-phase flow is conventionally investigated using air-water mixtures. Since production and control of air-water mixtures is simpler and cheaper in comparison to the other types, air-water flow is chosen for the present study. The selection has permitted taking advantage of the existing flow loop and the available dynamic test data points obtained at the same test section.

The air-water two-phase flow loop of the Fluid-Structure Interactions Laboratory at École Polytechnique de Montréal was used for the quasi-static force measurements. The test section of three columns of full cylinders bounded with sidewalls with fixed half cylinders was used to perform quasi-static measurement of forces. The quasi-static fluid force-field was measured in a rotated-triangle tube bundle (P/D=1.5 and D=30mm) for a series of void fractions and flow velocities in water and air-water flow. The forces were found to be strongly dependent on void fraction, flow rates and relative tube positions.

The quasi-static fluid force variations obtained in the present test section differ from those reported earlier using air in the same configuration with different pitch to diameter ratio and tube diameter. Although the two-phase flow results found at high void fractions are similar to those reported in air flow, the sharp changes in the lift coefficient in the cross-flow direction are absent in the present tube array. Interestingly, for void fractions below 40%, the variation of central cylinder lift coefficient in the cross-flow direction is the inverse of that in air flow. This means that for low void fractions, two-phase flow instability may be governed by the variation of force coefficients while for higher void fractions fluidelastic instability is mostly governed by time delay effects.

The fluid force field was then employed along with the quasi-steady model originally developed for single phase flows, to model the two-phase flow problem. Since the present tube bundle is not really infinite, introducing small modifications in the original formulation to account for different phase angles was inevitable.

The variation of the most important fluid force coefficients with the Re number been emphasized in the analysis. Taking into consideration these variations when evaluating stability at very low velocity (or Reynolds numbers) the "premature" prediction of instability in the quasi-static model is explained (as opposed to changes in gap velocity originally used to explain unreasonably narrow unstable regions).

Having one dynamic test data made it is possible to go beyond the quasi-steady model and to find the first order of the decay function using quasi-unsteady model. Using the approximate formula of decay function applying the dynamic data points and fluid force coefficients obtained experimentally, the first order of the decay function has been calculated for different void fractions.

The present work uncovers some of the complexities of the fluid force field in two-phase flows. The data are invaluable since they are the necessary inputs to the class of quasi-static, quasi-steady and quasi-unsteady fluidelastic instability theoretical models. This database opens a new research avenue on the feasibility of applying quasi-steady models to two-phase flow.

CONDENSÉ

Le phénomène de vibration induite par écoulement est devenu un problème majeur ces dernières années pour les concepteurs qui poussent les composants et les matériaux à leurs limites. Les structures sont ainsi devenues légères et plus flexibles ; augmentant ainsi la probabilité de vibration. Les défaillances des faisceaux de tubes ont fait du domaine de la vibration induite par écoulement une priorité.

Dépendants de la conception et des conditions de fonctionnement des faisceaux de tubes, les phénomènes de résonance due aux vortex, de vibration due à la turbulence, de résonance acoustique et d'instabilité fluide-élastique ont été identifiés en tant que sources possibles de ces vibrations. Pour les faisceaux de tubes soumis à un écoulement transversal, l'instabilité fluide-élastique est le type de vibration le plus grave.

La nature de l'instabilité fluide-élastique la rend complètement différente des autres mécanismes. Les forces induites par le fluide se produisent par le résultat direct du mouvement des cylindres. Par contre pour les autres mécanismes d'excitation, l'effet de ces forces est plutôt sous forme d'une source découplée d'excitation extérieure. En conséquence de cette différence, la mesure des forces fluide liées à l'instabilité fluide-élastique sur un corps rigidement fixé n'est pas suffisante.

Les premiers travaux pour analyser l'instabilité fluide-élastique pour les faisceaux de tubes ont été accomplies au début des années soixante par Robert. Par la suite beaucoup de modèles ont été proposés pour ce phénomène en écoulement monophasique. Ces méthodes sont soigneusement étudiées dans ce travail.

Bien que beaucoup de systèmes industriels fonctionnent en écoulement diphasique, la connaissance du phénomène d'instabilité fluide-élastique en écoulement transversal est beaucoup moindre que celle en l'écoulement monophasique. Avant 1980, peu de travaux ont ciblé la vibration induite en écoulement diphasique de faisceaux des tubes soumis à un écoulement transversal. Ceci n'est pas étonnant puisque la vibration induite par écoulement monophasique, un sujet encore plus simple, n'est pas complètement identifiée. L'étude de l'instabilité fluide-élastique soumise á un écoulement diphasique

présente plus de complexités ; telles que le régime d'écoulement et les effets de taux de vide. En effet, les expériences sur l'écoulement diphasique sont plus coûteuses et difficiles à effectuer parce qu'elles exigent des boucles complexes avec la capacité de produire des mélanges diphasiques uniformes.

L'instabilité fluide-élastique induite par écoulement diphasique est traditionnellement étudiée dans l'air-eau, vapeur-eau et d'autres mélanges de liquide-vapeur tels que le Fréon. Puisque la production et le contrôle d'un mélange air-eau est plus simple et moins coûteux par rapport aux autres types, la plupart des études expérimentales sur les instabilités fluide-élastiques en écoulement diphasique ont été effectuées en utilisant ce mélange. Ce dernier est également choisi pour la présente étude. Par conséquent, il est possible d'utiliser la base de données exhaustive, existante dans la littérature et en même temps d'éviter les complexités provenant des autres types de mélanges diphasiques.

La présente étude est faite dans le cadre d'un mémoire de maîtrise. Elle propose d'adapter des modèles originalement développés pour des écoulements monophasiques, vers des écoulements transversaux diphasiques dans des rangées triangulaires tournées de tubes. Comme il sera discuté plus tard, le modèle adapté exige la mesure des forces quasi-statiques exercées sur le faisceau des tubes pour une série de taux de vide et de vitesses d'écoulement. L'information sur le champ de force est une base de donnée cruciale pour les modèles théoriques d'instabilité fluide-élastique quasi-statiques, quasi-stationnaires et quasi-non-stationnaires.

Une étude de la littérature sur l'instabilité fluide-élastique met en évidence le manque de modèles appropriés pour prévoir l'instabilité fluide-élastique dans des mélanges diphasiques. L'existence de tels modèles dans des écoulements monophasiques nous a permis de les utiliser dans le cas diphasique. Comme discuté dans la section précédente, les modèles de *jet-switching*, quasi-statiques et l'écoulement non visqueux ont quelques problèmes qui les rendent non utilisables, même pour le cas le plus simple de l'écoulement monophasique. En outre, les modèles *CFD*, ne peuvent même pas prévoir l'instabilité fluide-élastique en écoulement monophasique. Bien que les modèles semi-analytiques fonctionnent comme des modèles quasi-stationnaires dans les écoulements monophasiques, ils sont limités par la connaissance du champ d'écoulement.

L'incertitude des modèles diphasiques suggère l'utilisation des modèles quasi-stationnaires ou non-stationnaires. La complexité des modèles instables limite leur utilisation à ce stade.

Maintenant, en tenant compte du modèle quasi-stationnaire choisi pour modéliser l'instabilité fluide-élastique dans l'écoulement diphasique, les objectifs de la présente étude sont énumérés comme suit :

1. Mesurer avec précision les forces fluides pour un certain nombre de vitesses d'écoulement et une gamme des taux de vides ;
2. Employer le champ de force mesuré dans un modèle quasi-stationnaire pour la prévision de instabilité fluide-élastique ;
3. Comparer la frontière prévue de seuil de l'instabilité fluide-élastique aux mesures.

Une fois le champ de force mesuré, le modèle quasi-stationnaire en écoulement diphasique homogène sera utilisé pour prévoir l'instabilité fluide-élastique pour un éventail de taux de vide dans un faisceau de tubes triangulaires tournés. Les mélanges air-eau qui sont choisis pour cette étude permettent de tirer profit des essais dynamiques des montages expérimentaux existants.

Le modèle théorique de Price et de ses collègues est récapitulé dans ce travail tout en présentant les modifications appropriées pour prendre en compte les faisceaux de tubes infinis et les écoulements diphasiques. Le faisceau de tubes fini est également considéré dans le modèle modifié.

L'introduction de l'écoulement diphasique dans le problème fluide-élastique ajoute deux nouveaux paramètres ; à savoir le taux de vide et le régime d'écoulement. Ces deux paramètres, absents en écoulement monophasique, affectent le comportement de l'écoulement.

Le champ de force fluide quasi-stationnaire est la donnée nécessaire à la classe des modèles théoriques d'instabilité fluide-élastique: quasi-statique, quasi-stationnaire et quasi-non-stationnaire. La boucle d'écoulement diphasique air-eau du laboratoire

d'interaction Fluide-Structure de l'École Polytechnique de Montréal a été employée pour les mesures.

Les modifications mineures d'un dynamomètre existant ont permis de mesurer les forces sur le cylindre central avec précision. Parmi ces modifications, coller des jauges sur les lamelles immergées pour le dynamomètre du cylindre central s'est avéré être un réel défi. Quoique l'existence de la symétrie dans le faisceau de tubes ait diminué le nombre de cylindres instrumenté, la mise à niveau de la section d'essai, est devenue un autre défi.

Bien que la structure du dynamomètre et la bonne installation des systèmes de mesures à l'intérieur des tubes de plexiglass puissent réduire au minimum le couplage des forces mesurées, les imperfections en assemblant différentes pièces causent un certain accouplement entre les deux directions. Cet accouplement a pu varier de 1/15 à 1/50 pour les deux genres de cylindres instrumentés.

La force de trainée étant ainsi environ dix fois supérieure à la force de portance (aux limites), il est important de considérer cet effet en mesurant les forces. Il peut être de même ordre de grandeur que les forces de portance dans le pire des cas. Concernant la mesure de la force de trainée, étant donné que la force de portance est dix fois plus petite, le couplage est négligeable.

Le couplage dans la direction de la traînée est évalué en laissant stagner l'eau au-dessus des tubes dans la section d'essai et en mesurant les forces dans les deux directions. Puisque la force résultante de flottabilité agit purement dans la direction de la traînée, n'importe quelle force mesurée de portance est induite par le couplage. Le rapport entre force de traînée et force de portance peut être alors utilisé comme indicateur de couplage pour tous les cylindres.

Les données acquises dans les essais comportent les forces liquides dans les directions de traînée et de portance pour cinq cylindres équipés de jauges de contrainte. Les forces de portance sont corrigées en tenant compte du couplage mesuré dans les essais hydrostatiques. Les résultats de vingt et un essais différents nous ont fournis

l'information nécessaire. Le rapport des forces de la trainée et de la portance pour chaque cylindre est ramené à une moyenne pour tous les essais.

La force de traînée à chaque point est multipliée par le rapport de couplage pour compenser l'erreur. Les résultats sont alors soustraits de la valeur mesurée de la force de portance afin d'obtenir la force réelle. La force de traînée ne souffre pas de l'erreur de couplage parce que la valeur de la traînée est au moins environ dix fois la force de portance. Par conséquent, l'effet de la portance en direction de la trainée est négligeable.

L'effet de la flottabilité est également pris en considération. La valeur de la force hydrostatique peut être employée comme force de flottabilité pour l'écoulement d'eau. La force est alors multipliée par la portion de l'eau qui existe dans le mélange pour trouver la flottabilité dans l'écoulement diphasique. La force résultante de flottabilité est soustraite de la force de traînée mesurée pour trouver la force corrigée. Pour l'écoulement diphasique la densité homogène du mélange diphasique est employée au lieu de la densité de l'eau.

Les variations des forces quasi-statiques obtenues diffèrent de celles rapportées plus tôt par Price et Païdoussis qui ont employé l'air dans la même configuration mais avec un rapport pas-diamètre différent. Bien que les résultats diphasiques d'écoulement trouvés à de hautes fractions vides soient semblables à ceux rapportés dans l'air, les changements brusques du coefficient de portance dans la direction transversale sont absents dans la rangée de tube. Pour les taux de vide en-dessous de 40%, la variation du coefficient de portance du cylindre central pour un déplacement transversal est l'inverse de celle dans l'air. Ceci signifie que pour un bas taux de vide, l'instabilité diphasique d'écoulement peut être régie par la variation des coefficients de force tandis que pour de plus hauts taux de vides, l'instabilité fluide-élastique est la plupart du temps définit par un retard de temps.

Les mesures nous permettent ainsi de trouver les dérivées des coefficients de force exigées pour le modèle fluide-élastique quasi-stationnaire. Les dérivées des forces sur les cylindres voisins suivant le déplacement du cylindre central sont traduits par la variation des coefficients de force du cylindre par rapport au déplacement du cylindre central.

Dans le travail présenté, la variation des forces avec le nombre de Reynolds est soulignée. Ces variations serviront plus tard à expliquer pourquoi l'instabilité fluide-élastique ne se produira pas à de basses vitesses réduites. À nos connaissances, c'est la première fois que ces variations sont employées pour expliquer le début de l'instabilité.

L'effet de la variation de la vitesse d'écoulement pour le cylindre central (dans l'écoulement d'eau) est démontré. Il est intéressant de noter qu'aux vitesses inférieures et en position d'équilibre, la force de trainée augmente (amortissement du fluide) tandis qu'en même temps le composant de déstabilisation le plus important (la dérivée de la force de portance dans la direction de l'écoulement transversal) diminue sensiblement. Ces valeurs tendent à approcher une valeur constante à des vitesses plus élevées. Ces résultats peuvent expliquer pourquoi des vitesses très basses d'instabilité ont été obtenues en utilisant des coefficients constants d'écoulement. Dans le travail actuel, quand les calculs mènent à une basse vitesse d'instabilité, l'effet des coefficients variables de force (c.-à-d. effet de nombre de Reynolds) est employé pour modifier la prévision. Pour des vitesses plus élevées, ce n'est pas le cas, parce que les coefficients de force sont presque constants.

Les forces liquides corrigées (après élimination des effets de la flottabilité et du couplage) sont lu par le code *Matlab*. La fonction de *polyfit* est utilisée pour l'interpolation en fonction de l'ordre du polynôme choisi. Les coefficients qui concernent la force elle-même et sa première dérivée sont sauvegardés. La moyenne du coefficient de la force trouvé dans les deux directions est employée comme meilleure approximation des coefficients de force à la position d'équilibre.

Un tableau regroupe les coefficients de force de trainée et portance aussi bien que les dérivés en fonction des déplacements du cylindre central. Les résultats obtenus en fonction du taux de vide superficiels en-dessous de 31% souffrent de l'inexactitude due aux mesures du débit d'air à la limite. Pour les taux de vide de 40%, la vitesse de l'écoulement n'est pas assez élevée pour que les forces atteignent leur valeur constante. En outre, le grand changement observé des forces mesurées aux fractions de vides au-

dessus de 80% est possiblement dû aux changements du régime d'écoulement. Le modèle homogène peut souffrir d'inexactitude dans ce secteur.

Avoir le champ de forces quasi-statiques permet d'employer le modèle quasi-stationnaire pour prévoir l'instabilité fluide-élastique. Les forces du fluide ainsi que leurs variations par rapport aux coordonnées locales obtenues plus tôt sont employées avec les modèles quasi-stationnaires, qui sont à l'origine développés pour des écoulements monophasiques, afin de modéliser le problème d'écoulement diphasique.

Des analyses de stabilité sont exécutées en utilisant le modèle d'un tube flexible aussi bien que l'analyse du mode contraint. Comme les travaux précédents, l'effet de la variation du paramètre de retard d'écoulement est examiné pour le modèle d'un tube flexible à divers taux de vides.

D'ailleurs, la variation des coefficients de force du fluide les plus importants avec le nombre de Reynolds est utilisée dans le travail actuel pour l'évaluation de la stabilité à vitesse réduite (pour l'eau). Les mesures complètes de tous les coefficients de force du fluide en fonctions du nombre de Reynolds permettent d'améliorer la prévision d'instabilité fluide-élastique aux bas paramètres masse-amortissement. L'application de ce concept pour l'écoulement diphasique exige des modèles diphasiques sophistiqués afin d'examiner les coefficients de force à différentes vitesses d'écoulement sans être préoccupé par les changements du taux de vide.

Un code Fortran est développé pour résoudre l'équation du mouvement obtenue en utilisant l'une ou l'autre des approches quasi-stationnaires. Les coefficients de force présentés en forme de tableaux fournissent les informations nécessaires pour former les matrices de rigidité et d'amortissements du fluide. Le programme détermine les valeurs propres des équations de l'état-espace du mouvement en changeant la vitesse de l'écoulement. Les parties réelles de toutes les valeurs propres sont examinées pour

trouver la première valeur propre avec une partie réelle zéro qui indique le début de l'instabilité. En choisissant l'ordre des équations simultanément avec la matrice de rigidité et d'amortissement ont permet au programme de résoudre le problème pour un seul tube flexible ou pour le modèle de rangée infini.

Le début de l'instabilité d'un seul tube flexible est cherché pour différents paramètres de retard. En plus du travail original, et puisque l'étude actuelle est en l'écoulement diphasique, le taux du vide est également changé pour étudier l'effet du paramètre de retard.

Puisque la pente des variations du coefficient de portance change constamment de signe (pour le taux de vide superficiel de zéro à cinquante pourcent), les erreurs de mesure de coefficient de force deviennent comparable aux valeurs mesurées à bas taux de vides. Par conséquent, la prévision a seulement été accomplie pour les valeurs raisonnables des coefficients de force (écoulement d'eau et taux de vides au-dessus de 50%).

Puisque le modèle d'un seul tube flexible fonctionne bien seulement pour des bas paramètre de masse-amortissement (pour les paramètres masse-amortissement élevées l'instabilité est plutôt gouvernée par le mécanisme de rigidité et a besoin de plus d'un tube flexible pour s'effectuer), les limites d'instabilité sont tronquées pour différents intervalles dû aux paramètres masse-amortissement, et cela pour tous les taux de vide. Le taux de vide est changé entre 50% et 90% pour chercher les limites d'instabilités. À noter qu'à la différence du travail en air, l'abscisse est le paramètre masse-amortissement total. Les résultats analytiques tendent à surestimer la vitesse critique réduite et tendent à s'approcher des essais dynamiques à hauts taux de vides.

Fixant les différences de phase $\theta_x = \varphi_x = \phi_y = 0$ et $\theta_y = \pi$, le tube peut vibrer dans la direction de l'écoulement transversal. Les plages d'instabilité sont également obtenues pour une rangée flexible en utilisant l'analyse mode contraint. Le paramètre de retard

$\mu = 1$ est considéré pour différents taux de vides (de nouveau, les résultats sont seulement présentés dans la région dans laquelle les coefficients de portance sont beaucoup plus grands que les erreurs expérimentales prévues).

En comparant les essais dynamiques avec le modèle d'un seul tube flexible et l'analyse mode contraint on trouve que le modèle d'un seul tube flexible surestime la valeur de la vitesse critique réduite. Par contre l'analyse mode contraint sous-estime cette dernière. Les deux prévisions mènent à un meilleur accord pour des plus hauts taux de vides superficiels.

Les multiples régions d'instabilité à basse vitesse ont toujours étés une énigme. Price et Païdoussis ont remis en cause le nombre de ces régions d'instabilité qui peuvent pratiquement exister. Ils ont conclus que les autres mécanismes d'instabilité empêcheraient la rangée restante d'être instable. Ils ont déduit que les régions étroites d'instabilité ne peuvent pas exister. En utilisant cet argument, ils ont considéré les régions avec une largeur en-dessous de 10% de vitesse réduite impraticables.

Dans la présente étude la variation des forces du fluide par rapport aux nombres de Reynolds est employée pour empêcher la prévision prématurée de l'instabilité dans le modèle quasi-statique. Les résultats de l'analyse mode contraint considérant la variation des coefficients les plus importants de force des fluides est comparés à ceux obtenus par les forces des fluides constants. Comme mentionné précédemment, l'augmentation du coefficient de traînée aux vitesses inférieures, augmente l'amortissement du fluide et diminue les forces de déstabilisation empêchant ainsi l'instabilité. Les résultats montrent que la mesure précise de toutes les forces du fluides à différentes vitesses libres mène à améliorer les prévisions.

Ayant les essais dynamiques, il est possible d'aller au delà du modèle quasi-stationnaire et d'employer le premier ordre des estimations des paramètres de Granger pour

modéliser la fonction décroissante. Employer la formule approximative présentée par Granger, l'application des points de repères dynamiques et les coefficients de force donne la fonction décroissante pour différents taux de vides.

Les résultats d'analyse de stabilité sont comparés avec les essais dynamiques disponibles et donne un bon accord. Les résultats pour l'analyse d'un seul tube flexible et multiples tubes flexibles pour des hauts taux de vide tendent à coïncider au bas amortissement structural. Les résultats principaux du travail actuel sont les suivants :

- La variation du coefficient C_{LC} avec le déplacement transversal $\tilde{y}$, dans le cas monophasique (écoulement d'eau) diffère du cas diphasique (air-eau). Alors que la force de portance quasi-statique est orientée vers la position d'équilibre du cylindre dans l'écoulement diphasique à des hauts taux de vide (taux de vide superficiel de plus de 40%), elle est dirigée vers la direction opposée de l'écoulement d'eau à des taux des vides bas.
- La courbure de C_{DC} avec le déplacement transversal $\tilde{y}$, dans le cas monophasique (écoulement d'eau) diffère du cas diphasique (air-eau). Alors que la courbure de force quasi-statique de trainée est positive dans l'écoulement diphasique (minimum C_{DC} à la position d'équilibre) a haut taux de vide (taux de vide superficiel de plus de 40%), elle change de signe pour l'écoulement d'eau à de bas taux de vide.
- Les mesures de force en écoulement monophasique (écoulement d'eau) ont démontré que la force de trainée augmente quand le nombre de Reynolds diminue, ce qui indique que la stabilités accrue pour de basse vitesses.
- Les mesures de force en écoulement monophasique (d'écoulement d'eau) ont également prouvé les diminutions de la dérivé de coefficient de portance (ce qui est déstabilisant) avec le nombre de Reynolds, qui indique une autre fois la stabilité accrue pour des vitesses réduites inférieures.
- Le point auquel la tendance des variations des forces des fluides change dans le faisceau de tubes a été établi expérimentalement (un taux de vide superficiel d'environ 40%).

- Il a été démontré que le modèle d'un seul tube flexible peut être adapté avec succès pour modéliser l'instabilité fluide-élastique dans le cas d'un écoulement transversal diphasique pour prévoir la limite supérieure du seuil d'instabilité.
- Il a été également démontré que l'analyse mode contraint adaptée pour modéliser l'instabilité fluide-élastique dans des écoulements diphasiques mène à une limite inférieure du seuil d'instabilité.
- Une comparaison des résultats avec des essais dynamiques montre que les prévisions à hauts taux de vide sont plus fiables que celles à bas taux de vide.
- La variation des coefficients de force ont été employées avec succès pour améliorer la prévision fluide-élastique dans l'analyse mode contraint et la fonction masse-amortissement modifiée a été obtenue en utilisant les essais dynamiques et le modèle présentés par Granger.

Afin de terminer les travaux actuels il est nécessaire d'accomplir les tâches qui sont énumérées comme suit :

- Faire des essais dynamiques avec des paramètres masse-amortissement plus élevés pourrait valider l'analyse mode contraint. En outre, d'avoir différent essais dynamiques, il sera possible d'employer des ordres plus élevés de modèle quasi-instable (modèle de Granger).
- Déterminer la carte d'écoulement diphasique pour le faisceau de tubes actuel pourrait expliquer l'amélioration des résultats en écoulements diphasiques à haut taux de vide. Il serait également possible de déterminer le moment où les mesures doivent être prises afin d'éviter les erreurs dues aux changements de régime.
- Adopter un modèle diphasique sophistiqué fournirait les moyens de faire des expériences à de diverses vitesses libres sans être inquiété par les changements de taux de vide réel. Cette étape pourrait également améliorer la prévision de la masse ajoutée.

TABLE OF CONTENTS

LIST OF FIGURES

LIST OF TABLES

LIST OF SYMBOLS

a	ratio of gap to free stream velocity
Cap	capillary number
$[C]$	structural damping matrix
C_D, C_L	drag and lift coefficients based on free stream velocity
C_{D0}, C_{L0}	drag and lift coefficients based on free stream velocity at zero position
D	cylinder diameter
$[\tilde{D}]$	fluid damping
$[E]$	structural stiffness matrix
f_n	structural natural frequency
F_i	force in "i" direction
$\{\tilde{F}\}$	fluid force per unit area
$\tilde{g}, g_i$	delay functions
$[I]$	identity matrix
$[\tilde{K}]$	fluid stiffness matrix
K, b	Connor's constants
L, T	distance of cylinders in-flow and cross-flow directions
m_S, m_h, m_T	structural, hydrodynamic and total mass per unit length
$[M]$	total mass matrix
P	pitch between cylinders
Q_g, Q_l	volumetric flow rate of gas and water
p, q	row and columns in tube bundle
s	slip ratio

S	center to center of cylinders
t	time
U_∞, U_G, U_r	free stream, gap velocity and relative velocity
U_{pc}	critical pitch velocity
Re	Reynolds number
α, α_i	angle of attack
β	homogeneous void fraction
ε	real mean void fraction
$\tilde{x}, \tilde{y}$	dimensionless displacements with respect to D
$\{\tilde{z}\}$	dimensionless displacement vector with respect to D
$,i$	partial derivative with respect to i
δ	structural logarithmic decrement
$\delta(t)$	Dirac delta-function
σ	surface tension
Δt	time delay
χ, η	local coordinates in-flow and cross-flow directions
ν_g, ν_l	kinematic viscosity of air and water
ϕ, θ	phase lags
λ	complex eigenvalue
ρ	homogeneous density
μ, τ	flow retardation parameter, time delay
ω	circular frequency of vibration in air
ξ, ζ	structural and total damping ratio

LIST OF APPENDIXES

CHAPTER 1

INTRODUCTION

Flow induced vibration has become more important in recent years because designers are pushing components and materials to their limits. Structures have become lighter and more flexible thus; the likelihood of vibration has increased. Failures in tube bundles have made flow induced vibration a primary concern.

Depending upon the design and operating condition of tube bundles, vortex shedding, turbulent buffeting, acoustic resonance and fluidelastic instability have all been identified as possible sources of these vibrations [1]. In cylinder arrays subjected to cross-flow, it is widely believed that fluidelastic instability is the most severe type of flow- induced vibration among the above mentioned sources [2].

The nature of fluidelastic instability makes it completely different from the other flow-induced vibration mechanisms. In fluidelastic instability, the destabilizing fluid forces occur as a direct result of cylinder motion whereas in the other forms of flow-induced vibration, these forces act more like an external decoupled excitation source. Consequently unlike the other forms of flow-induced vibration, simply measuring the fluid forces associated with fluidelastic instability on a rigidly held body is not sufficient [3].

The first attempt to analyze fluidelastic instability of cylinder arrays goes back to the early 1960's by Roberts [3]. Many models for this phenomenon were later proposed in the case of single-phase flow. These methods are carefully reviewed in this chapter.

Although many industrial components operate in two-phase flow, the knowledge of fluidelastic instability in two-phase cross-flow is much less than that of single-phase flow. Prior to 1980, very little work had been done to study flow-induced vibration of tube bundles subjected to two-phase cross-flow [4]. This is not surprising since single-phase flow-induced vibration, a simpler topic, is still not yet fully understood [5]. The

study of fluidelastic instability in two-phase flow presents more complexities such as flow regime and void fraction effects. Moreover, experiments in two-phase flow are more expensive and difficult to carry out because they require complex loops with the ability to produce uniform two-phase mixtures.

Fluidelastic instability in two-phase flow is conventionally investigated in air-water, steam-water and other liquid-vapor mixtures such as Freon. Since production and control of air-water mixtures is simpler and cheaper in comparison to the other types, most of the two-phase flow fluidelastic experimental studies have been conducted using air-water mixtures. Air-water is also chosen for the present study. Hence, it is possible to take advantage of the comprehensive existing database in the literature and at the same time avoid the complexities arising in the other types of two-phase mediums.

The present study is done in the framework of a master's thesis. It proposes to adapt models originally developed for single-phase flows, to two-phase cross-flow in a rotated triangular tube array. As will be discussed later, the adapted model requires quasi-static fluid force field measurement in the tube bundle for a series of void fractions and flow velocities. The valuable force field information is the necessary input to the class of quasi-static, quasi-steady and quasi-unsteady fluidelastic instability theoretical models.

In this chapter, first, the nature of fluidelastic instability will be discussed; subsequently different models for dealing with single-phase fluidelastic instability will be presented. Next, one of the models, which is deemed to best suit two-phase flows will be adapted for two-phase flow problem. Consequently, the objectives of the present study will be enumerated and the structure of the thesis will be outlined.

1.1 Fluidelastic instability

Consider a typical tube array subjected to cross-flow as depicted in Figure 1.1. It is evident that movement of a tube within a tube bundle changes the fluid forces acting on its neighbors and by extension the bundle as a whole. This can lead to instability if the energy input of the cylinder exceeds the energy damped by the system. This type of

instability is known as *fluidelastic instability* (in heat exchangers) or *wake galloping* (in power transmission lines). This phenomenon can lead to violent vibration and even clashing of the tubes within array.

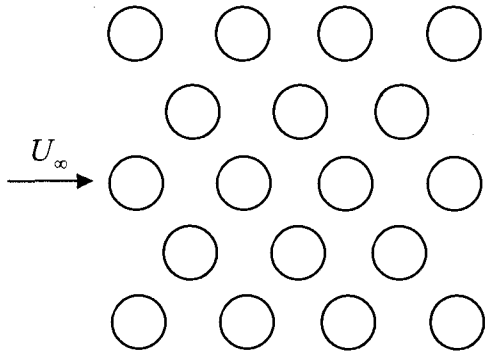

Figure 1.1 A typical tube array subjected to two-phase cross-flow

Fluidelastic instability can be subdivided into two distinct categories, damping (or velocity) controlled and stiffness (or displacement) controlled mechanisms. It is believed that for low mass damping parameters the instability is due to damping controlled mechanism while for high mass damping parameters it is mostly governed by stiffness controlled mechanism [6].

1.1.1 Stiffness controlled instability

Fluidelastic stiffness controlled instability is the dynamic instability caused by forces related to displacement. It is also called coupled mode flutter because a minimum of two degrees of freedom is necessary to produce this kind of instability. The non-symmetrical fluid stiffness matrix is known as the source of this kind of instability[7]. Since the destabilizing fluid force is in-phase with cylinder displacement, it is also referred to as a displacement mechanism[3].

1.1.2 Damping controlled instability

This kind of instability is caused by non-conservative fluid damping forces. This phenomenon mainly occurs by the phase difference between cylinder vibration velocity and displacement [3] (because of time delay). This mechanism can take place within a system with only one degree of freedom so it may alternatively be called *single mode flutter*.

1.2 Fluidelastic instability models

1.2.1 Jet switch model

Roberts [8, 9] took advantage of experimental evidence available at the time thus proposing that fluidelastic instability occurs in the flow direction and suggested that the fluid jet which flows through the minimum cross section area between two neighboring cylinders. Supposing imaginary boundaries passing through the cylinders, he suggested that the flow, which hit the imaginary plates, is responsible for instability. Although his assumption about the direction in which fluidelastic instability first takes place was not correct, he made fundamental hypotheses that are considered correct (i.e. consideration of time lag, hysteresis and the form of basic equations). His model was modified and used by Connors [3] but it still contains the following shortcomings. The instability in this approach needs at least two flexible cylinders, so it cannot predict single mode flutter. Furthermore, the Connors equation is solely dependent on structural mass, damping and natural frequency and lacks any contributions from the fluid [2].

1.2.2 Quasi-static model

This model suggests that the fluid-dynamic characteristics of cylinders oscillating in flow, at any instant of time, are the same as stationary cylinders at identical instantaneous position. Connors used the quasi-static approach and developed his famous expression, which was later rederived by Blevins [3].

Connors observed the elliptical motion of cylinders and measured the forces quasi statically on the central cylinder. He knew that the forces of the jet-switch

mechanism were not responsible for instability so he subtracted the part pertaining to jet switching and calculated the work in both the in flow and cross-flow directions. Using the measured fluid stiffness Connors obtained energy balances in the in flow and cross-flow directions. Solving these equations simultaneously leads to the well-known Connors equation.

$$U_{pc}/f_n D = K\left(\frac{m_s \delta}{\rho D}\right)^b \tag{1.1}$$

where U_{pc} is the critical pitch velocity, f_n the structural natural frequency, m_s the structural mass per unit length, δ the structural logarithmic decrement, D the tube diameter and ρ the density of fluid. K and b stand for the constants of Connors equation.

The constants in the Connors equation were later modified by himself [10], Gorman [11], Païdoussis [12], and Pettigrew [13]. Chen has shown that this model is a very special case of his general unsteady model [7].

1.2.3 Quasi-steady and quasi-unsteady models

The quasi-steady model assumes that the cylinder motion only modifies the relative velocity vector so that the drag and lift coefficients are defined according to cylinder position (in the Quasi-Static model does not count for this modification). It suggests that the force coefficients are unchanged from those measured, or calculated, on a stationary object, which means the body immediately feels the relative motion of the relative velocity vector. If the velocity of vibration can be considered negligible comparing to the flow velocity, the quasi-steady assumption is correct, otherwise, this is not an accurate assumption. Blevins [3] concluded that quasi-steady model is valid, only if the reduced velocity is greater than 10. Yet, Price & Wang suggested that this restriction is more severe for closely spaced cylinders [3].

The first attempts to predict instability where performed by Gross in late 1975 and Price and Païdoussis in the early 1980's [3]. They related the reduced velocity and the mass-damping parameter with the derivative of the lift coefficient with respect to the

angle of attack. Price and Païdoussis possibly incorrectly [3] tried to relate this derivative to the derivative of force coefficient with respect to Cartesian counterparts in their first attempts.

Later in 1984 and 1988, Price and Païdoussis [14, 15] refined their model to account for the movement of neighboring cylinders and considered the time lag mechanism, which was earlier proposed by Flower and Simpson [16]. They related the flow retardation to an exponential factor. Afterwards, Païdoussis *et al.* [15] employed a constrained mode analysis and decoupled a cluster of arrays for their analysis which was two cylinders for staggered array and four cylinders for an in-line array. Before long Price, Païdoussis and Cheng [3] showed that the cluster could be further reduced to one cylinder for inline arrays.

At low mass-damping parameters, both single flexible cylinder and multiple flexible cylinder models lead to multiple instability regions the same as the regions predicted using the Leaver and Weaver model. Price and Païdoussis [3] suggested that when the cylinder becomes unstable it would not restabilize so the lower value of the stable region shall be considered.

Granger and Païdoussis [17] modified their model under the name of quasi-unsteady to account for a memory effect. They used convolution to account for a memory effect and expressed it as a series of decaying exponentials. Their effort matches much better with the experimental data but they needed extra constants, which are dependent on knowledge of vibration response. The second disadvantage is that it is restricted to single cylinder vibration and cannot account for a group of flexible cylinders [2]. It shall be noted that this model does not predict multiple instability regions [2].

1.2.4 Inviscid flow models

The inviscid or potential flow models are based on the assumption that the wake region behind the cylinder is small and negligible. In these models, normally, the velocity potential is estimated and the impermeability boundary condition on cylinder

surfaces applied. Consequently, the unsteady Bernoulli equation is solved to find the unsteady fluid force field.

The pioneers of this method (Dalton and Helfinstine), considered a row of oscillating cylinders and an array in stagnant fluid. They represented the cylinders with doublets [18]. Unfortunately the results of the potential flow or semi potential models [19] are far from reality because although the wake region is small, the interstitial flow is more complex than can be taken care of with the potential flow theory [3]. Although, in general, potential flow theory cannot lead to good results in predicting fluidelastic instability it can be used as a powerful tool to obtain the added mass [20].

1.2.5 Unsteady models

These models are based on the direct measurement of unsteady fluid forces acting on the oscillating cylinder. Measurements of unsteady forces go back to the 1980's [21]. Tanaka and Takahara the first to measure the unsteady forces for a wide range of reduced velocities and considered the motion of cylinder itself along with its neighbors. Their results show that fluid force coefficients are strongly dependent on reduced velocity for low reduced velocities [21]. They also showed that there is a discontinuity, dependent on the value of logarithmic damping factor, in the variation of reduced instability velocity with respect to the dimensionless mass damping parameter. Their results show that below the discontinuity most of the motion is in the cross-flow direction but above that point, it contains a significant amount of in-flow motion. They also showed that for a single cylinder free to move only in the cross-flow direction, the critical velocity is only slightly higher than that of a flexible bundle. Thus, the instability is damping controlled.

Later, the results of the above fluid forces where employed by Chen [7] in his analytical model. He demonstrated that there are two distinct instability mechanisms: damping controlled and stiffness controlled. He showed that the damping controlled mechanism normally occurs at low values of reduced velocity with a single-degree-of-

freedom while the stiffness-controlled mechanism needs at least two degrees-of-freedom and takes place at high values of reduced velocity.

Chen predicted multiple instability regions and showed that quasi-static and quasi- steady models are only special cases of his more general unsteady model [7]. Although it is agreed that the unsteady model gives the best results among all the existing fluidelastic models the extensive effort to find the fluid force coefficients is a major difficulty.

1.2.6 Semi-analytical models

Lever and Weaver proposed the first semi-analytical model [3]. They assumed a single flexible cylinder surrounded by a cluster of tubes. They believed that the sudden change in flow area could produce a perturbation in velocity and pressure. Therefore, the flow was divided into channel flow and wake region. The continuity, momentum and energy equations were solved for a one-dimensional inviscid channel flow using these perturbations.

Later Lever and Weaver [22] included the movement in both in-flow and cross-flow directions in their modified model. Afterwards, Yetisir and Weaver [23] modified the flow perturbation to mitigate the perturbation magnitude with increasing distance from the oscillating cylinder. They found multiple instability regions at low values of reduced velocity and concluded that because perturbations due to turbulence can change the phase lags in this region, the multiple instability points are physically unreasonable, concluding that if the cylinder goes unstable, nonlinear effects would prevent re-stabilization[3].

1.2.7 Computational fluid mechanics models

The advances in computer technology have persuaded a number of researchers to use computational fluid dynamics (CFD), to predict fluidelastic instability numerically. The flow inside cylinder arrays is viscous and highly turbulent so a

comprehensive CFD model must be capable of accounting for such a flow along with moving boundaries [3].

In 1997, the $k-\varepsilon$ model was used to avoid the adjustable constants in the other turbulent models to predict fluidelastic instability in six different tube bundles for realistic Reynolds numbers [24]. A finite volume and a Cartesian mesh refinement around the cylinders were used in this effort. Kassera and Strohmeier [24] solved the flow field, found the forces, displacements and velocities in one time step, reproduced the mesh in a new position, and proceeded with the new mesh. Although they showed that the results were good for low and medium pitch to diameter ratios, Price [2] has questioned their results and suggested that at present accurate CFD-based models of fluidelastic instability are not realizable.

Later, Schröder and Gelbe [25], tried to predict fluidelastic instability and the RMS amplitudes using $k-\varepsilon$ and $k-\omega$ models. Their results show a lower critical velocity and higher RMS amplitudes. They concluded that the results might be improved by using a three-dimensional analysis.

Even if a new method has been developed to simulate single-phase flow with an acceptable accuracy, the existence of such a method is dubious for the more complicated two-phase flow field for the moment.

1.3 Fluidelastic instability in two-phase flow

Although two-phase flow fluidelastic instability can be found in many industrial components such as nuclear steam generators, condensers and boilers and that the cost of plant shutdown due fluidelastic instability failures is very high, the current knowledge in two-phase flow is much less than that of single-phase flow.

Pettigrew *et al.* [26] reported a comprehensive experimental work carried out in air-water flow for different array geometries in 1985. Similar to the other studies on fluidelastic instability pertaining to nuclear steam generators they conducted their tests in arrays having pitch to diameter ratio of 1.5. Later in 1989, they reported their complete results on the hydrodynamic mass and damping in two-phase flows [27].

Pettigrew and his coworkers published an ample review on fluidelastic instability in two-phase flow in 1994 [4]. Interested readers can refer to their review on damping to find the available guidelines in this domain [28].

Most of the work in two-phase flows has been carried out to find design guidelines, predict added mass, two-phase flow damping and fluidelastic instability constants. To the author knowledge, there is only one published work, aimed to predict fluidelastic instability in two-phase flow. In 1992, Marn and Catton tried to use Bottoni and Sengpiel equations to overcome uncertainties arising in the two-phase flow. They assumed a horizontal arrangement to artificially exclude the gravity effect and the slip between air and water phases [29]. They also neglected the effects of vortices in front and behind the cylinders, which plays an important role in single-phase flow. Marn and Catton used finite differences to solve the governing differential equations and tried to estimate Connors fluidelastic instability constants, which is rightfully questioned by Price [2].

In 1996, Mureithi, Nakamura and their coworkers [30] reported the results of unsteady fluid-force measurements in steam-water cross-flow. Afterwards they used their own results to calculate the instability boundaries [31]. Their theoretical analysis showed that instability in homogeneous or nearly homogeneous two-phase flows could be predicted with reasonable accuracy

1.3.1 Modeling void fraction

Although the detailed flow measurements [32] show that the void fraction changes continuously in a tube bundle, the changes in each half pitch interval tends to homogenize the mixture. Most of the researchers have used the homogenous model to model the two-phase flow in a fluidelastic instability problem. The exception is the Feenstra *et al.* model in the fluidelastic instability literature [33].

The homogeneous model is obtained by assuming that the velocities of each phase in the mixture are equal (the slip ratio is equal to one.). Although there is a large difference in the density of air and water phases, which causes the gas phase to travel

faster, it can be argued that the continual change of the void fraction in different half pitches can mitigate the slip ratio so the slip ratio is almost one [32]. This assumption greatly simplifies the calculations and can lead to explicit relations. The disadvantage of this method is that completely ignoring the existence of slip between phases can lead to a false comparison of cases with different void fractions.

The Feenstra *et al.* model considers the slip between gaseous and liquid phases. It uses the surface tension, a new interpretation of capillary number and Richardson number to calculate the slip between phases. Using this formulation can lead to implicitly complicated relations. Feenstra *et al.* tried to justify their model by measuring void fraction using a Gamma ray densitometer at the entrance of the test section, which can be considered as a weak point in their experiments because the void fraction can change throughout the test section. Their analysis leads to small slip ratios for high void fractions (at most 1.1 for superficial void fractions of 60% and 80%).

Comparing the above void fraction models and considering the complexity that arises from the Feenstra *et al.* model leads us to choose a homogeneous model throughout this work. However, having all the data acquired during the tests enables one to use the data for more sophisticated two-phase modeling.

1.4 Objective of present study

A review of the literature on fluidelastic instability shows a lack of appropriate models to predict fluidelastic instability in two-phase media. The existence of such models in single-phase flows makes one try using these models in two-phase flow. As discussed in the previous section, jet switching, quasi-static and inviscid flow models have some problems that make them not feasible, even for the simpler case of single-phase flow. Furthermore, CFD models, cannot predict fluidelastic instability in single-phase flow. Although semi-analytical models work as well as quasi-steady models in single-phase flows, they are restricted to the knowledge of flow field.

The uncertainty about the accuracy of two-phase flow models suggests using quasi-steady or unsteady models to overcome the uncertainties arising in two-phase flows. The complexity of unsteady models limits their usage at this stage.

Keeping in mind that the quasi-steady model is chosen to model the two-phase flow fluidelastic instability, the objectives of present study are enumerated as follows:

1. Detailed and accurate measurement of the fluid forces for a number of flow velocities and a range of void fractions
2. Use the measured force field in a quasi-steady model for FES prediction
3. Compare predicted FEI boundary with measurements

The measured force field, the quasi-steady model along with homogeneous two-phase flow will be employed to predict fluidelastic instability for a wide range of void fractions in a rotated triangular tube bundle. Air-water mixtures are chosen for the present study. Therefore, it is possible to take advantage of the existing dynamic test data and experimental apparatus.

1.5 Structure of the thesis

The outline of the report is as follows: after the introduction to the problem, the theory will be explained in chapter two. The experimental setup used to conduct the experiments is described in chapter three. Chapter four presents the force field data that form the engine of the quasi-steady model. In chapter five, the quasi-static forces and their variations will be used to predict fluidelastic instability in two-phase flow using quasi-steady models. Finally, the last chapter is dedicated to the main conclusions and suggestions for future works.

CHAPTER 2

THEORY

As mentioned in the previous chapter, there are different approaches to modeling fluidelastic instability. Among the methods found to work well in single-phase flow, analytical modeling requires little or no experimental fluid force data whereas semi-empirical analysis requires experimental fluid force data. The latter may be either the fully unsteady data or steady time averaged data [6]. The first approach, because of the complexity of the physics, cannot be adapted to the two-phase flow problem. The analysis using unsteady data, on the other hand requires a vast amount of experimental work. Requiring a moderate amount of experimental input, the quasi-steady theory can provide an acceptable solution. The quasi-steady theory has therefore been chosen for the present stability analysis of two-phase flows. The model of Price and his co-workers [6], [15] and [34] is summarized bellow while at the same time the appropriate modifications are introduced to account for infinite tube bundles and two-phase flows.

Considering one flexible cylinder or a fully flexible array subjected to cross-flow free to move in plane as shown in Figures 2.1 and 2.2, the equation of motion can be written as follows [6]:

$$[M]\{\ddot{\tilde{z}}\}+[C]\{\dot{\tilde{z}}\}+[K]\{\tilde{z}\}=\{\tilde{F}\} \tag{2.1}$$

Considering a parallel tube bundle with no mechanical coupling between cylinders (and between two directions) the above equation can be written as:

$$m_r[I]\{\ddot{\tilde{z}}\}+2\omega\xi m_s[I]\{\dot{\tilde{z}}\}+m_s\omega^2[I]\{\tilde{z}\}=\{\tilde{F}\} \tag{2.2}$$

The fluid force vector on the right hand side will be estimated using the quasi-steady approach whilst considering a time delay mechanism as discussed below.

2.1 Fluid Forces

The quasi-steady approach states that the cylinder motion only modifies the relative velocity vector. Considering a typical cylinder in an array, free to move in the in-flow or cross-flow directions, the relative velocity can be written as a function of gap flow velocity [34] and cylinder velocity. The angle of attack, relative velocity and fluid forces are shown in Figure 2.1. The figure shows that considering small displacements the relative velocity can be defined as:

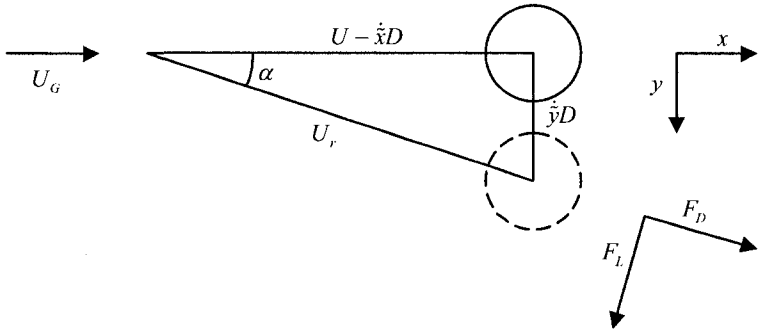

Figure 2.1 Angle of attack, relative velocity and fluid forces on a typical cylinder

$$U_r = U_G\left(1-\frac{\dot{x}D}{U_G}\right) \tag{2.3}$$

The angle of attack, α ,can be related to the velocity of the cylinder in cross-flow direction as follows [34]:

$$\cos(\alpha)=\frac{U_G-\dot{x}D}{U_r}\simeq 1\ ;\ \sin(\alpha)=\frac{\dot{y}D}{U_r} \tag{2.4}$$

Finally, assuming small displacements, the forces in the cross-flow and in-flow directions can be expressed in terms of the drag and lift coefficients in the standard quasi-steady method developed by Price and Païdoussis [6]:

$$F_x = \frac{1}{2}\rho S U_\infty^2 \left(C_D - 2\frac{\dot{\tilde{x}} D}{a U_\infty} C_D + \frac{\dot{\tilde{y}} D}{a U_\infty} C_L \right)$$
$$F_y = \frac{1}{2}\rho S U_\infty^2 \left(C_L - 2\frac{\dot{\tilde{x}} D}{a U_\infty} C_L - \frac{\dot{\tilde{y}} D}{a U_\infty} C_D \right) \tag{2.5}$$

2.1.1 Time delay

In 1983, Price and Païdoussis did not consider the changes in fluid velocity and could not find instability in airflow [34]. Later they modified their analysis using Flower and Simpson [16] correlation for the time delay. Price and Païdoussis argued that the force coefficients do not change instantly and need some time to reach the quasi-static value. They suggested that the order of magnitude of the time delay, produced by the presence of the stagnant body, should be the same as that of an isolated cylinder. They used the Flower an Simpson correlation to find the time delay [6]:

$$\Delta t = \frac{\mu D}{U_G} \; ; \mu \sim O(1) \tag{2.6}$$

Price and Païdoussis assumed a harmonic cylinder motion and deduced that the delay can be expressed as the following factor multiplied by quasi-static force coefficients to compensate for unsteady effects:

$$\tilde{g} = \exp\left(\frac{\lambda \mu D}{U_G}\right) \tag{2.7}$$

Later, they applied the same concept to their constrained mode analysis and suggested that the motion in the in-flow direction shall experience the same effect. They used the first approximation and concluded that the time delay sensed by the surrounding cylinders in a tube bundle can be expressed as [15]:

$$\tau_i = \frac{S_i}{U_G} \tag{2.8}$$

Following the same argument, they supposed that the time delay has the same asymptotic form for neighboring cylinders (in the triangular tube bundle, the distances are equal so the time delay is the same for all neighboring cylinders):

$$g_i = \exp(\lambda \tau_i) \tag{2.9}$$

Usage of time delay enabled them to go beyond the limit of the pure quasi-steady model. Consequently, the new model can predict instability for single flexible tube as well as multiple stability regions (the latter was considered as the weak point of the quasi-steady model by Chen [7]). In the present study, the same time delay mechanism is used to account for unsteady effects.

2.1.2 Passing from local to global coordinate system

Applying the time delay hypothesis, Price *et al.* [15] expressed the motion of surrounding cylinders from a coordinate system attached to the central cylinder in the flow direction:

$$\begin{aligned} \chi_i(\textit{as viewed from the central cylinder}) &= x_i(t-\tau_i) + \tau \dot{x}_i(t-\tau_i) \\ \eta_i(\textit{as viewed from the central cylinder}) &= \qquad\quad y_i(t-\tau_i) \end{aligned} \tag{2.10}$$

Price *et al.* [15] supposed a simple harmonic motion in the in-flow and cross-flow directions as follows:

$$x_i(t) = x_{io} \exp(\lambda t) \; ; \; y_i(t) = y_{io} \exp(\lambda t) \tag{2.11}$$

Therefore, using the time delay only in the flow direction they combined (2.10) and (2.11) to obtain:

$$\begin{aligned} \chi_i(\textit{as viewed from the central cylinder}) &= g_i x_i(t)(1+\lambda \tau_i) \\ \eta_i(\textit{as viewed from the central cylinder}) &= \qquad g_i y_i(t) \end{aligned} \tag{2.12}$$

Furthermore, the effect of changes in angle of attack demonstrated in Figure 2.1 is combined with the time delay mechanism. Considering a local coordinate system parallel and normal to flow direction and attached to the central cylinder results in the local coordinate changes arising from the angle of attack changes.

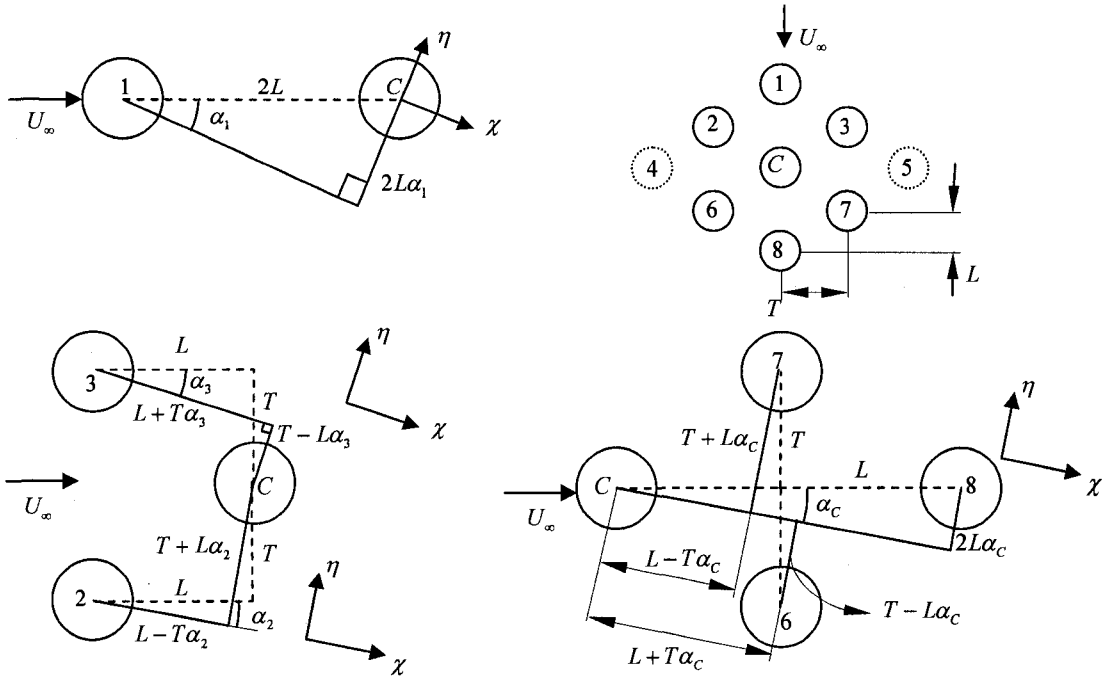

Figure 2.2 Effect of angle of attack on local coordinate system attached to each cylinder neglecting the effect of distant cylinders [15] (cylinder 4 and 5)

Figure 2.2 describes the effect of angle of attack on modifying the local coordinate viewed from the central cylinder. These changes are summarized in (2.13):

$$\begin{aligned}
\Delta\eta_1 &= -2L\alpha_1 & \Delta\chi_1 &= 0 & \Delta\eta_6 &= L\alpha_C & \Delta\chi_6 &= T\alpha_C \\
\Delta\eta_2 &= -L\alpha_2 & \Delta\chi_2 &= T\alpha_2 & \Delta\eta_7 &= L\alpha_C & \Delta\chi_7 &= -T\alpha_C \\
\Delta\eta_3 &= -L\alpha_3 & \Delta\chi_3 &= -T\alpha_3 & \Delta\eta_8 &= 2L\alpha_C & \Delta\chi_7 &= 0
\end{aligned} \tag{2.13}$$

where the effect of the time delay is considered in the calculation of angle of attack:

$$\alpha_i(t-\tau_i)=\frac{\dot{\tilde{y}}_i(t-\tau_i)D}{U_\infty} \tag{2.14}$$

Combining the local coordinate changes due to time delay (2.12) and due to the angle of attack (2.13) while considering the time delay effect on angle of attack variations (2.14) leads to (2.15) which defines the local coordinate system in terms of global coordinates:

$$\begin{aligned}
&\chi_C = x_C && \eta_C = y_C \\
&\chi_1 = g_1 x_1(1+\lambda\tau_1) && \eta_1 = g_1 y_1(1-2L\lambda/U_G) \\
&\chi_2 = g_2[x_2(1+\lambda\tau_2)+y_2 T\lambda/U_G] && \eta_2 = g_2 y_2(1-L\lambda/U_G) \\
&\chi_3 = g_3[x_3(1+\lambda\tau_3)-y_3 T\lambda/U_G] && \eta_3 = g_3 y_3(1-L\lambda/U_G) \\
&\chi_6 = g_6 x_6(1+\lambda\tau_6)+y_C T\lambda/U_G && \eta_6 = g_6 y_6 + y_C L\lambda/U_G \\
&\chi_7 = g_7 x_7(1+\lambda\tau_7)-y_C T\lambda/U_G && \eta_7 = g_7 y_7 + y_C L\lambda/U_G \\
&\chi_8 = g_8 x_8(1+\lambda\tau_8) && \eta_8 = g_8 y_8 + 2y_C L\lambda/U_G
\end{aligned} \tag{2.15}$$

Having expressed the local coordinate system in terms of the global counterpart the next step is to calculate the force coefficients.

2.1.3 Fluid force coefficients

Using the standard quasi-steady approach while applying the unsteady time delay multiplier (2.7), Price *et al.* [15] expressed the fluid force coefficients on the central cylinder in terms of the forces on the central cylinder and the derivative of the forces with respect to neighboring tubes local coordinates. In the present work, the effect of Tubes 4 and 5 (Figure 2.2) is neglected to simplify the test apparatus knowing that the effect of cylinders in close vicinity is far more important than the distant ones. This approximation is expected to be even more valid for two-phase flows compared to single-phase flows. The fluid forces can be expressed as follows:

$$\begin{aligned}
C_{DC} &= C_{D0} + \tilde{g}\sum_{C,i=1}^{8}(\chi_i C_{DC,\xi_i} + \eta_i C_{DC,\eta_i}) \qquad i \neq 4,5 \\
C_{LC} &= C_{L0} + \tilde{g}\sum_{C,i=1}^{8}(\chi_i C_{LC,\xi_i} + \eta_i C_{LC,\eta_i}) \qquad i \neq 4,5
\end{aligned} \tag{2.16}$$

2.1.4 Application of symmetry

The existence of symmetry in triangular tube bundles greatly simplifies the measurements and calculations. Because of symmetry, when moving in the cross-flow direction, the drag coefficient variations shall be zero for tube "1", "C" and "8" therefore:

$$C_{DC,\eta_C} = C_{DC,\eta_1} = C_{DC,\eta_8} = 0 \tag{2.17}$$

On the other hand, the lift coefficients of the above-mentioned cylinders are zero when the cylinders move in the flow direction along the symmetry axis:

$$C_{LC,\chi_C} = C_{LC,\chi_1} = C_{LC,\chi_8} = 0 \tag{2.18}$$

The same arguments lead to the following additional simplifications:

$$\begin{aligned} C_{DC,\eta_3} &= -C_{DC,\eta_2} & C_{LC,\eta_3} &= C_{LC,\eta_2} \\ C_{DC,\eta_7} &= -C_{DC,\eta_6} & C_{LC,\eta_7} &= C_{LC,\eta_6} \\ C_{DC,\chi_3} &= C_{DC,\chi_2} & C_{LC,\chi_3} &= -C_{LC,\chi_2} \\ C_{DC,\chi_7} &= C_{DC,\chi_6} & C_{LC,\chi_7} &= -C_{LC,\chi_6} \end{aligned} \tag{2.19}$$

The center to center distances are equal in a rotated triangular tube bundle therefore the time delays τ_i's and subsequently the g_i's are constant for surrounding cylinders:

$$\tau_i = \tau \qquad g_i = g \tag{2.20}$$

Applying the symmetry conditions (2.17) through (2.20) in (2.16) and rewriting the local coordinates in terms of global coordinate system (2.15) leads to the following form of the fluid force coefficients:

$$
\begin{aligned}
C_{DC} = C_{D0} + \tilde{g}\{ & x_C C_{D\,C,\chi_C} + g_1 x_1 (1+\lambda\tau_1) C_{D\,C,\chi_1} \\
& + g[x_2(1+\lambda\tau) + y_2 T\lambda / U_G] C_{DC,\chi_2} + g y_2 (1 - L\lambda / U_G) C_{DC,\eta_2} \\
& + g[x_3(1+\lambda\tau) - y_3 T\lambda / U_G] C_{DC,\chi_2} - g y_3 (1 - L\lambda / U_G) C_{DC,\eta_2} \\
& + [g x_6 (1+\lambda\tau) + y_C T\lambda / U_G] C_{DC,\chi_6} + [g y_6 + y_C L\lambda / U_G] C_{DC,\eta_6} \\
& + [g x_7 (1+\lambda\tau) - y_C T\lambda / U_G] C_{DC,\chi_6} - [g y_7 + y_C L\lambda / U_G] C_{DC,\eta_6} \\
& + g x_8 (1+\lambda\tau) C_{DC,\chi_8} \}
\end{aligned}
\tag{2.21}
$$

$$
\begin{aligned}
C_{LC} = \tilde{g}\{ & y_C C_{LC,\eta_C} + g y_1 (1 - 2L\lambda / U_G) C_{LC,\eta_1} \\
& + g[x_2(1+\lambda\tau) + y_2 T\lambda / U_G] C_{LC,\xi_2} + g y_2 (1 - L\lambda / U_G) C_{LC,\eta_2} \\
& - g[x_3(1+\lambda\tau) - y_3 T\lambda / U_G] C_{LC,\xi_2} + g y_3 (1 - L\lambda / U_G) C_{LC,\eta_2} \\
& + [g x_6 (1+\lambda\tau) + y_C T\lambda / U_G] C_{LC,\xi_6} + [g y_6 + y_C L\lambda / U_G] C_{LC,\eta_6} \\
& - [g x_7 (1+\lambda\tau) - y_C T\lambda / U_G] C_{LC,\xi_6} + [g y_7 + y_C L\lambda / U_G] C_{LC,\eta_6} \\
& + [g y_8 + 2 y_C L\lambda / U_G] C_{LC,\eta_8} \}
\end{aligned}
\tag{2.22}
$$

The variation of the fluid forces versus local coordinates will be determined experimentally. It should be noted that in the absence of cylinder velocity (quasi-static force measurements) the angles of attack do not change thus the local coordinates are no longer different from global ones.

2.2 Two-phase flow considerations

Introduction of two-phase flow into the fluidelastic instability problem adds two new parameters; namely void fraction and flow regime. Both of these parameters, which are absent in single-phase flow, affect the fluidelastic instability behavior.

Traditionally researchers have relied on the homogeneous model to determine fluid parameters such as density, void fraction and flow velocity for fluidelastic instability problems. However, one can find other models like that of Feenstra *et al.* [33] which take into account the slip ratio between phases. The draw back of the Feenstra *et al.* model is that it is only verified with Gamma ray measurements at the entrance of the tube bundle.

The flow regime in tube bundle can seriously affect the results. Unfortunately, unlike internal (pipe) flow, only a few researchers have tried to predict the flow regime in tube bundles. Among these attempts, are the flow maps obtained by Grant [35] and Ulbrich [36] (Figure 2.3). For the moment, supposing that the flow regime can be simply controlled by changing flow rates, the flow velocities may be chosen so that flow remains in the bubbly regime. The experimental test conditions are compared to these flow maps in chapter four (It should be kept in mind that the results are to be compared with dynamic tests, which are conducted at higher free stream velocities[37]).

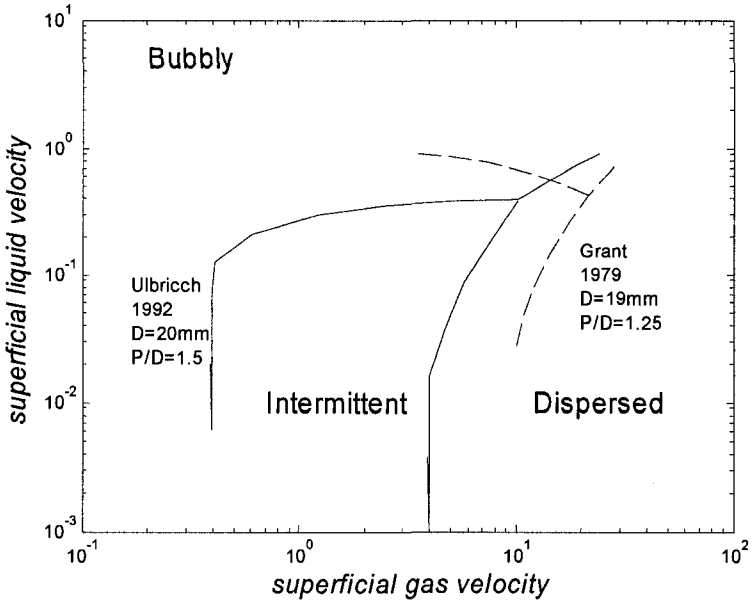

Figure 2.3 Flow maps obtained by Grant (- -) [35] and Ulbrich (—) [36]

2.2.1 Homogeneous model

The homogeneous model states that the velocities of both phases are equal. Considering the same velocity for liquid and gaseous phase enables one to deal with the homogeneous mixture as a medium with averaged properties. Although the big difference in densities of air and water (1:830) can make the gaseous phase travel faster

[33] , the continuous mixture of phases at each half tube pitch can cancel this effect and produce an almost homogeneous flow in a triangular tube bundle [32].

The simplicity of the homogeneous model makes it a powerful tool to examine fluidelastic instability in two-phase flow. This assumption will not restrict the quasi-steady model. Other two-phase models can simply be adapted to investigate instability using the same approach.

The homogeneous void fraction is defined as the ratio of volumetric flow rate of gas divided by total volumetric flow rate.

$$\beta = \frac{Q_g}{Q_g + Q_l} \tag{2.23}$$

Assuming homogeneous flow greatly simplifies prediction of the fluid properties. The void fraction can simply be used as a weight function to calculate average fluid properties such as density and viscosity.

$$\begin{aligned} \rho &= \beta\rho_g + (1-\beta)\rho_l \\ \nu &= \beta\nu_g + (1-\beta)\nu_l \end{aligned} \tag{2.24}$$

Finally, the average free stream velocity can be approximated dividing the total volumetric flow rate by the free stream area:

$$U_\infty = \frac{Q_g + Q_l}{A_\infty} \tag{2.25}$$

Although this assumption greatly simplifies the calculations one should bear in mind that a small slip exists between the phases. The variation of the slip ratio at various flow rates can produce errors in comparing the same void fraction at different free stream velocities. In order to avoid such problems one should limit the variation of flow velocities to a small range while using the homogeneous model.

2.2.2 Feenstra *et al.* model

Feenstra *et al.* [33] proposed a new void fraction model considering slip between phases. They used gamma densitometry to measure the average density upstream of the tube bundle. They correlated the slip between phases as:

$$s = 1 + 25.7(Ri.Cap)^{1/2}(P/D)^{-1} \tag{2.26}$$

where the Richardson number, Ri, is calculated by:

$$Ri = 9.81\Delta\rho^2.(P-D)/G_p^2 \tag{2.27}$$

and the capillary number, Cap, is related to surface tension as:

$$Cap = \mu_L U_G / \sigma \tag{2.28}$$

with the gaseous phase velocity expressed in terms of real void fraction and quality:

$$U_G = \frac{xG_p}{\varepsilon\rho_g} \tag{2.29}$$

where the void fraction itself is a function of the slip ratio:

$$\varepsilon = \frac{x}{x + s\frac{\rho_g}{\rho_l}(1-x)} \tag{2.30}$$

The slip ratio can be found using the superficial void fraction as an initial guess and finding the slip ratio and void fraction respectively. A trial and error iterative

process will lead to the answer with an acceptable error. As mentioned earlier, the measurement of flow velocity upstream of the tube bundle is the major draw back of this method and it is not evident that the small-calculated slip ratio between phases is worth complicating the problem. However, one can easily include this correlation into the fluidelastic instability model.

2.2.3 Approximation of added mass

Although the added mass, an important fluid dynamic parameter, is almost independent of viscosity and can be dealt with inviscid models the existence of two-phase flow makes direct usage of such methods complicated. This important flow parameter can be approximated using the correlation introduced by Rogers *et al.* [38]. The hydrodynamic mass per unit length can be approximated as follows:

$$m_a = \frac{\pi}{4}\rho D^2 \left[\frac{\left(D_e/D\right)^2 + 1}{\left(D_e/D\right)^2 - 1} \right] \tag{2.31}$$

where for a triangular tube bundle

$$D_e/D = \left(0.96 + 0.5\,P/D\right)P/D \tag{2.32}$$

The homogeneous void fraction can be used in the above correlation to calculate the density as a first approximation.

2.3 Single flexible tube analysis

For low mass damping parameters, one can neglect the effect of surrounding cylinders on the central tube. Neglecting the above-mentioned effects will simplify the form of the force coefficients (2.21) and (2.22) as follows:

$$C_{DC} = C_{D0} + \tilde{g}\tilde{x}_C C_{D\,C,\chi_C}$$
$$C_{LC} = \tilde{g}\tilde{y}_C C_{LC,\eta_C} \tag{2.33}$$

Combining (2.33) and (2.5) using first order approximation, will lead to the following fluid forces appearing on the right hand side of equation of motion

$$\{\tilde{F}\} = Q\{\tilde{F}_0\} + Q[\tilde{D}]\{\dot{\tilde{z}}\} + Q\tilde{g}[\tilde{K}]\{\tilde{z}\} \tag{2.34}$$

where,

$$\{\tilde{F}_0\} = \begin{Bmatrix} C_{D0} \\ 0 \end{Bmatrix} ; \ [\tilde{D}] = \frac{-DC_{D0}}{aU_\infty}\begin{bmatrix} 2 & 0 \\ 0 & 1 \end{bmatrix} ; \ [\tilde{K}] = \begin{bmatrix} C_{D,\chi} & 0 \\ 0 & C_{L,\eta} \end{bmatrix}$$
$$\{\tilde{z}\} = \begin{Bmatrix} \tilde{x} \\ \tilde{y} \end{Bmatrix} ; \ Q = \frac{1}{2}\rho U_\infty^2$$

The above formulation was first introduced by Price and Païdoussis [6] to predict fluidelastic instability in single-phase flow. The two-phase flow parameters such as density, added mass and free stream velocity could be modeled using the void fraction models introduced earlier. The resulting forces will be introduced into (2.1) to form the general governing equation.

The eigenvalues of the homogeneous differential equation may be obtained by solving the state space equations for different mass damping parameters. The minimum velocity at which the real value of any eigenvalue becomes positive indicates the instability boundary.

2.4 Constrained mode hypothesis

Although the simplicity of the single flexible model makes it a useful tool to interpret the results, it is limited to low mass damping parameters. Price *et al.* [15] developed their constrained mode analysis to overcome this shortcoming in 1988. Although the method is based on an infinite cylinder array, the constrained mode

hypothesis brings down the number of variables to a kernel of two cylinders for staggered tube bundles.

Figure 2.4 helps to describe the constrained mode model. The generalized constrained mode analysis states that when moving in flow and cross-flow direction in either of the kernels of hatched or dotted cylinders, a certain phase difference occurs in in-flow and cross-flow motion for each degree of freedom such that

$$x_{q,p} = x_0 \exp(\lambda t + ip\phi_x + iq\theta_x)$$
$$y_{q,p} = y_0 \exp(\lambda t + ip\phi_y + iq\theta_y) \tag{2.35}$$

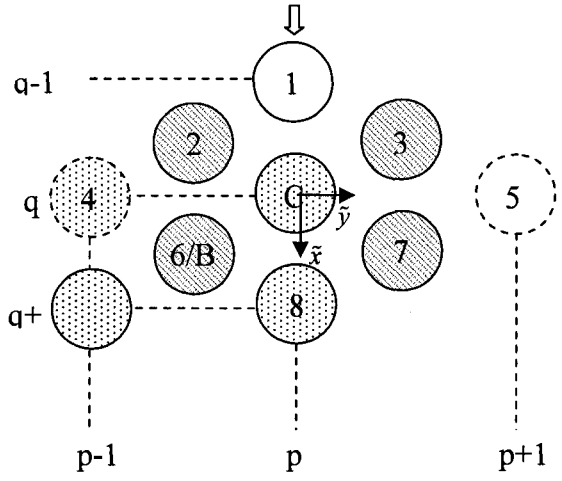

Figure 2.4 The hatched and dotted cylinders indicate two different kernels. The row and column indices are zero for the cylinders centered at 'B' or 'C'

In a finite tube bundle, the results of dynamic test analysis show different behaviors [37]. The kernel of dotted cylinders seems to be more affected by the left wall while that of the hatched ones is under the influence of the right wall. The formulation is modified to account for this effect. Unfortunately, the number of flexible rows does not permit measuring the two distinct phase angles and the new formulation shall be used with unique kernel phase angles [15].

Considering the general case with two different phase angles, the motion of each cylinder can be expressed in terms of Cylinder 'C' or 'B'. Motion of Cylinder '1' and '8' can be expressed in terms of Cylinder 'B' as:

$$\begin{aligned} x_1 &= x_{p,q}^B e^{-i\theta_{xb}}, y_1 = y_{p,q}^B e^{-i\theta_{yb}} \\ x_8 &= x_{p,q}^B e^{i\theta_{xb}}, y_8 = y_{p,q}^B e^{i\theta_{yb}} \end{aligned} \tag{2.36}$$

while the movement of Cylinder '2', '7', '3' and '6' can be related to that of Cylinder 'C' supposing:

$$\begin{aligned} x_{p,q}^{BB} &= x_{p,q}^C e^{-i\phi_{xc}} e^{i\theta_{xc}} \\ y_{p,q}^{BB} &= y_{p,q}^C e^{-i\phi_{yc}} e^{i\theta_{yc}} \end{aligned} \tag{2.36}$$

this leads to:

$$\begin{aligned} x_2 &= x_{p,q}^{BB} e^{-i\theta_{xc}} &&= x_{p,q}^C e^{-i\phi_{xc}} &&, y_2 = y_{p,q}^{BB} e^{-i\theta_{yc}} = y_{p,q}^C e^{-i\phi_{yc}} \\ x_7 &= x_{p,q}^{BB} e^{i\phi_{xc}} &&= x_{p,q}^C e^{i\theta_{xc}} &&, y_7 = y_{p,q}^{BB} e^{i\phi_{yc}} = y_{p,q}^C e^{i\theta_{yc}} \\ x_3 &= x_{p,q}^{BB} e^{i\phi_{xc}-i\theta_{xc}} &&= x_{p,q}^C &&, y_3 = y_{p,q}^{BB} e^{i\phi_{yc}-i\theta_{yc}} = y_{p,q}^C \\ x_6 &= x_{p,q}^C e^{-i\phi_{xc}} e^{i\theta_{xc}} &&&&, y_6 = y_{p,q}^C e^{-i\phi_{yc}} e^{i\theta_{yc}} \end{aligned} \tag{2.37}$$

Having defined the motion of every cylinder in terms of either cylinder 'C' or 'B', the fluid forces for the constrained mode can be written as:

$$\begin{Bmatrix} \tilde{F}_{Cx} \\ \tilde{F}_{Cy} \\ \tilde{F}_{Bx} \\ \tilde{F}_{By} \end{Bmatrix} = \frac{1}{2}\rho U_\infty{}^2 \begin{Bmatrix} C_{D0} \\ 0 \\ C_{D0} \\ 0 \end{Bmatrix} + \frac{1}{2}\rho U_\infty^2 \frac{d}{aU_\infty} C_{D0} \begin{bmatrix} -2 & 0 & 0 & 0 \\ 0 & -1 & 0 & 0 \\ 0 & 0 & -2 & 0 \\ 0 & 0 & 0 & -1 \end{bmatrix} \begin{Bmatrix} \dot{\tilde{x}}_C \\ \dot{\tilde{y}}_C \\ \dot{\tilde{x}}_B \\ \dot{\tilde{y}}_B \end{Bmatrix}$$
$$+ \frac{1}{2}\tilde{g}\rho U_\infty^2 \begin{bmatrix} K_{11} & 0 & K_{13} & K_{14} \\ 0 & K_{22} & K_{23} & K_{24} \\ K_{31} & K_{32} & K_{33} & 0 \\ K_{41} & K_{42} & 0 & K_{44} \end{bmatrix} \begin{Bmatrix} \tilde{x}_C \\ \tilde{y}_C \\ \tilde{x}_B \\ \tilde{y}_B \end{Bmatrix} \tag{2.38}$$

where,

$$K_{11} = CD_{C,\xi_C} + g_1 e^{-i\theta_{cx}}(1+\lambda\tau_1)CD_{C,\xi_1} + g_8 e^{i\theta_{cx}}(1+\lambda\tau_8)CD_{C,\xi_8}$$

$$K_{12} = 0$$

$$K_{13} = (1+e^{i\phi_{bx}})[g_2 e^{-i\theta_{bx}}(1+\lambda\tau_2)CD_{C,\xi_2} + g_6(1+\lambda\tau_6)CD_{C,\xi_6}]$$

$$K_{14} = g_2 e^{-i\theta_{by}}(1-e^{i\phi_{by}})[T\lambda/U_G CD_{C,\xi_2} + (1-L\lambda/U_G)CD_{C,\eta_2}] + g_6 CD_{C,\eta_6}(1-e^{i\phi_{by}})$$

$$K_{21} = 0$$

$$K_{22} = CL_{C,\eta_C} + g_1 e^{-i\theta_{cy}}(1-2L\lambda/U_G)CL_{C,\eta_1} + 2\lambda/U_G(TCL_{C,\xi_6} + LCL_{C,\eta_6}) + [g_8 e^{i\theta_{cy}} + 2L\lambda/U_G]CL_{C,\eta_8}$$

$$K_{23} = (1-e^{i\phi_{bx}})[g_2 e^{-i\theta_{bx}}(1+\lambda\tau_2)CL_{C,\xi_2} + g_6(1+\lambda\tau_6)CL_{C,\xi_6}]$$

$$K_{24} = g_2 e^{-i\theta_{by}}(e^{i\phi_{by}}+1)[T\lambda/U_G CL_{C,\xi_2} + (1-L\lambda/U_G)CL_{C,\eta_2}] + g_6(1+e^{i\phi_{by}})CL_{C,\eta_6} *$$

$$K_{31} = (e^{-i\phi_{xc}}+1)[g_2(1+\lambda\tau_2)CD_{C,\xi_2} + g_6 e^{i\theta_{xc}}(1+\lambda\tau_6)CD_{C,\xi_6}] *$$

$$K_{32} = (e^{-i\phi_{yc}}-1)\{g_2[T\lambda/U_G CD_{C,\xi_2} + (1-L\lambda/U_G)CD_{C,\eta_2}] + g_6 e^{i\theta_{yc}} CD_{C,\eta_6}\}$$

$$K_{33} = CD_{C,\xi_C} + g_1 e^{-i\theta_{xb}}(1+\lambda\tau_1)CD_{C,\xi_1} + g_8 e^{i\theta_{xb}}(1+\lambda\tau_8)CD_{C,\xi_8}$$

$$K_{34} = 0$$

$$K_{41} = (e^{-i\phi_{xc}}-1)[g_2(1+\lambda\tau_2)CL_{C,\xi_2} + g_6 e^{i\theta_{xc}}(1+\lambda\tau_6)CL_{C,\xi_6}] *$$

$$K_{42} = (e^{-i\phi_{yc}}+1)\{g_2[T\lambda/U_G CL_{C,\xi_2} + (1-L\lambda/U_G)CL_{C,\eta_2}] + g_6 e^{i\theta_{yc}} CL_{C,\eta_6}\} *$$

$$K_{43} = 0$$

$$K_{44} = CL_{C,\eta_C} + g_1 e^{-i\theta_{yb}}(1-2L\lambda/U_G)CL_{C,\eta_1} + 2\lambda/U_G(TCL_{C,\xi_6} + LCL_{C,\eta_6}) + (g_8 e^{i\theta_{yb}} + 2L\lambda/U_G)CL_{C,\eta_8}$$

The coefficients which are marked by "*" differ from those originally presented in [15] due to small typing errors in the latter. Once more, the eigenvalues of the homogeneous differential equation may be obtained by solving state space equations for different mass-damping parameters.

2.5 State space equations

The modal analysis suffers from a damping matrix with different distribution than the stiffness matrix. The existence of fluid stiffness and damping matrices with different behaviors for various mass-damping parameters makes one search for alternative methods to solve the eigenvalue problem. The state space method does not

experience the above-mentioned shortcoming. However, usage of state spaces doubles the size of all complex nonlinear matrices.

The new state variable, which changes the second order differential equations to the first order equations, can be defined as follows:

$$\{x^*\} = \begin{Bmatrix} \{\tilde{z}\} \\ \{\dot{\tilde{z}}\} \end{Bmatrix} \tag{2.39}$$

therefore the displacement and velocity vectors are related to the new vector as:

$$\begin{aligned} \{\tilde{z}\} &= [[I] \quad [0]] \times \{x^*\} \\ \{\dot{\tilde{z}}\} &= [[0] \quad [I]] \times \{x^*\} \end{aligned} \tag{2.40}$$

the above equations can be written as the form of additional identity transformation:

$$[[I] \quad [0]] \times \{\dot{x}^*\} - [[0] \quad [I]] \times \{x^*\} = 0 \tag{2.41}$$

the governing equation also can be written in terms of state variables:

$$[M][[0] \quad [I]]\{\dot{x}^*\} + [C^*][[0] \quad [I]]\{x^*\} + [K^*][[I] \quad [0]]\{x^*\} = 0 \tag{2.42}$$

Equations (2.41) and (2.42) can be expressed in matrix form:

$$[S] \times \{\dot{x}^*\} - [R] \times \{x^*\} = 0 \tag{2.43}$$

where:

$$[S] = \begin{bmatrix} [I] & [0] \\ [0] & [M] \end{bmatrix} \quad ; \quad [R] = -\begin{bmatrix} [0] & [I] \\ [K^*] & [C^*] \end{bmatrix}$$

It should be noted that, unlike classical mechanical vibrations, the stiffness matrix is not symmetric. Therefore, the multiplication of identity transformation by stiffness matrix does not make the equation symmetric and only complicates the calculations. This is why the R and S matrices appear in an unusual non-symmetric form.

The resulting complex nonlinear eigenvalue problem can be solved using IMSL libraries. It will be enough to call CALCEIG subroutine to solve this complicated problem.

2.6 Consideration of memory effect

In 1996, Granger and Païdoussis modified the single flexible tube model [17]. The pure quasi-steady model states that the variation of forces takes place instantaneously. Therefore, the consideration of time delay only retards the variation of forces due to fluid inertia or because of the delay experienced by fluid impinging a stationary body. They argued that in reality, instead of the time delay introduced in earlier models, the force coefficients should vary smoothly with a series of decaying functions.

They showed that the consideration of time delay, which only considers one decaying function, is a special case of their quasi-unsteady model. They used dynamic test data along with parameter estimation techniques to calculate the new decay functions. Although the new method can provide a better understanding of flow retardation, it implies that dynamic tests are required.

Considering that the instability often first occurs in the cross-flow direction, the fluid forces in the cross-flow direction in single flexible tube analysis (2.34) can be written as:

$$\tilde{F}_y = Q\tilde{F}_{0y} - Q\frac{DC_{D0}}{aU_\infty}\dot{\tilde{y}} + Q\tilde{g}C_{L,\eta}\tilde{y} \tag{2.44}$$

Application of the quasi-unsteady theory replaces the $\tilde{g}$ function by an appropriate convolution integral:

$$\tilde{g}^* = h_{Ly}(\tau) * \tilde{y} \tag{2.45}$$

where,

$$h_{Ly}(\tau) = {d\Phi_{Ly}}/{d\tau} + \Phi_{Ly}(0)\delta(\tau) \tag{2.46}$$

knowing $\delta(\tau)$ is the Dirac delta-function and Φ_{Ly} is defined as follows:

$$\Phi_{Ly} = \sum_{i=1}^{N} \alpha_i e^{-\delta_i \tau} \tag{2.47}$$

The single flexible tube model of Price and Païdoussis can be found by setting: N=1 and $h_{Ly}(\tau) = \delta(\tau - \mu)$. The verification of this method requires more dynamic data points at different mass-damping parameters.

As it can be seen in all quasi-steady models, the application of these methods requires the knowledge of quasi-static force variations. The next chapter is devoted to the experimental setup, which enable us to measure the quasi-static force variations in a rotated triangular tube bundle.

CHAPTER 3

EXPERIMENTAL SETUP AND TEST PROCEDURE

As described in previous chapters, the quasi-steady fluid force field is the necessary input to the class of quasi-static, quasi-steady and quasi-unsteady fluidelastic instability theoretical models. The air-water two-phase flow loop of the Fluid-Structure Interactions Laboratory at École Polytechnique de Montréal was used for the experimental measurements.

Minor modifications of an existing dynamometer made it possible to measure the forces on the central cylinder precisely. Among these modifications, sealing the immersed strain gauges on the central cylinder beams proved to be quite a challenge. Even though the existence of symmetry in the tube bundle decreased the number of instrumented cylinders, the leveling of the test section, became another challenge.

The large number of data points made it necessary to connect all the sensors to the data acquisition system. However, electrical noise became another problem. The existence of various strain indicators and strain gages installed on different materials and the vicinity of rotating machinery necessitated a careful selection of excitation voltage and amplification.

This chapter is devoted to the experimental setup, instrumentation and measurement methodology.

3.1 Flow loop

A schematic of the flow loop and test section is shown in Figure 3.1. The flow loop consists of a 2500 liter tank that serve as a reservoir, a variable speed (by varying the frequency) centrifugal pump with a maximum flow rate of 25 l/s, a turbine flow meter, a mixer for producing a uniform two-phase mixture upstream of the test section, a test section and related piping.

The university air supply is connected to the flow loop upstream of the mixer. It can provide up to 200 l/s air at ambient pressure and temperature (P=1.01 bar, T=20 C). Two orifice plates are installed on the airline to enable accurate measurement of air at high and low flow rates.

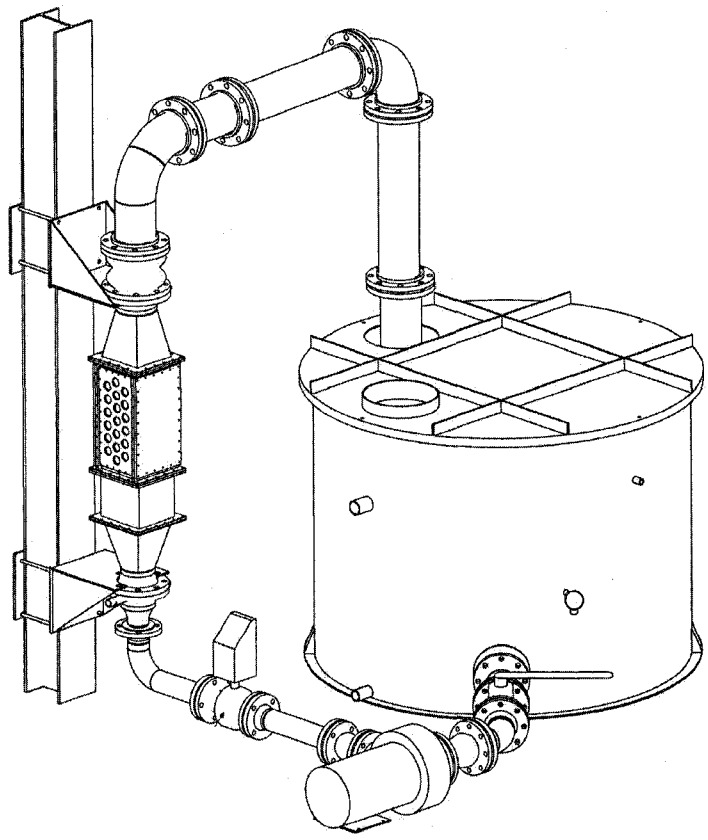

Figure 3.1 Schematic of flow loop and test section

3.2 Test section

Two different test sections can be used in the flow loop. The smaller test section contains only one column of full cylinders and the larger one holds three columns of full cylinders. Fixed half cylinders are added on the sidewalls of each test section to simulate the effect of neighboring tubes. The force measurements were taken using the larger test section with three columns of full cylinders. Figure 3.2 illustrates the test section used in the force measurements.

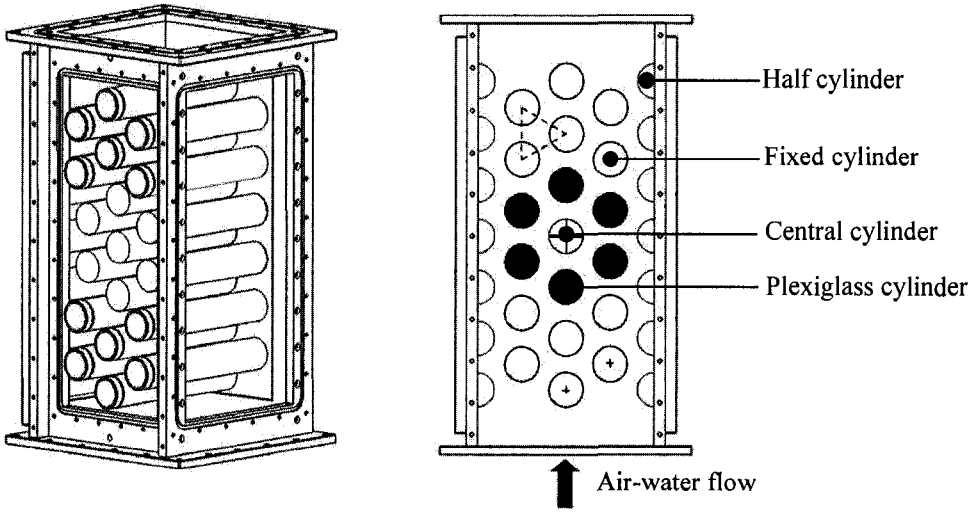

Figure 3.2 Larger test section used to measure fluid forces

Three kinds of tubes are installed in the test section. Fixed tubes and instrumented tubes that may be either, hollow plexiglass tubes, or the dynamometer.

3.2.1 Fixed tubes

The rigid aluminum tubes are 38 mm in diameter. They simply slide inside the test section holes. The O-rings installed at the ends of these tubes ensures good sealing.

3.2.2 Instrumented tubes

Two types of instrumented tubes are used to measure the quasi-static forces on the central tube and its neighbors:

- Plexiglass tubes: the plexiglass tubes are instrumented with four strain gages (Figure 3.3). The strain gages are connected to form two half bridges that measure strain in both in-flow and cross-flow directions on the cylinders. Four bolts fasten the tubes to the test section faces. Special care was needed to level these tubes (using a level it is possible to put the cylinders at the same position where the calibrating has been done).

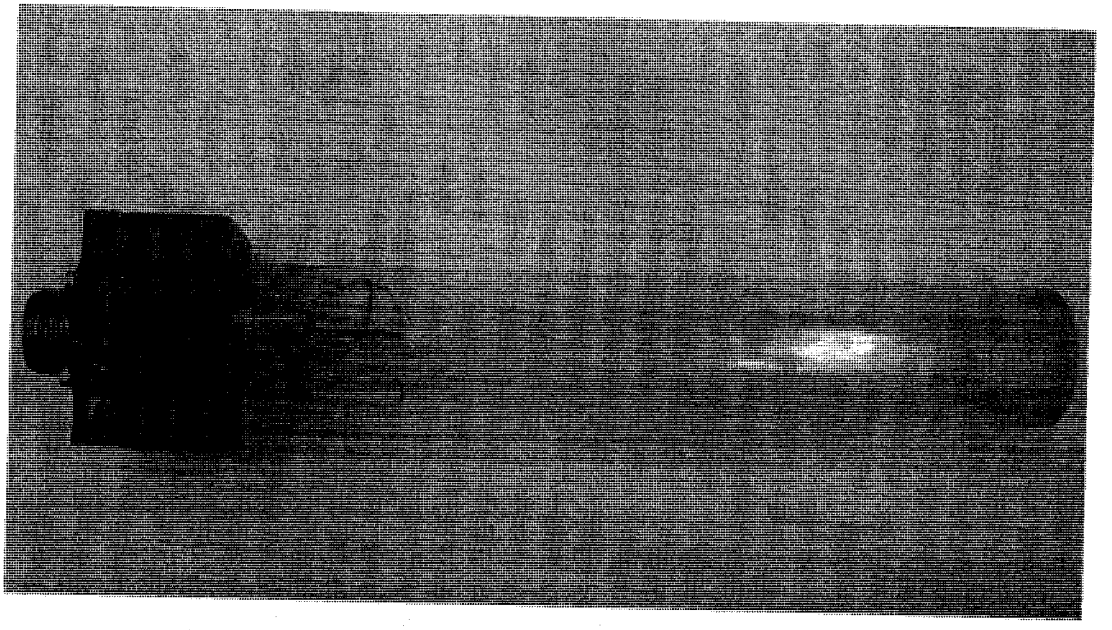

Figure 3.3 Plexiglass tube instrumented with four strain gages inside the tube

- Central tube and dynamometer: Since the position of the central tube has the strongest effect on measured fluid forces this system was developed to achieve high precision measurements. Figure 3.4 and 3.5 show pictures of the central cylinder and dynamometer installed on the displacement system. The dynamometer acts under pure shear so; it is not sensitive to the position of load (Figure 3.7). Each of the four thin steel plates are equipped with two strain gages connecting the four strain gages found at each direction in a full bridge, the forces could be measured precisely in each direction. The dynamometer is attached to the displacement system so that the quasi-static fluid forces can be measured for different positions of central cylinder.

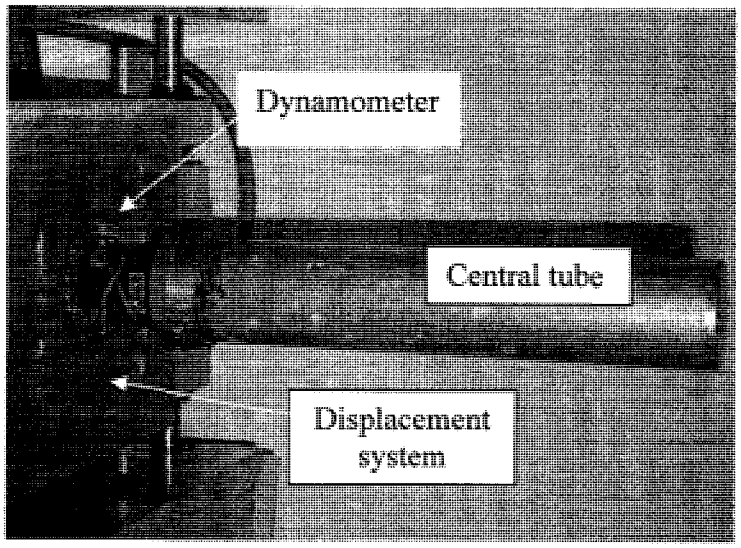

Figure 3.4 Central tube, dynamometer and displacement system assembly

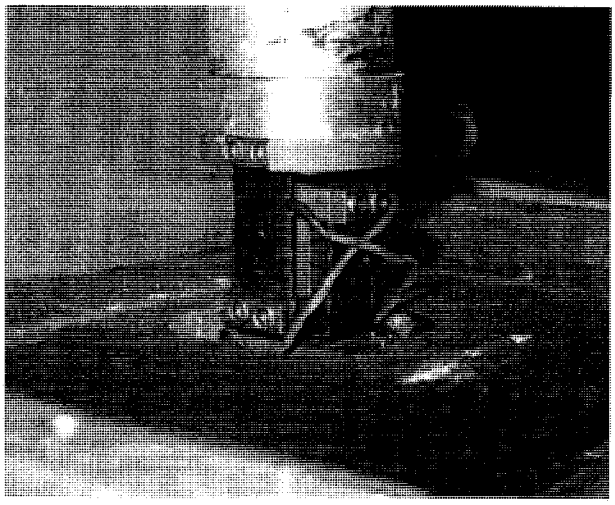

Figure 3.5 A closer view of dynamometer and displacement system assembly

3.3 Displacement system

The variation of the force coefficients with to position in the quasi-steady formulation (Chapter 2) necessitates quasi-static measurements of forces for different positions in both the cross-flow and in-flow directions. The displacement system is designed to allow the accurate positioning of the central cylinder within the surrounding

cylinders. The variation of force coefficients of the surrounding cylinders versus the displacement of the central cylinder will be interpreted later as the derivatives of the central tube force coefficients with respect to the displacement of the neighboring cylinders.

Two power screws enable vertical and horizontal positioning of the central cylinder within a $12x12mm^2$ area. A pair of displacement transducers is attached to the positioning system to measure the position of the central tube with a precision of 0.3 millimeters.

3.4 Dynamometer strain gage sealing

The dynamometer was designed to ensure precise measurement of forces in the vertical and horizontal directions. Since the dynamometer strain gages are immersed in water, the sealing process requires special attention. A five-layer sealant, which was chosen according the recommendations of the manufacturer (Vishay), ensured proper sealing of the strain gages.

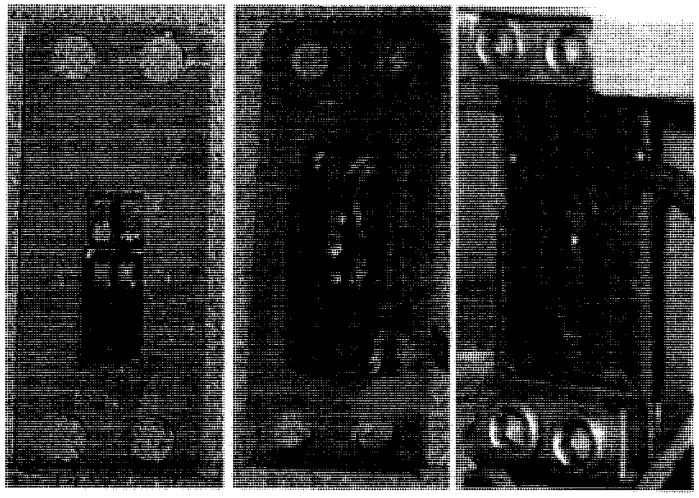

(a) (b) (c)

Figure 3.6 (a) installation of gages, (b) attachment of Teflon band and (c) covering with aluminum foil sandwiched in Butyl rubber sealant

A thin layer of nitrile rubber forms the first flexible coating. The wires attached to the gages are also protected against moisture with the same sealant. A Teflon band covers the initial layer. The whole installation is protected with a thin aluminum foil sandwiched between two layers of flexible Butyl rubber sealant. The surfaces and wires were properly cleaned before installation. Figure 3.6 shows pictures taken after the installation of the gages, attachment of the Teflon band and finally with the aluminum foil cover sandwiched in Butyl rubber sealant.

3.5 Calculation of excitation voltage

The centrifugal pump being near the strain gage installation caused unwanted extraneous noise. To minimize the problem it was desirable to increase the excitation voltage while reducing the amplification. This improves the signal to noise ratio although it can create other problems.

Strain gages are seldom damaged by excessive excitation voltages. The usual result is a gradual change of the output due to the heat generated in the gages. Rather than gage failure, the higher voltage applied to the strain gage bridge generates more electrical power loss in each arm, which must be dissipated in the form of heat. The heat generated in the gage causes a temperature rise in the gage filament, which is a function of heat-sink capacity and the gage power level (the problem directly depends on requirements of every particular installation).

The strain gages are installed on either stainless steel (central cylinder installation) or hollow plexiglass tubes (plexiglass surrounding tubes). The stainless steel acts like a good heat sink whereas plexiglass is a poor heat conductor. Thus, strain measurement on plastic requires special considerations. Knowing the installed strain gages and heat sink properties it is possible to calculate the excitation voltage (It is sufficient to introduce the strain gage and heat sink properties in Vishay excitation voltage calculator). In this case, the excitation voltage for plexiglass tubes should be

inferior to 4.6 volts otherwise, continuous changes of strain gage output due to the thermal effects may be observed.

3.6 Strain indicators

Inter technology P-3500 units were used for preliminary tests while the final tests (most of the tests) were conducted using a COOPER DCM160 Bridge sensor along with a 2110A signal conditioner.

3.6.1 P-3500 strain indicator

These strain indicators were less sensitive to external noise but the wiring and calibration of ten separate P-3500 units needed special care. The P-3500 units are battery/adaptor supplied. Since the units were properly isolated from other units and other electric supplies, they were less sensitive to electrical noises than other strain indictors were. The excitation voltage of these units was only 2 volts so it could be used for indicating strain in both strain gages installed on plexiglass tubes and those installed on stainless steel plates of dynamometer.

3.6.2 COOPER DCM160 bridge sensor

The COOPER DCM160 bridge sensors were used to measure strain in the full bridge of the central cylinder. This apparatus contains eight channels two of which were used to conduct the experiments. The excitation voltage of the bridge could vary between 4-10 volts. Since the central cylinder gages were installed on steel, which is a good heat sink, the excitation voltage was set to the maximum for the DCM160 unit.

3.6.3 Model 2110A signal conditioner/amplifier

This signal conditioner also contains eight channels. The excitation voltage of each of them could be independently adjusted between zero and ten volts. Since the unit was connected to the half bridges installed on plexiglass, the selection of the excitation voltage proved to be very important. A proper earth connection reduced the noise

produced by the centrifugal pump (adding a jumper allows the simulation of other resistances on half bridge installations).

3.7 Displacement indicators

Two OMEGA potentiometers were used to measure, in each direction, the position of the central cylinder supported by the displacement system. The output of these potentiometers was connected to an OMEGA CCT-90 device, which converts position linearly to the voltage. The voltage could be read either on the LEDs attached to the panel or through the external data acquisition card connected to the computer. Because the connecting wires passed next to the centrifugal pump, shielding of these wires proved to be of great importance.

3.8 Flow indicators

Two types of indicators were used in measuring water and air flow rates. The MEG 5000 turbine type flow meter, which had been installed an acceptable distance from the pump, measured water flow rates while two Rosemont orifice plates, which were installed on the airlines, measured air flow.

The precision of the water flow meter was about 0.5 percent of the value read on flow meter while for the orifice plates the airflow rates measured were within an accuracy of 1.5%. The two orifice plates enabled precise measurements of air flow in two different ranges. The flow rate of water and air should not exceed 25l/s and 200 l/s respectively.

The signals of all flow meters could either be read on screen or be transferred to the external data acquisition card, which was connected to the computer. The direct recording of flow rates in the computer prevented possible human errors and made it possible to average the fluctuations of either of these flow rates.

3.9 SCB-68 connector data accusation card

The variation of flow rates and forces as well as recording fourteen variables in every test made it necessary to use data acquisition techniques. The fourteen data points include ten strains, two displacements and two flow rate signals. Apart from the risk of error that may occur in manual recording of these signals, the averaging and reporting for twenty-six different positions for every void fraction takes a considerable effort.

The SCB-68 data acquisition card with sixteen 5-volt differential channels made it possible to acquire reliable data in a short time. Furthermore, using LABVIEW enabled averaging the samples recorded every 0.001 sec. The transition of signals to the data acquisition card was through properly shielded cables installed as far as possible from the potential sources of noise.

3.10 Noise control

The existence of potential electric noise sources such as variable speed pump (which functions with varying frequency), fluorescent lamps and amplifiers induces noise in measurement circuits. The closer the measurement system to the potential noise sources the greater is the induced noise. The induced noise superimposes on the real signals and can lead to incorrect and inaccurate interpretation of the signals. Ground connections, shielding, amplification and unnecessarily long wires were thoroughly verified and corrected to reduce the noise effect to an acceptable level.

3.10.1 Ground connections

Generally, when shielding against electrostatic noises below 20 kHz, it is not good practice to ground the shield at more than one point. Multiple ground points may have different voltage levels, which can produce unwanted currents in the wires called ground loops. The precise investigation of every single ground connection helped preventing such a problem.

3.10.2 Shielding

The long instrument cables may act like an antenna and pick up noises. The most effective strategy is to limit the length of cables and to cover them with properly grounded shields. Foiled shields, which can provide the best protection for cables, were chosen to do this task.

3.10.3 Amplification

A high amplification level in the strain indicators can lead to unwanted amplification of noises along with the main signal. The best technique is to try mitigating the amplification level while increasing the excitation voltage to the allowable limit calculated in section 3.5.

3.10.4 Excessive wires

No matter how hard one may try to provide perfect shielding, there always remain some unshielded wires near the strain gages. Minimizing the length of these wires and weaving them together minimized this effect.

3.11 Cross coupling

Although the structure of the dynamometer and the straight installation of the gages inside the plexiglass tubes can minimize the cross coupling of the forces measured in drag and lift directions, the imperfections in assembling and machining different parts causes some coupling between the two directions. This coupling could vary from 1/15 to 1/50 for both kinds of instrumented cylinders.

Considering that, the drag force can be about ten times the lift forces (at the limits) one has to consider this effect when measuring the forces in the lift direction. This effect can be the same order of magnitude as the lift forces for the worst case. On the other hand, since the lift forces are small compared to the drag forces, cross coupling has a negligible effect when measuring drag forces.

The cross coupling in drag direction can be evaluated by letting the water rise above the instrumented tubes in the test section and measuring the forces in both directions. Since the resulting buoyancy force acts purely in drag direction, any measured lift force is cross coupling induced. The ratio of lift to drag forces may be used as the index of cross coupling for every cylinder.

3.12 Measurement methodology

This section describes the experimental methods and techniques used to obtain and interpret the quasi-static fluid force coefficients. The first section, calibration, describes the set of operations that establish, under specified conditions, the relationship between the values indicated by the measuring instrument and the corresponding known values. Then the measured fluids forces are corrected to take into account the buoyancy and cross-coupling effects.

3.12.1 Calibration

The data acquisition system can collect fourteen variables in a single step. These signals are in volts and represent fluid forces, air and water flow rates and finally the displacement in the lift and drag directions. The measured values are converted to real units that are respectively Newtons, liters per second and meters.

Peaces of pipe with two different thicknesses were cut to the length of instrumented tubes and used as distributed weights to calibrate instrumented cylinders. Each cylinder was installed on sidewalls and the weights (the pipes that were cut to almost the same length of pipes) were put over the instrumented cylinder to establish the relation between the distributed force and the value read in millivolts. Then the sidewall was turned ninety degrees, held fix in the clamp and the same procedure was repeated to find the ratio between force in Newtons and the read value in millivolts in the lift direction. These values were recorded to enable the program to read the forces in Newtons in both directions.

The flow meters were calibrated using the values read on the earlier calibrated LED's. The read values in millivolts were compared to the value read on LED to find the correct multiplier that gives the flow rate in the known unit. The use of two different orifice plates resulted in two different multipliers for airflow measurements.

The displacement system was first placed at the zero position. This location was found by putting plates on the neighboring cylinders and moving the displacement system until it contacts the plates. The values read at each limit were subtracted and divided by two to find the real zero position. Putting the cylinder in the central position and measuring the distances between the fixed and moving parts of the displacement system gave an indication for zero position. The displacement system was then moved a known distance (3 mm) in each direction and the resulting signal was again used to find the required multiplier for measuring displacements.

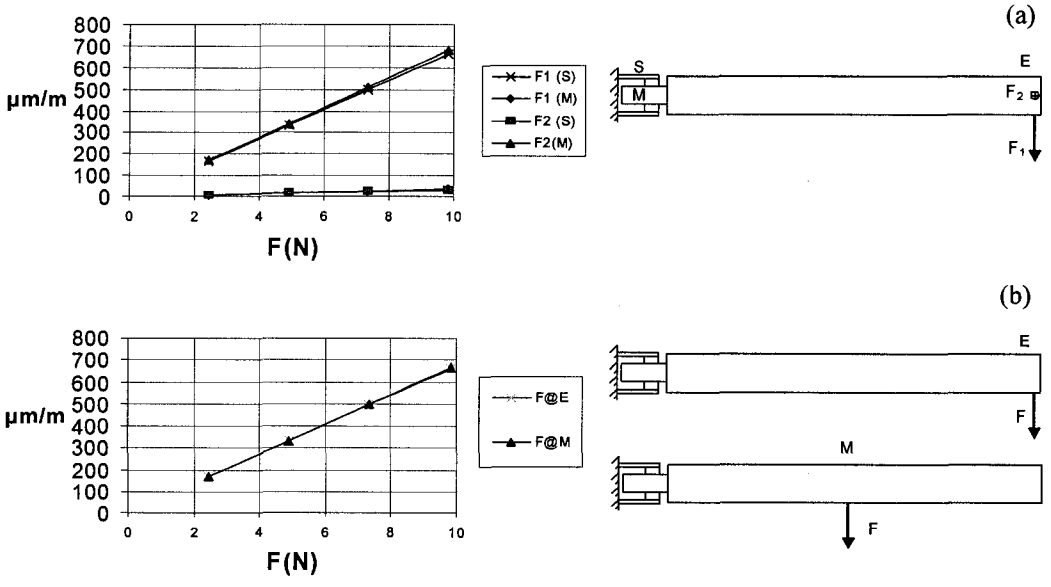

Figure 3.7 (a)effect of cross coupling for the two dynamometer axes, (b) comparison for two force locations 'E' and 'M'

Each set of tests contains two auxiliary data sets. The first set was taken after setting all variables to zero before starting the air and water flow. The second set, which helped calculating the correct coupling, was taken in stagnant water filled to a level above the instrumented tubes in the test section. The ratio of the forces in the lift and drag directions for each tube is used as the indication of cross coupling.

Figure 3.7(a) demonstrates the cross-coupling effect experienced in both directions. Initially different concentrated weights were measured then the cylinder was turned 90 degrees and the experiment repeated. The experiment showed neither the coupling effect nor the true read out considerably change in both directions.

In the second experiment (Figure 3.7 (b)), the location of the concentrated load was changed from the end of the cylinder to the middle location. The same read out showed that unlike the classical cases, the dynamometer works under pure shear rather than pure bending. Both experiments exhibit the linear behavior of the dynamometer.

3.12.2 Calculation of fluid forces

The data acquired in the tests comprises the fluid forces in drag and lift directions for five instrumented cylinders. The forces in the lift direction are corrected taking into account the cross coupling measured in hydrostatic tests. The results of twenty-one different tests provided us with the necessary cross coupling information. The ratio of drag and lift forces for each cylinder is averaged for all the tests to find cross coupling for every individual cylinder.

The drag force at each point is multiplied by the cross coupling ratio to compensate for the error due to the cross coupling. Then the results are subtracted from the corresponding reading in lift direction to calculate the corrected lift force. The drag force does not suffer from the cross coupling error because the value of drag is at least about ten times of the lift force. Therefore, the effect of lift is negligible in the drag direction.

The effect of buoyancy is also taken into account. The value of the hydrostatic drag force can be used as the buoyancy force for water flow. The force is then multiplied by the void fraction to find the buoyancy in two-phase flow. The resulting buoyancy force is subtracted from the drag force to find the corrected drag force.

The corrected fluid forces are used along with the average void fraction and homogeneous two-phase density and velocity to determine the fluid force coefficients. For convenience, the fluid force coefficients are calculated using the free stream velocity, though they can be converted to any needed reference velocity. The next chapter deals with the calculation of the fluid force coefficients.

CHAPTER 4

QUASI STATIC FLUID FORCE COEFFICIENTS

The calibration and correction factors obtained in Chapter 3 provide the necessary information for calculation of the force coefficients and their derivatives. The quasi-static force coefficients are calculated using the homogeneous two-phase flow model and free stream velocity. The test results are stored to permit a later analysis with more sophisticated two-phase models.

The quasi-static fluid force variations obtained in the present test section differ from those reported earlier by Price and Païdoussis [6] who used air in the same configuration with different pitch to diameter ratio and tube diameter. Although the two-phase flow results found at high void fractions are similar to those reported in air flow, the sharp changes in the lift coefficient in the cross-flow direction are absent in the present tube array. Interestingly, for void fractions below 40%, the variation of central cylinder lift coefficient in the cross-flow direction is the inverse of that in air flow. This means that for low void fraction, two-phase flow instability may be governed by the variation of force coefficients while for higher void fractions fluidelastic instability is mostly governed by time delay.

In the present chapter, the variation of fluid forces with Reynolds number is emphasized. These variations will serve to explain why fluidelastic instability will not occur at low free stream velocities. To the author's knowledge, it is the first time that these variations are used to explain the onset of instability.

Finally, curve fitting allows finding the required force coefficient derivatives for the quasi-steady fluidelastic instability model. The derivatives of the fluid forces on neighboring cylinders versus the displacement of the central cylinder shall be converted to the variation of the central cylinder force coefficients with respect to the displacement of the central cylinder.

4.1 Force coefficients in single-phase flow

In all the results that follow, the measured force coefficients are presented as functions of the dimensionless displacements $\tilde{x}$ and $\tilde{y}$ of the central cylinder, 'C'. For cylinders one to four, the force coefficients directly represent the effect of the central cylinder motion on its neighbors. The numbering used in the experiments is shown in Figure 4.1. Using the numbering shown in Figure 4.1, simplifies the passage from a tube bundle with a moving central cylinder to a tube bundle with moving surrounding cylinders as will be explained in Section 4.5.

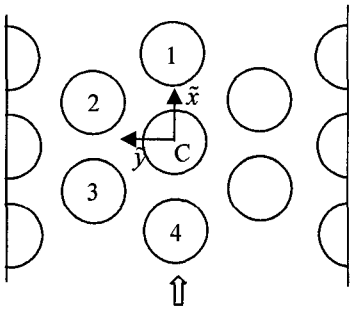

Figure 4.1 Numbering system used in experimental data presentation

Although one can find single-phase quasi-static force variations in the open literature, some tests are conducted in single-phase water flow. These data are free from the uncertainties arising from two-phase flow. Experiments in water flow, permit exploring the effect of Reynolds number without being worried about the changes in two-phase flow parameters. Besides, it will be possible to compare the quasi-static fluid force variations of single and two-phase flows.F

Figure 4.2 shows the measured lift and drag coefficients for cylinder 'C'. The lift coefficient remains essentially zero as the cylinder is displaced in the drag direction (Figure 4.2(a)). This makes sense from symmetry considerations. The drag coefficient increases as the cylinder is displaced in the downstream direction (Figure 4.2(c)). The slight increase may be associated with increased blockage of the flow channels, downstream of the cylinder.

The lift coefficient strongly depends on the transverse displacement ($\tilde{y}$). As seen in Figure 4.2(b), the lift force is always directed away from the cylinder equilibrium (zero) position. The negative value of $C_{LC,\tilde{y}C}$ the derivative can be

directly responsible for instability in the quasi-steady model. For cylinder 'C', C_{DC} varies only slightly with transverse displacement (Figure 4.2(d)). In particular, the $C_{DC,\tilde{y}}$ is zero, as would be expected from symmetry considerations.

The displacement of cylinder 'C' has the strongest effect on tube 'C' itself, and Tube 4 immediately upstream where C_L varies significantly only with transverse displacement for both of the tubes. As seen in Figures 4.4(b) and 4.5(b) the lift coefficients corresponding to Cylinders 2 and 3 in the neighboring column, show less sensitivity to tube 'C' displacements in the transverse direction. The Tube 2 and 3 drag coefficients are more sensitive to the displacement. The drag coefficient decreases for Cylinder 3 when Cylinder 'C' moves upstream (Figure 4.5 (c)) while the drag coefficient only slightly increases for Cylinder 2 (Figure 4.4(c)). Interestingly, when the central cylinder moves in the transverse direction, the drag coefficient of Cylinder 3 remains almost unchanged (Figure 4.5 (d)) while an increase in Cylinder 2 drag coefficient is observed (Figure 4.4 (d)).

The drag coefficients the of the central tube, Tube 1 as well as Tube 4 experience an extremum while the central cylinder moves in the cross-flow direction (Figures 4.2, 4.3 and 4.6 (d)). Furthermore, the slope of the lift coefficient curve for the same tubes is almost zero, when the central cylinder moves in the flow direction (Figures 4.2, 4.3 and 4.6 (a)). These results indicate that the symmetry of tube bundle is an acceptable assumption, which can be used throughout the present work.

4.2 Force coefficients in a typical two-phase flow

The primary set of results to be presented is for 80% homogeneous void fraction, the void fraction of interest within the U-bend region of nuclear steam generators. Figure 4.7 shows the measured lift and drag coefficients for Cylinder 'C'. As expected from symmetry, the lift coefficient remains essentially zero when the cylinder is displaced in the drag direction (Figure 4.7(a)).The central cylinder lift coefficient is strongly dependent on the transverse displacement. As Figure 4.7(b) shows, the lift force is always directed toward the cylinder equilibrium (zero) position. The negative value of the derivative $C_{LC,y}$ shows that instability in the quasi-steady model is governed by time delay rather than the variation of force coefficients.

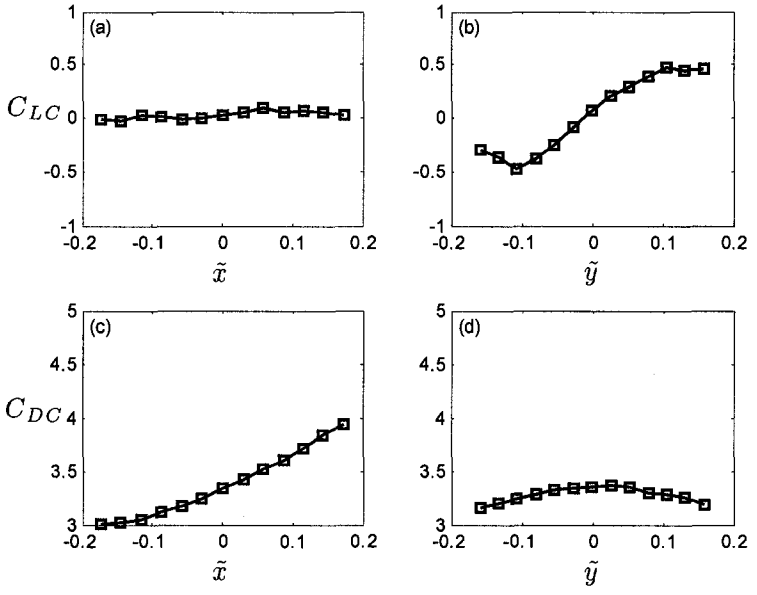

Figure 4.2 The effect of Tube 'C' displacement on the measured (a,b) lift and (c,d)drag force coefficients for Tube 'C' (water flow)

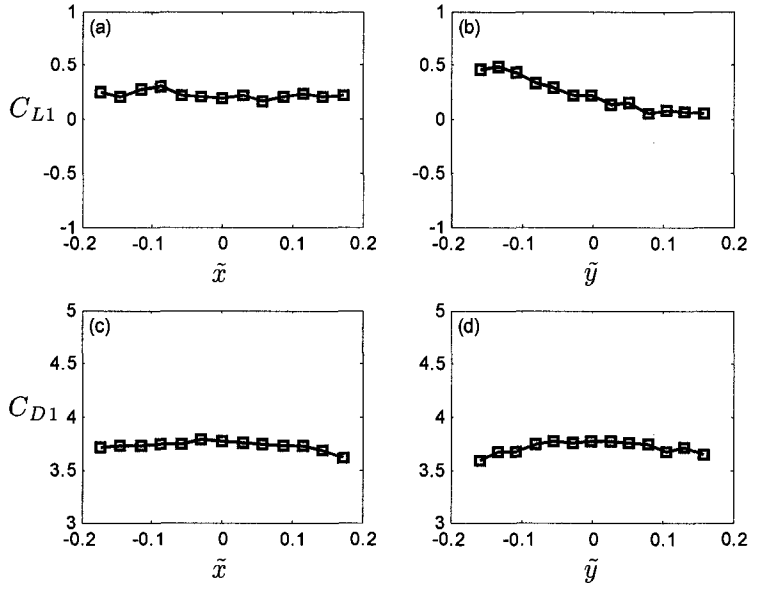

Figure 4.3 The effect of Tube 'C' displacement on the measured (a,b) lift and (c,d)drag force coefficients for Tube 1 (water flow)

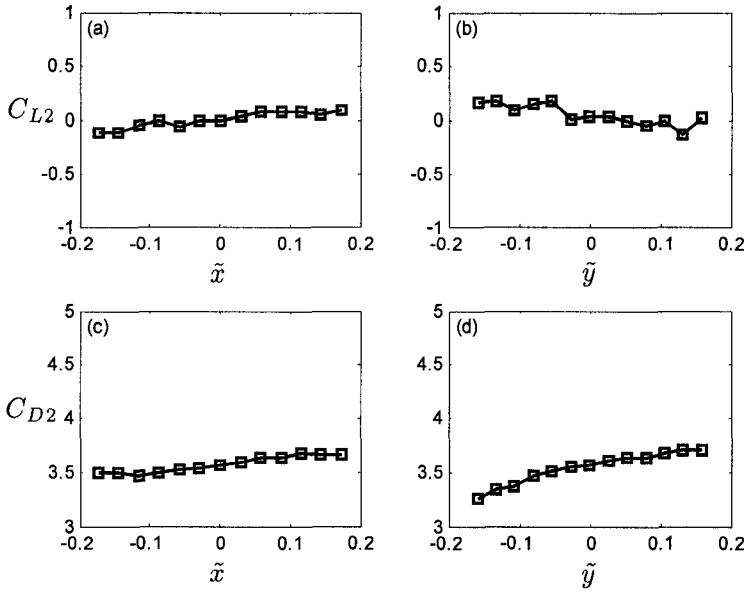

Figure 4.4 The effect of Tube 'C' displacement on the measured (a,b) lift and (c,d)drag force coefficients for Tube 2 (water flow)

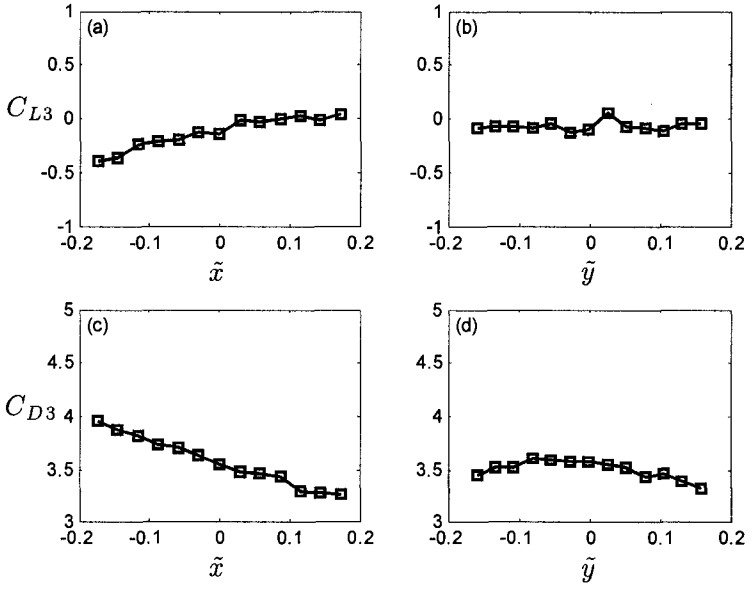

Figure 4.5 The effect of Tube 'C' displacement on the measured (a,b) lift and (c,d)drag force coefficients for Tube 3 (water flow)

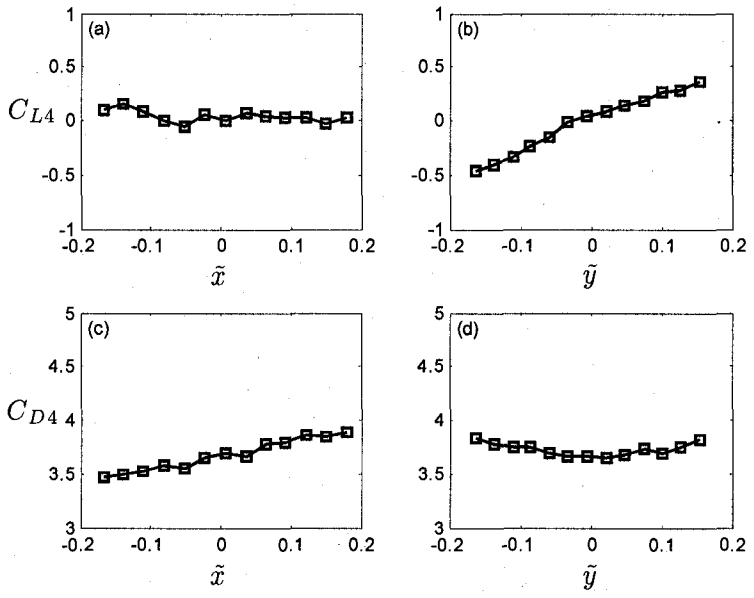

Figure 4.6 The effect of Tube 'C' displacement on the measured (a,b) lift and (c,d)drag force coefficients for Tube 4 (water flow)

The drag coefficient increases as the cylinder is displaced in the downstream direction (Figure 4.7 (c)). The slight increase may be due to increased blockage of the flow channels downstream of the cylinder. Once more dictated by symmetry condition, the variation of the drag coefficient in the cross-flow direction falls in an extremum at the zero position (Figure 4.7 (d)).

The effect of Tube 'C' displacements on Tube 1 lift and drag forces is shown in Figure 4.8. Once more because of symmetry, the lift coefficient of Tube 1 located directly downstream of central tube, remains constant as the central tube moves from upstream to downstream (Figure 4.8 (a)). Figure 4.8 (b) shows that the cross-flow displacement of the central cylinder has the strongest effect on the Tube 1 lift coefficient. This effect is the opposite of what observed for the central cylinder itself. In line displacement of Tube 'C' decreases the drag coefficient of Tube 1 as the Cylinder falls in the wake of cylinder 'C' (Figure 4.8 (c)). Figure 4.8 (d), as expected from symmetry, shows that the slope of drag coefficient at the equilibrium position is zero.

The displacement of Cylinder 'C' has the strongest effect on Tube 'C' itself, and Tube 1 immediately downstream while $C_{L1,\tilde{y}}$ varies significantly for both tubes. As seen

in Figure 4.9 and Figure 4.10, Cylinders 2 and 3 in the neighboring column show less sensitivity to Tube 'C' displacements. The lift coefficients of Cylinders 2 and 3 essentially remain unchanged in Figures 4.9(a) and 4.10(a) respectively for the displacement of Tube 'C' in the x-direction. The Tube 2 and 3 drag coefficients show an increasing trend with $\tilde{x}$ for both cylinders. Interestingly, C_{D2} increases as Cylinder 'C' approaches Cylinder 2 in the transverse direction, while C_{D3} is insensitive to transverse displacements.

Figure 4.11 shows the results for Tube 4, located directly upstream of Tube 'C'. The displacements of Tube 'C' only has a measurable effect on the drag coefficient C_{D4} as Cylinder 'C' is displaced parallel to the flow direction (Figure 4.11 (c)).

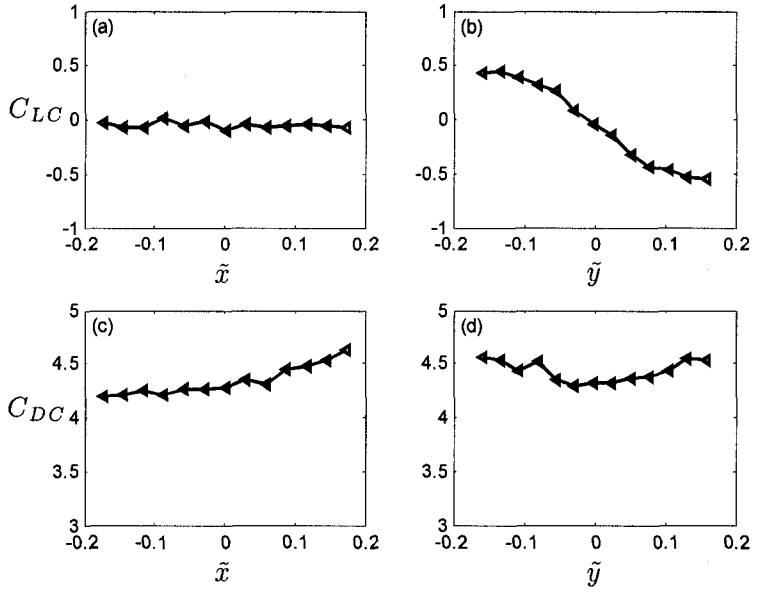

Figure 4.7 The effect of Tube 'C' displacement on the measured (a,b) lift and (c,d)drag force coefficients for Tube 'C' ($U_\infty = 1.32 m/s$, $\beta = 80\%$)

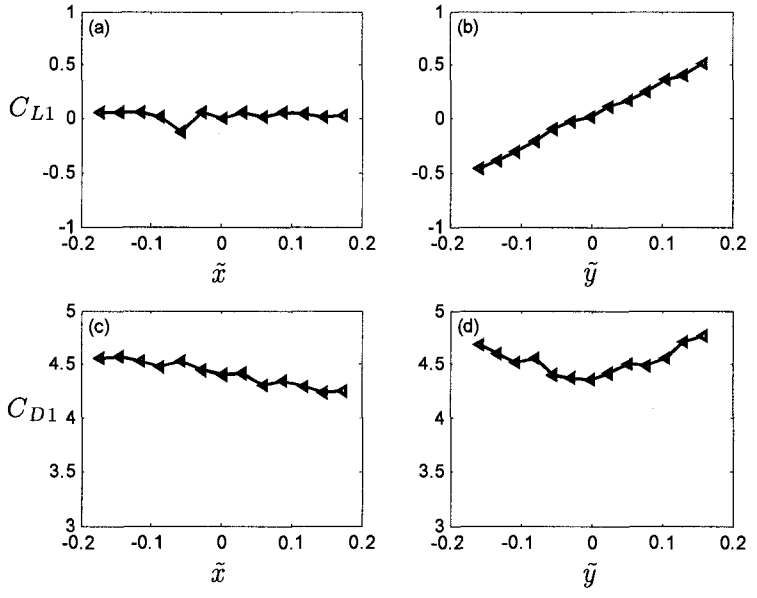

Figure 4.9 The effect of Tube 'C' displacement on the measured (a,b) lift and (c,d)drag force coefficients for Tube 2 ($U_\infty = 1.32m/s$, $\beta = 80\%$)

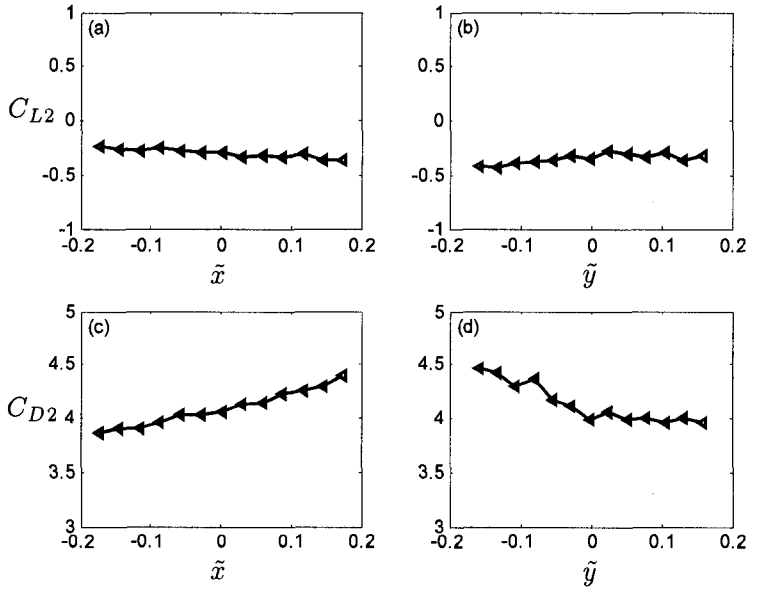

Figure 4.8 The effect of Tube 'C' displacement on the measured (a,b) lift and (c,d)drag force coefficients for Tube 1 ($U_\infty = 1.32m/s$, $\beta = 80\%$)

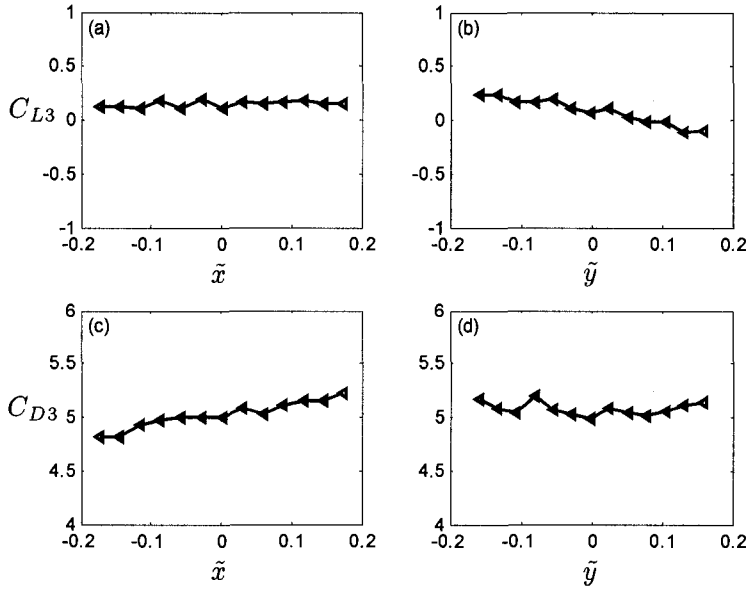

Figure 4.10 The effect of Tube 'C' displacement on the measured (a,b) lift and (c,d)drag force coefficients for Tube 3 ($U_\infty = 1.32m/s$, $\beta = 80\%$)

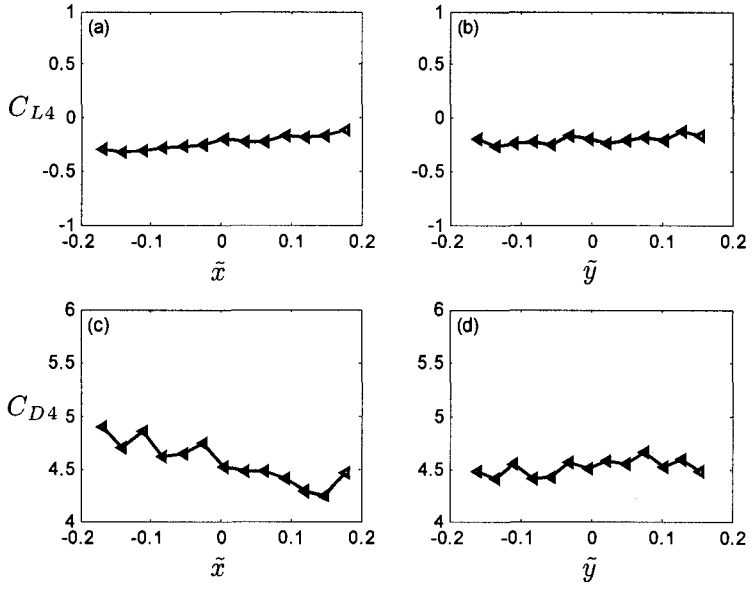

Figure 4.11 The effect of Tube 'C' displacement on the measured (a,b) lift and (c,d)drag force coefficients for Tube 4 ($U_\infty = 1.32m/s$, $\beta = 80\%$)

4.3 Variation of force coefficients with superficial void fraction

The fluid force coefficients have also been measured in various superficial void fractions. The variation of the superficial void fraction has a significant effect on the fluid force coefficients. The results for the primary Cylinder 'C' are presented in Figure 4.12.

The most distinct difference is in the variation of C_{LC} with the traverse displacement $\tilde{y}$. While the steady lift force is directed towards the cylinder equilibrium position for the high void fraction two-phase flow case (higher than 40% superficial void fraction), it is directed in the opposite direction comparing to water flow, Figure 4.12(b). The derivative $C_{LC,\tilde{y}c}$ varies continuously from a positive value at 0% void fraction to a large negative value at 100% void fraction.

For the drag coefficient variation in Figure 14.12(d), the curvature of the drag coefficient changes gradually from negative in water flow to positive in air-water flow. The change of curvature occurs at superficial void fraction of approximately 20%. The difference between the void fraction at which the curvature of lift and drag coefficient changes may be attributed to the errors originating from calculation of void fraction, measurement of fluid force coefficients and measurement of fluid flow rates.

The results obtained at very high superficial void fractions (above 80%) do not follow the same trend as that observed at low superficial void fractions (80% and bellow). This effect might be due to a change of flow regime in this area. Furthermore, the drag coefficient at 95% superficial void fraction is very different from other measured void fractions, which can be because of assumption of homogeneous model (the slip ratio increases at higher superficial void fractions).

The variation of lift coefficient in the cross-flow direction at 21% and 31% void fractions is not zero therefore the measured fluid forces in this cases is not as accurate as for void fractions above 31% .

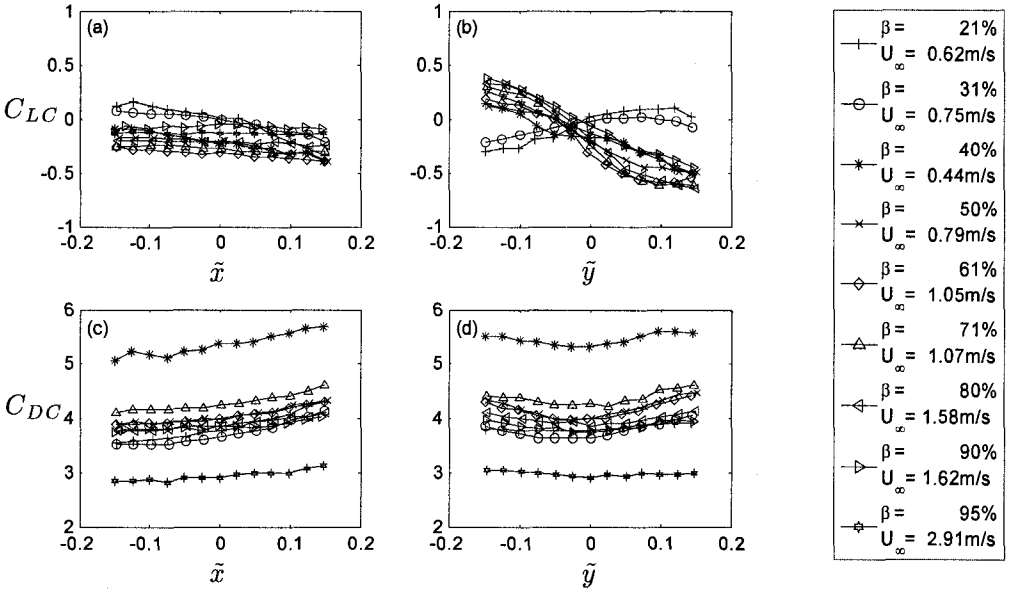

Figure 4.12 The effect of Tube 'C' displacement on the measured (a,b) lift and (c,d)drag force coefficients for Tube 'C' (various void fractions)

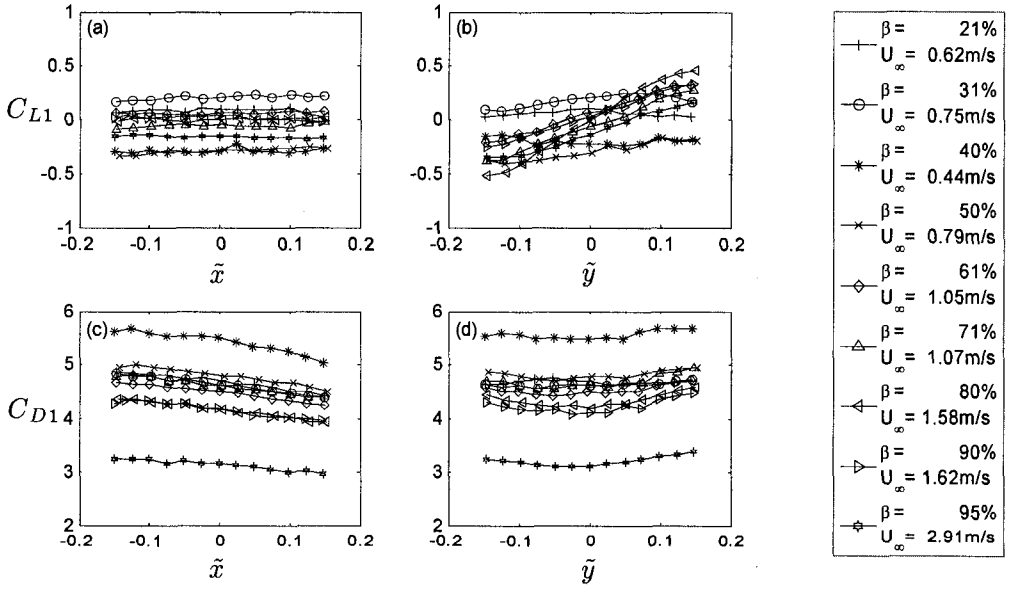

Figure 4.13 The effect of Tube 'C' displacement on the measured (a,b) lift and (c,d)drag force coefficients for Tube 1 (various void fractions)

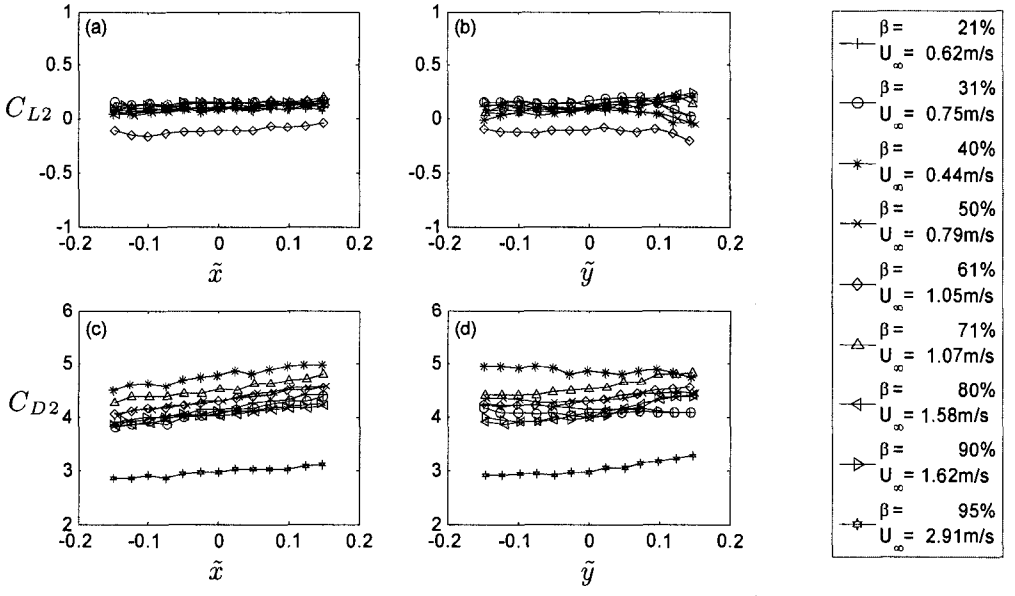

Figure 4.14 The effect of Tube 'C' displacement on the measured (a,b) lift and (c,d)drag force coefficients for Tube 2 (various void fractions)

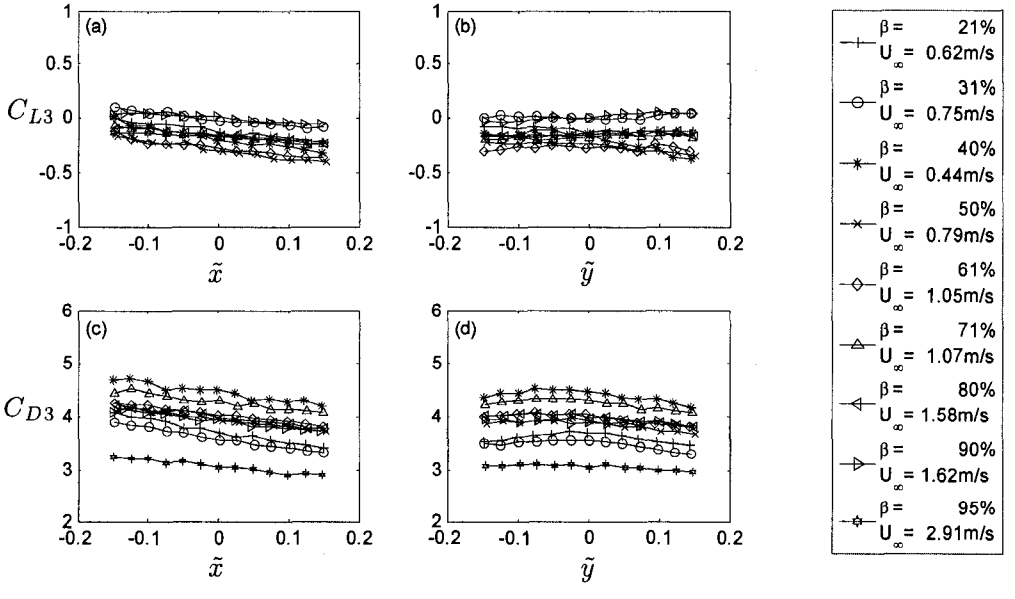

Figure 4.15 The effect of Tube 'C' displacement on the measured (a,b) lift and (c,d)drag force coefficients for Tube 3 (various void fractions)

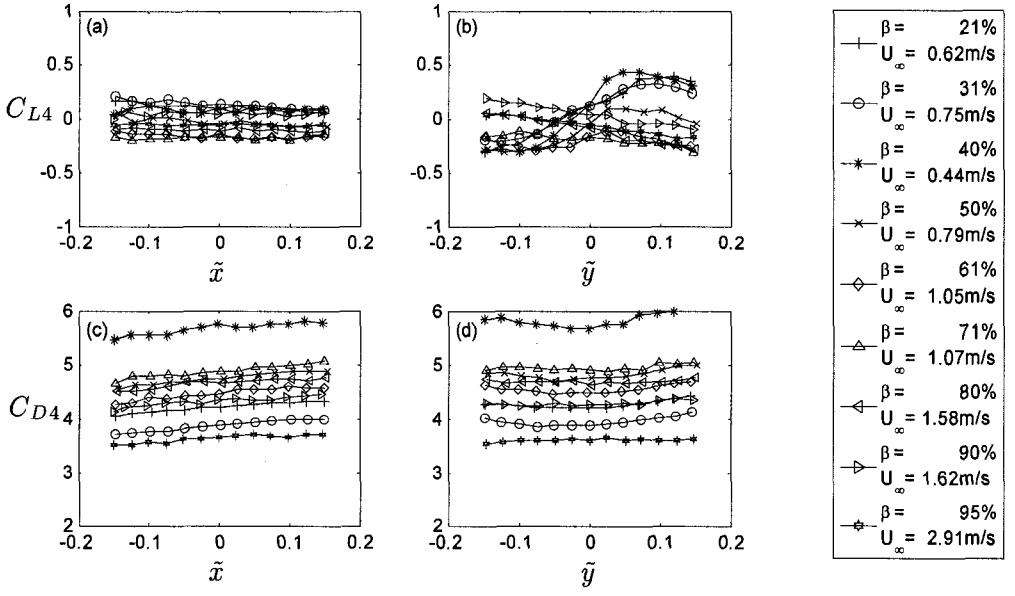

Figure 4.16 The effect of Tube 'C' displacement on the measured (a,b) lift and (c,d)drag force coefficients for Tube 4 ($U_\infty = 1.32m/s$, $\beta = 80\%$)

The drag force for 40% superficial void fraction is higher than for all other cases. As it will be shown in Section 4.4, the Reynolds number at which the test is conducted has a great influence on the results. Taking into account the low Reynolds number at which the 40% void fraction test was conducted, it is not surprising that a drag coefficient greater than all the cases is obtained.

4.4 Variation of force coefficients with Re number

The effect of variation of flow velocity for the central cylinder (in water flow) is demonstrated in Fig.4.17. It is interesting to note that at lower velocities the drag force in the equilibrium position increases (fluid damping) while at the same time the most important destabilizing component, the derivative of the lift force in the cross-flow direction, decreases dramatically. These values tend to approach a constant value at higher velocities. These results may explain why very low instability velocities were obtained using constant flow coefficients[6]. In the present work, when calculations lead

to a low instability velocity, the effect of variable force coefficients (i.e. Reynolds number effect) is used to modify the prediction. For higher velocities, it is not the case because the force coefficients are almost unchanged at sufficiently high Re numbers.

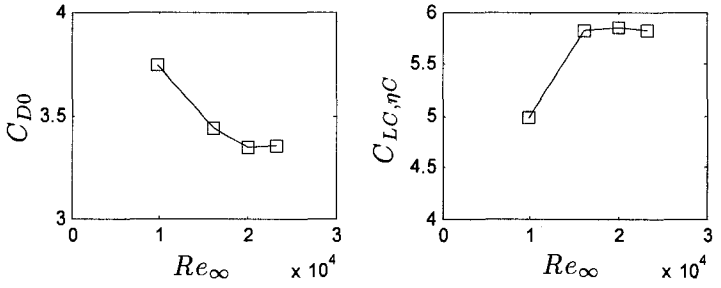

Figure 4.17 Variation of most important fluid force coefficients $C_{D0}, C_{LC,\eta C}$ with Reynolds number in water flow

4.5 Force coefficient derivatives

The fluid forces depend on the drag coefficient (fluid damping) as well as the derivatives of lift and drag coefficients (fluid stiffness) at equilibrium position in quasi-steady formulation (Equation 2.38). The proper values of these variables can be found by means of an appropriate curve fitting method. Afterwards, the fluid force derivatives with respect to central cylinder movement should be translated into the variation of the central cylinder fluid forces with respect to the displacement of surrounding cylinders.

4.5.1 Curve fitting

Measurement of fluid force coefficients, positions and two-phase flow variables inevitably contains some inherent errors. These errors result from the sources of noise and uncertainties during measurements. The derivative of fluid forces is even more sensitive to the superfluous detail related to second-level effects. Approximating the force coefficients with suitable functions only holds the most important information and deliberately strips off the unwanted second-level details.

Since the accuracy of individual measured force coefficients are subject to experimental uncertainty, it is unreasonable that the approximated function pass through

all the measured points. The least-square polynomials instead of requiring that the approximating polynomial pass through all data points help to average out the inherent individual data point errors.

Carefully selected polynomials should be chosen so that they represent the behavior of the experimental data points. In the present work, the highest degree of chosen polynomials does not exceed three. Using higher order polynomials leads to unreasonable variations rather than improving the approximation.

Once a proper polynomial is chosen for the variation of each force coefficient, finding the derivatives is an easy task. It is enough to take the zero order term as the fluid force coefficient while the derivative corresponds to the coefficient of the linear term.

The corrected fluid forces (after eliminating the cross-coupling effects and buoyancy) were read in *Matlab*. The input of the *polyfit* function was the data points used for interpolation and the order of the chosen polynomial. The coefficients of the zero and first order terms were stored respectively as the force coefficient itself and its first derivative. The average of the force coefficient found in two directions $(\tilde{x}, \tilde{y})$ is used as a better approximation of force coefficients at the equilibrium position.

4.5.2 Interpretation of the derivatives

As mentioned earlier, the quasi-steady formulation depends on the variation of the central cylinder force coefficients with respect to the displacement of the neighboring cylinders. Since designing a mechanism to displace surrounding cylinders and to measure the forces on the central cylinder is far more expensive than measuring the forces on fixed neighboring tubes, the central cylinder is displaced and the forces are measured on the surrounding cylinders.

The assumption of an infinite tube bundle enables one to deduce the required data from the measured force coefficients. The numbering system of Figure 4.1 can ease the task. For example, for an infinite tube bundle, measuring the forces on Tube 3 when it moves toward Tube 'C' shall have the same effect as measuring the forces on Tube 'C' while it approaches Tube 3 in the numbering introduced in Figure 2.3. Therefore considering the numbering introduced in Figure 4.1 directly leads to the needed fluid force variations. This conversion can conveniently be summarized as follows:

$$
\begin{aligned}
\left(C_{DC,\chi_1}\right)_{\text{old}} &= \left(C_{D1,\chi_C}\right)_{\text{new}} \qquad \left(C_{LC,\eta_1}\right)_{\text{Price}} = \left(C_{L1,\eta_C}\right)_{\text{new}} \\
\left(C_{DC,\chi_2}\right)_{\text{old}} &= \left(C_{D2,\chi_C}\right)_{\text{new}} \qquad \left(C_{LC,\chi_2}\right)_{\text{Price}} = \left(C_{L2,\chi_C}\right)_{\text{new}} \\
\left(C_{DC,\eta_2}\right)_{\text{old}} &= \left(C_{D2,\eta_C}\right)_{\text{new}} \qquad \left(C_{LC,\eta_2}\right)_{\text{Price}} = \left(C_{L2,\eta_C}\right)_{\text{new}} \\
\left(C_{DC,\chi_6}\right)_{\text{old}} &= \left(C_{D3,\chi_C}\right)_{\text{new}} \qquad \left(C_{LC,\chi_6}\right)_{\text{Price}} = \left(C_{L3,\chi_C}\right)_{\text{new}} \\
\left(C_{DC,\eta_6}\right)_{\text{old}} &= \left(C_{D3,\eta_C}\right)_{\text{new}} \qquad \left(C_{LC,\eta_6}\right)_{\text{Price}} = \left(C_{L3,\eta_C}\right)_{\text{new}} \\
\left(C_{DC,\chi_8}\right)_{\text{old}} &= \left(C_{D4,\chi_C}\right)_{\text{new}} \qquad \left(C_{LC,\eta_8}\right)_{\text{Price}} = \left(C_{L4,\eta_C}\right)_{\text{new}}
\end{aligned}
\tag{4.1}
$$

The subscripts (old and new) respectively indicate the coordinate system originally used by Price (Figure 2.3) and the new coordinate system (Figure 4.1) chosen to ease the transformation.

4.5.3 Fluid force derivatives

In the stability analysis outlined in Chapter 2, it was demonstrated that in the quasi-steady theory, the fluid forces and their derivatives are the necessary inputs to these models. These derivatives, at the equilibrium position ($\tilde{x} = 0, \tilde{y} = 0$) are estimated from curve fitting to the data presented in Figures 4.2 through 4.16. Table 1 shows the force coefficients C_D, C_L as well as the derivatives with respect to Tube 'C' displacements.

The results for superficial void fractions between 50% and 80% are closely similar. Besides the effect of the force field on the tube itself, Tube 'C's influence is felt by the tubes downstream. Tubes in the same column are also significantly affected even when located upstream of the moving tube. However, it should be noted that the upstream Tube 4 is affected in the drag direction, while the downstream Tube 1 is influenced in lift direction. Figure 4.17 and Table 4.1 give useful insight into the stability behavior of the tube bundle.

For superficial void fractions between 50% and 80%, the derivative $C_{L,\eta C}$ is the most important; indicating that Tube 'C' transverse displacement has the most influence on the Tube 'C' fluid forces. The next largest influence is that on Tube 1 immediately downstream again in the lift direction. This is followed by Tube 2 affected in the drag direction. Figure 4.18 shows a visual representation of the influence of Tube 'C' on its

neighbors for lift or drag direction displacements. The length and thickness of the arrows reflect the level of influence. Only the most significant effects are shown.

The results obtained at superficial void fractions below 31% suffer from inaccuracy due to using the orifice plates to measure the air flow at their lower limits. Since the velocity at 40%, the superficial void fraction is not high enough the fluid forces have not reached the constant value at this void fraction. Finally, the big change observed in the measured fluid forces at void fractions above 80% may be because of the flow regime changes. The homogeneous model may suffer from inaccuracy in this area.

The next logical step, which will be accomplished in Chapter 5, is a quantitative stability analysis of the tube bundle using the force derivatives of Table 4.1.

Table 4.1 Force coefficients and their derivatives

	i	$C_{D,\chi i}$	$C_{L,\chi i}$	$C_{D,\eta i}$	$C_{L,\eta i}$	Comments
$C_{D0} = 3.34$	C	3.06	0.25	0	5.85	The results have reached a constant value, symmetry is excellent, and the forces are large enough to lead to a reasonably good prediction.
$\beta = 0\%$	1	-0.49	-0.28	-0.5	-1.69	
$U_\infty = 0.53 m/s$	2	0.68	1.3	0.97	-1.06	
$\mathrm{Re}_\infty = 1.94\times10^4$	6	-2.03	1.25	-0.51	-0.12	
	8	1.06	0.2	0.21	2.89	
$C_{D0} = 3.78$	C	2.57	-1.38	0.61	2.81	The results have reached a constant value, symmetry is not good, the airflow rate is small and do not lead to a reasonably good prediction.
$\beta = 21\%$	1	-1.45	0.09	-0.65	-0.09	
$U_\infty = 0.62 m/s$	2	1.85	0.06	-0.47	0.63	
$\mathrm{Re}_\infty = 5.92\times10^3$	6	-2.28	-0.78	-0.42	-0.11	
	8	0.95	-0.24	0.39	2.33	
$C_{D0} = 3.66$	C	2.14	-0.97	1.31	0.84	The results have reached a constant value, symmetry is not good, the airflow rate is small and do not lead to a reasonably good prediction.
$\beta = 31\%$	1	-1.34	0.09	0.38	0.76	
$U_\infty = 0.77 m/s$	2	2.28	0.17	0.45	0.76	
$\mathrm{Re}_\infty = 5.43\times10^3$	6	-1.87	-0.66	-0.56	-0.05	
	8	1.13	-0.38	0.7	2.59	
$C_{D0} = 5.32$	C	2.26	-0.86	0.9	-0.15	The results have not reached a constant value so it is not possible to use them for prediction of instability in higher velocities.
$\beta = 40\%$	1	-1.68	0.18	0.73	-0.65	
$U_\infty = 0.44 m/s$	2	1.79	0.2	-0.63	0.93	
$\mathrm{Re}_\infty = 2.52\times10^3$	6	-1.52	-0.88	-1.39	-1.15	
	8	1.07	0.11	0.91	7.26	
$C_{D0} = 3.99$	C	1.27	-0.66	0.97	-3.83	The results have reached a constant value, symmetry is good, and the forces are large enough to lead to a reasonably good prediction.
$\beta = 50\%$	1	-1.59	0.17	0.71	1.26	
$U_\infty = 0.79 m/s$	2	1.79	0.38	1.02	0.38	
$\mathrm{Re}_\infty = 3.73\times10^3$	6	-1.69	-0.92	-0.89	-0.32	
	8	1.09	-0.38	0.59	4.63	

Table 4.1 Force coefficients and their derivatives (continued)

	i	$C_{D,\chi i}$	$C_{L,\chi i}$	$C_{D,\eta i}$	$C_{L,\eta i}$	Comments
$C_{D0} = 3.93$	C	1.00	0.08	0.21	-5.41	The results have reached a constant value, symmetry is excellent, and the forces are large enough to lead to a reasonably good prediction.
$\beta = 60\%$	1	-0.89	-0.03	-0.05	3.26	
$U_\infty = 1.31 m/s$	2	1.57	-0.42	-1.71	0.32	
$\mathrm{Re}_\infty = 5.27\times10^3$	6	0.83	0.03	0.35	0.56	
	8	-0.66	0.95	1.38	0.21	
$C_{D0} = 4.24$	C	1.51	-0.46	0.34	-5.97	The results have reached a constant value, symmetry is good and the forces are large enough to lead to a reasonably good prediction.
$\beta = 71\%$	1	-1.38	-0.1	0.69	1.83	
$U_\infty = 1.07 m/s$	2	1.71	0.31	1.82	0.7	
$\mathrm{Re}_\infty = 3.70\times10^3$	6	-1.32	-0.54	-1.15	0.44	
	8	1.17	-0.01	-0.1	-0.01	
$C_{D0} = 4.31$	C	0.89	-0.11	-0.24	-5.21	The results have reached a constant value, symmetry is excellent and the forces are large enough to lead to a reasonably good prediction.
$\beta = 80\%$	1	-1.16	0.39	0.15	2.87	
$U_\infty = 1.33 m/s$	2	1.34	-0.33	-1.90	0.44	
$\mathrm{Re}_\infty = 4.12\times10^3$	6	0.69	0.18	-0.38	-1.10	
	8	-2.23	0.51	1.16	0.34	
$C_{D0} = 3.79$	C	0.34	-0.07	0.14	-3.5	The results have reached a constant value, symmetry is good, but the trend changes may indicate a change in flow pattern. The homogeneous model may have problems in this flow regime.
$\beta = 90\%$	1	-1.78	-0.17	0.57	2.05	
$U_\infty = 1.62 m/s$	2	0.89	0	1.52	0.22	
$\mathrm{Re}_\infty = 4.51\times10^3$	6	-1.7	-0.45	-0.54	0.36	
	8	0.53	-0.06	0.13	-1.09	
$C_{D0} = 2.93$	C	0.98	0.03	-0.04	-2.59	The results have reached a constant value, symmetry is good, but the trend changes may indicate a change in flow pattern. The homogeneous model may have problems in this flow regime.
$\beta = 95\%$	1	-0.81	-0.04	0.82	2.35	
$U_\infty = 2.91 m/s$	2	1.04	0.09	1.43	0.35	
$\mathrm{Re}_\infty = 7.70\times10^3$	6	-1.14	-0.26	-0.37	0.32	
	8	0.85	0.07	0.19	-0.97	
Data extracted from Price et al. (1988)						
$C_{D0} = 6.8$	C	-5.2	-	-	-243	-
$\beta = 100\%$	1	-3.8	-	-	72	
$\mathrm{Re}_\infty = 1.85\times10^4$	2	0	35.4	1.6	-16.7	
$P/D = 1.375$	6	-5.1	-25.2	3.4	26.6	
	8	3.6	-	-	13.2	

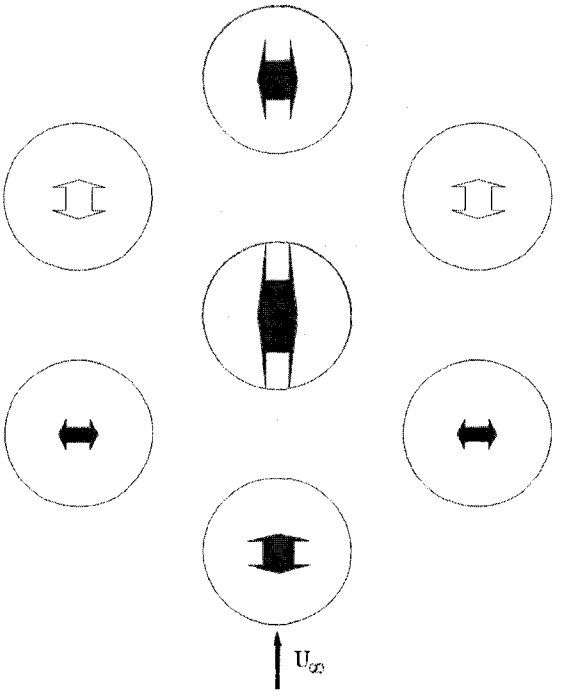

Figure 4.18 Influence of Tube 'C' on its neighbors for $\beta = 80\%$ each arrow indicates the magnitude and direction of the most important force derivative. Open arrows indicate that the Cylinder 'C' direction of motion is normal to the cylinder force direction.

CHAPTER 5

STABILITY ANALYSIS

Having found the fluid forces and their derivatives makes it possible to use the quasi-steady model to predict fluidelastic instability. The fluid forces together with their variations versus local coordinates obtained in Chapter 4 are used with the quasi-steady models, originally developed for single-phase flows, to model the two-phase flow problem.

Stability analyses are performed using the single flexible tube model [6] as well as constrained mode analysis [15]. Similarly to previous work [6], the effect of variation of the flow retardation parameter is examined for the single flexible tube model at various void fractions.

Moreover, variation of the most important fluid force coefficients with the Re number emphasized in Chapter 4 is taken into consideration when evaluating stability at very low velocity (or Reynolds numbers). The comprehensive measurements of all fluid force coefficients and their derivatives make it possible to improve fluidelastic instability prediction at low mass damping parameters. The application of this concept to two-phase flow requires improved two-phase flow models to examine fluid force coefficients at different flow velocities without being concerned about the changes in the real void fraction.

5.1 Solution of the equations

A FORTRAN program was developed to solve the equation of motion obtained using either of the quasi-steady approaches introduced in Chapter 2. The force coefficients presented in Table 4.1 provide the necessary information for forming fluid stiffness and damping matrices. The program determines the eigenvalues of the state-

space equations of motion by varying the free stream velocity. The real parts of all eigenvalues are examined to find the first eigenvalue with a zero real parts that indicates the onset of instability. Choosing the order of equations simultaneously while introducing the correct stiffness and damping matrices allows the program to solve the problem for a single flexible tube or an infinite flexible array model.

5.2 Single flexible tube analysis results

The onset of instability of a single flexible tube is sought for various flow retardation parameters. In addition to the original work, since the present work is in two-phase media, the void fraction is also changed to investigate the flow retardation parameter effect in two-phase flow.

5.2.1 Flow retardation parameter effect

The instability results presented in Figures 5.1 and 5.2 are based on mass damping parameters (based on structural mass and structural damping) originally used by Price and Païdoussis [6]. Presenting the results in terms of the structural mass damping enables us to compare the results with those obtained in earlier work.

Varying the flow retardation parameter μ has the same effect as that mentioned by Price in his comprehensive review [3]. As can be seen, in both water flow and later for a typical two-phase flow ($\beta = 80\%$) (in Figure 5.2) the prediction remains almost unchanged by varying flow retardation for lower structural mass damping parameters. By increasing structural mass damping, in both cases, the decrease in flow retardation results in higher predicted critical velocities.

As mentioned in Chapter 2, the flow the order of magnitude of the retardation parameter is one. Trying different values of μ shows that the minimum value of μ that leads to an infinite critical velocity in water flow is 1. Figure 5.1 shows the prediction for $\mu = 1, 3$ and 5.

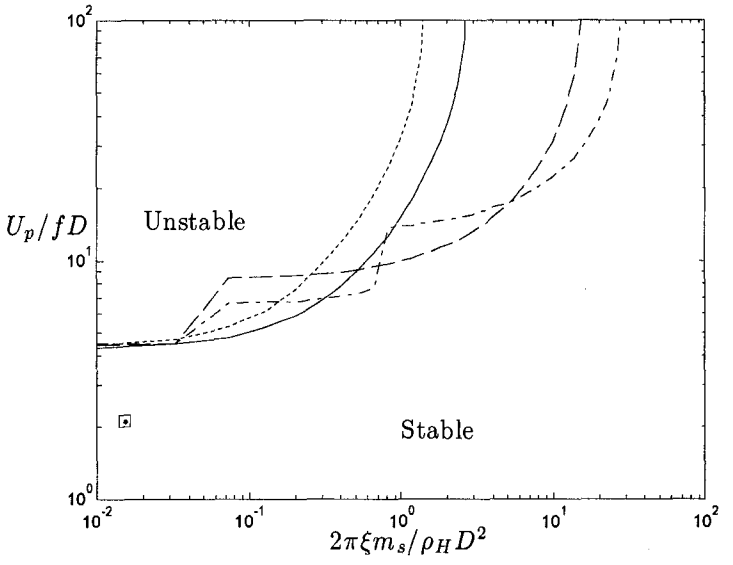

Figure 5.1 Stability boundary for a single-flexible tube model in water flow with $\mu = 0.8$ (.....), $\mu = 1$ (—), $\mu = 3$ (- - -) and $\mu = 5$ (— - —). The abscissa is calculated using structural mass and damping; (□ dynamic tests).

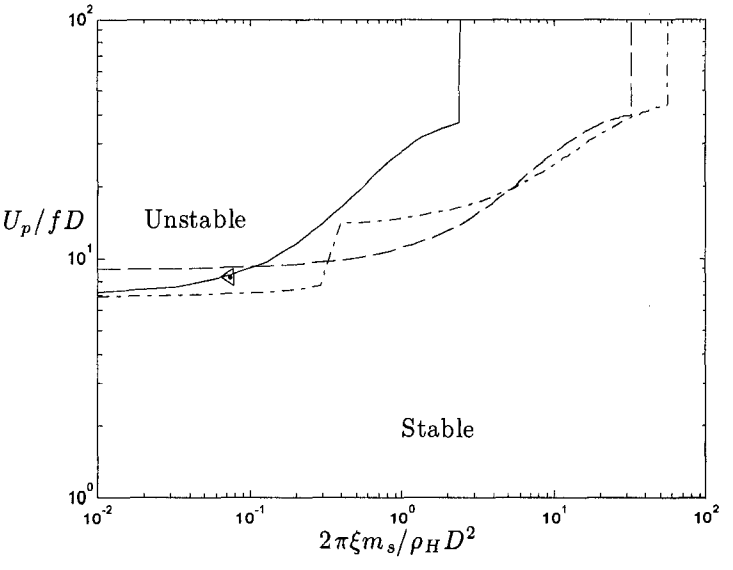

Figure 5.2 Stability boundary for a single-flexible tube model in air-water flow $\beta = 80\%$ with $\mu = 1$ (—), $\mu = 3$ (- - -) and $\mu = 5$ (— - —). The abscissa is calculated using structural mass and damping; (◁ dynamic tests).

Figure 5.2 shows the variation of the fluidelastic instability boundary by different retardation parameters. The value of $\mu = 0.8$ lead to an infinite critical velocity at $\beta = 80\%$. This may indicate an increment of the actual time delay due to increasing void fraction. Although the damping ratio is constant for all the tests ($\xi = 0.0011$) the changes in density have caused a considerable shift in the position of the dynamic tests along the x-axis.

Since the predicted critical velocities for all cases is close to the region in which fluid force coefficients and their variations become constant, it is not necessary to apply the variation of coefficients with Re number discussed in Chapter 4.

5.2.2 Onset of instability at various void fractions

Since the single flexible tube model only works well for low mass damping parameters (at higher mass damping parameters the instability is controlled by stiffness mechanism and normally needs more than one flexible tube), the instability boundaries are truncated at the higher superficial void fraction. Figures 5.3 and 5.4 respectively show the variation of predicted instability for superficial void fractions up to and above 60%. It should be noted that the abscissa is changed to the total mass damping parameter [37].

Since the slope of the lift coefficient changes continuously from positive to negative (from zero to fifty percent superficial void fraction) the force coefficient measurement errors become comparable with the measured values at low void fractions. Therefore, the prediction has only shown for the logical values of force coefficients (water flow and void fractions above 50%).

The analytical results tend to overestimate the reduced critical velocity and, as it can be seen in Figures 5.3 and 5.4, they tend to approach the dynamic test data at higher void fractions.

It should be noted that, although the density in the denominator reduces with increasing void fraction, the simultaneous decrease in the total damping makes the total mass damping parameter at 90% superficial void fraction less than at 80% air-water flow.

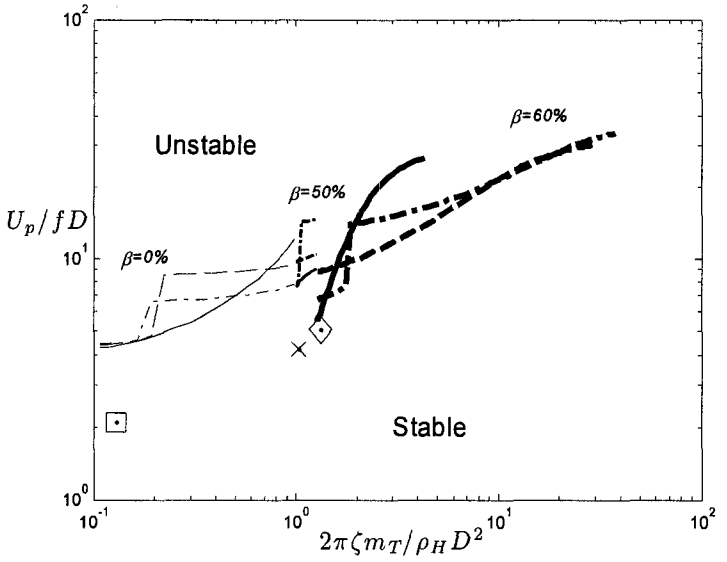

Figure 5.3 Onset of instability obtained using single-flexible tube model in air-water flow $\beta = 50\%$ and 60%. $\mu = 1$ (—), $\mu = 3$ (- - -) and $\mu = 5$ (— - —). The dynamic test data are respectively (□) $\beta = 0\%$, (x) $\beta = 50\%$ and (◇) $\beta = 60\%$.

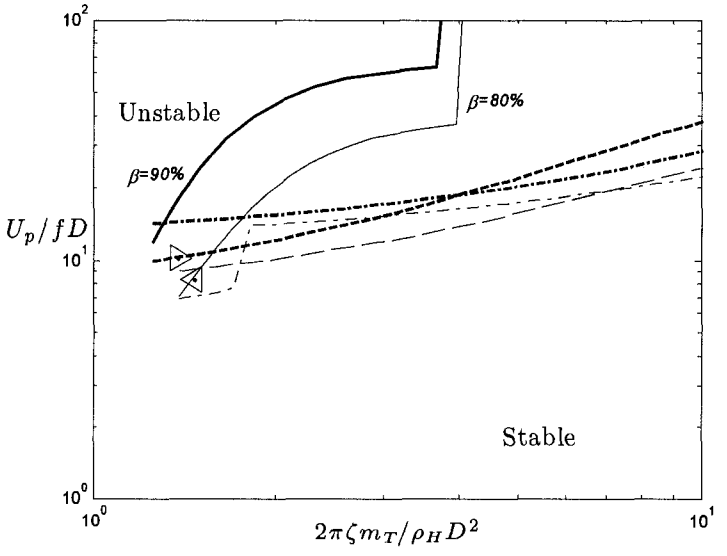

Figure 5.4 Onset of instability obtained using single-flexible tube model in air-water flow $\beta = 80$ and 90%. $\mu = 1$ (—), $\mu = 3$ (- - -) and $\mu = 5$ (- . -). The dynamic test data are respectively (◁) $\beta = 80\%$ and (▷) $\beta = 90\%$.

5.3 Constrained mode analysis results

Fixing the phase angles $\theta_x = \varphi_x = \phi_y = 0$ and $\theta_y = \pi$ forces the tube to vibrate in the cross-flow direction. The fluidelastic instability boundary is obtained assuming $\mu = 1$ for different void fractions (once again, the results are only presented in the region in which the lift coefficients are much greater than the expected experimental errors).

The low values of predicted instability velocity for low values of mass damping parameters ($2\pi\xi m_s/\rho_H D \ll 1$) are not acceptable since it was shown that at lower velocities, the force coefficients changes dramatically. The effect of fluid force changes will be discussed in the next section.

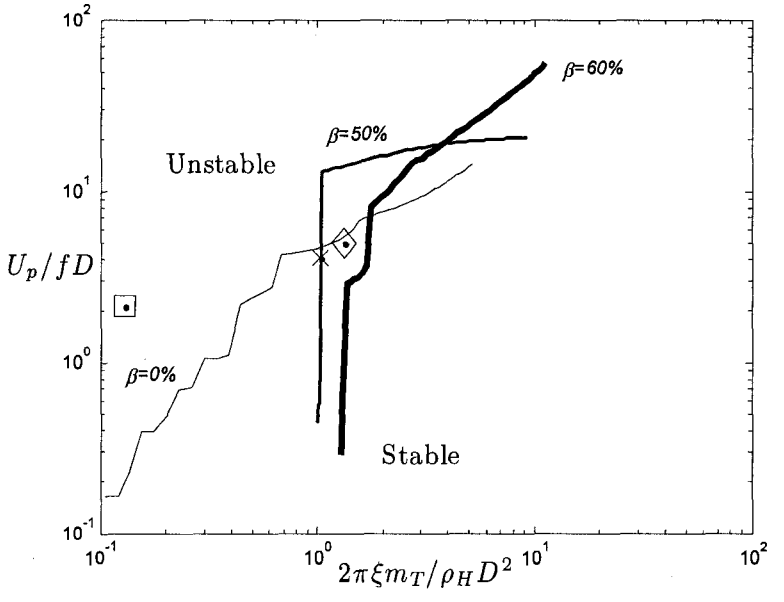

Figure 5.5 Onset of instability obtained using flexible array model in air-water flow. $\beta = 0\%$ (—), $\beta = 50\%$ (—) and $\beta = 60\%$ (—).The dynamic test data are respectively (□) $\beta = 0\%$, (x) $\beta = 50\%$ and (◇) $\beta = 60\%$.

The results obtained using the constrained mode analyses tend to underestimate the critical reduced flow velocity. Once more, with increasing void fraction, the

fluidelastic instability prediction approaches the dynamic test data points (all the dynamic test data are obtained with a low structural damping $\xi = 0.0011$).

Since the stiffness-controlled instability occurs at high mass damping parameters, the model should also be validated with dynamic test data obtained for higher values of this parameter.

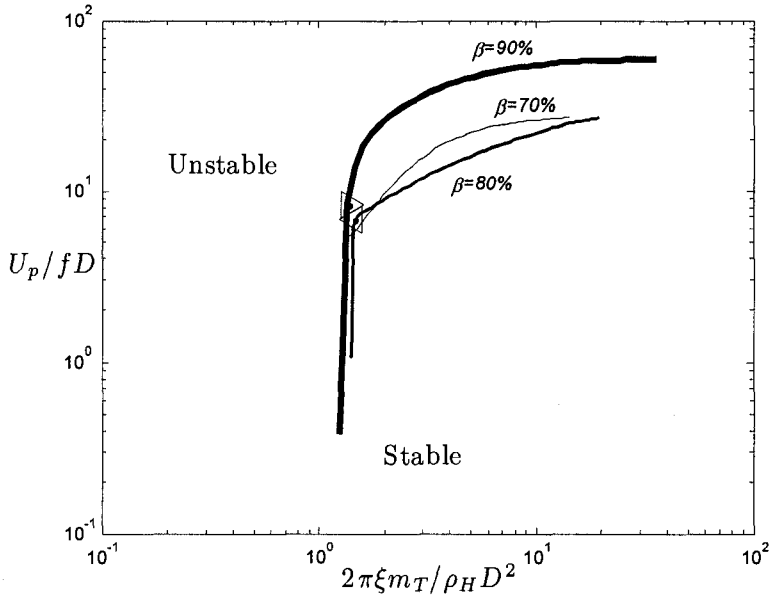

Figure 5.6 Onset of instability obtained using flexible array model in air-water flow. $\beta = 70\%$ (—), $\beta = 80\%$ (—) and $\beta = 90\%$ (—).The dynamic test data are respectively $\beta = 80\%$ ($\triangleleft$) and $\beta = 90\%$ ($\triangleright$).

Comparing the dynamic test data with the single flexible tube model and constrained mode analysis results shows that the single flexible tube model overestimates the value of the reduced critical velocity while the constrained mode analysis underestimates this velocity. Both predictions lead to a better agreement at higher superficial void fractions.

5.3.1 Consideration of variable force coefficients

The multiple instability areas and predicted low instability velocities have always been an enigma. Price and Païdoussis [6] questioned the number of these instability regions that can practically exist. They reasoned that the other instability mechanisms would prevent the array from remaining unstable with the same gap velocity. They deduced that the narrow instability regions could not exist. Using this argument, they considered the regions with width below 10% of reduced velocity as impractical.

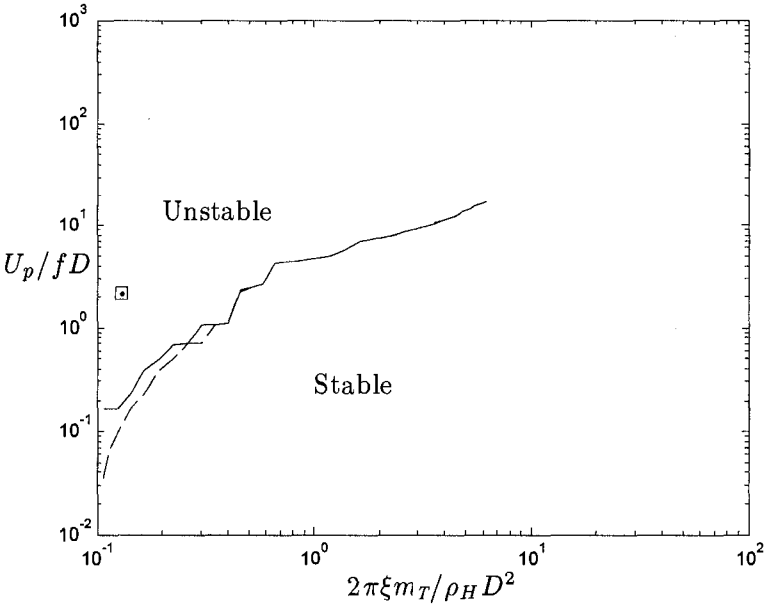

Figure 5.7 Onset of instability obtained using flexible array model in water flow using both variable and constant fluid forces. (--) analysis with constant drag force and (—) analysis with variable drag coefficient.

In the present work, for the first time to the author knowledge, variation of fluid forces is used to prevent premature prediction of instability in the quasi-static model. In Figure 5.7, the constrained mode analysis results considering the variation of the most

important fluid force coefficients is compared to those obtained with constant fluid forces (shown in Figure 4.17).

As mentioned, earlier the increase in the drag coefficient at lower velocities increases fluid damping and decreases the destabilizing forces thus prevents instability. The results presented in Figure 5.7 suggest that precise measurement of all fluid force derivatives at different free stream velocities leads to better predictions.

The measurement of fluid forces in two-phase flow at various free stream velocities necessitates enhanced two-phase models. The variation of flow conditions may also change the actual void fraction, which can lead to comparison of cases at not necessarily the same conditions. Furthermore, taking a look at the two-phase results (Figures 5.5 and 5.6) the predicted instability velocity in two-phase flow (for the same structural damping) leads to reduced velocities large enough to avoid the region of varying fluid forces.

5.4 Application of Granger's Model to approximate decay function

Having one dynamic test data it is possible to go beyond the quasi-steady model and to use the first order of the Granger's model [17], and parameter estimation techniques to approximate the decay function. Using the approximate formula introduced by Granger and applying the dynamic data points and fluid force coefficients obtained in Chapter 4, α_1 and β_1 (Equation 2.47) are calculated for different void fractions (Table 5.1).

It should be noted that with the data obtained using water flow Φ_{Ly} behaves as an unbounded function instead of the expected decay function. This may be due to the change of the slope of lift coefficient variations from negative (in two-phase flow) to positive (in water flow). Since the theory is based on the truncation of a series of decay functions, the unlimited first term shows that the first order approximation is not sufficient for water flow.

Table 5.1 Approximation of decay function

	β	C_D	$C_{LC,\eta C}$	U_{PC}	δ_1	α_1	Comments
$\Phi_{Ly} = \sum_{i=1}^{N} \alpha_i e^{-\delta_i \tau}$ $N = 1$	0	3.34	5.85	2.0	-5.57	4.61	*Not acceptable needs more terms*
	50	3.99	-3.83	4.5	2.26	3.51	
	60	3.93	-5.41	5.5	1.10	1.86	
	80	4.31	-5.21	9.5	0.46	1.41	
	90	3.79	-3.5	12.0	0.42	1.51	
	Data extracted from Granger, S., and Païdoussis, M.P. (1995)						
	100	3.8	-19.2	-	1.42	0.14	*Normal triangle, P/D=1.375*
	100	2.3	-73	-	1.10	0.04	*Square in line, P/D=1.5*

5.5 Recap of results of stability analysis

The stability analysis results are compared with dynamic stability tests [37] and show reasonable agreement. The results for single flexible tube analysis and multiple flexible tubes for high void fractions tend to coincide at low structural damping as expected. The key findings from the stability analysis are the following:

- The changes of the flow retardation parameter do not significantly affect the results at low mass damping parameters. At high mass damping parameters, a decrease of flow retardation tends to postpone the instability. The minimum flow retardation parameter at which an infinite solution obtains increases with increasing void fraction that may be an indication of increment of the flow retardation, by increasing void fraction.
- The variation of force coefficients may help to explain "premature" prediction of instability in the quasi-static model (unlike the changes in gap velocity originally used by price *et. al.* [6] to explain unreasonably narrow unstable regions).
- Normally the instability happens at higher velocities compared to those at which the measurement of forces takes place. Looking at the flow regime maps, increasing the velocity may change the flow regime at higher void fractions. Therefore, the measurements at lower void fractions may not necessarily show the precise force variations in the instability velocity.

CHAPTER 6

CONCLUSIONS AND RECOMMENDATIONS FOR FUTURE WORK

An experimental program to measure quasi-static force coefficients in single-phase (water) flow and two-phase (air-water) flow was completed in the present work. An existing dynamometer design was modified and forces were measured within a rotated triangular tube array on a kernel of seven instrumented tubes. The measured forces were used to predict fluidelastic instability with a single flexible tube as well as a fully flexible array model using a constrained mode hypothesis.

The main conclusions drawn from the current work are as follows:

- The variation of the coefficient C_{LC} with the transverse displacement, $\tilde{y}$, in single-phase (water flow) differs from two-phase (air-water flow). While the steady lift force is directed towards the cylinder equilibrium position in two-phase flow at higher void fractions (more than 40% superficial void fraction), it is directed in the opposite direction for water flow and lower void fractions.

- The curvature of C_{DC} with the transverse displacement, $\tilde{y}$, in single-phase (water flow) differs from two-phase (air-water flow). While the steady drag force curvature is positive in two-phase flow (minimum C_{DC} at equilibrium position) at the higher void fractions (more than 40% superficial void fraction), the curvature changes to negative for water flow and lower void fractions (hence maximum drag at equilibrium position) .

- Single-phase (water flow) force measurements showed the drag force (fluid damping) increases with decreasing Re number, which indicates increased stability at lower reduced velocities.

- Single-phase (water flow) force measurements also showed that the lift coefficient derivative (which is destabilizing) decreases with Re number, which again indicates increased stability at lower reduced velocities.
- The point at which the trend of fluid force variations changes in the tube bundle was established experimentally (about a superficial void fraction of about 40%)

- It has been demonstrated that the single flexible tube model can successfully be adapted for modeling fluidelastic instability in two-phase cross-flow to predict the upper bound for the threshold of instability.

- It has also been demonstrated that the constrained mode analysis adapted for modeling fluidelastic instability in two-phase flows leads to a lower bound for the threshold of instability.

- A comparison of the results with dynamic test data shows that, the predictions at higher void fractions are more reliable than that at lower void fractions.

- The variation of force coefficients were successfully used to improve the fluidelastic prediction in the constrained mode analysis and the modified damping function was obtained using the dynamic test data and the model introduced by Granger[17].

In order to complete the present work it is necessary to fulfill the tasks that are listed hereby:

- Doing dynamic tests at higher structural mass damping values would help to validate the flexible array analysis. Furthermore, having more dynamic test data points, it will be possible to use higher orders of parameter estimation techniques in the quasi-unsteady (Granger) model.

- Determination of the two-phase flow map for the present tube bundle could explain the improvement of the results at high void fraction two-phase flows.

It would also lead to the determination of point at which the quasi-steady force measurements should take place to avoid the errors due to the flow regime changes.

- Adopting sophisticated two-phase model would provide the means of carrying out experiments at various free stream velocities without being worried about changes in real void fraction. This step may also improve the prediction of added mass.

- Having better instrumented tubes would make it possible to investigate variation in fluid forces on neighboring cylinders as a function of Re number.

REFERENCES

1. Blevins, R.D., *Flow-Induced Vibration.* 1990, United States: New York, NY (USA) ;Van Nostrand Reinhold Co., Inc. Pages: (451 p).

2. Price, S.J. *An Investigation on the Use of Connors' Equation to Predict Fluidelastic Instability in Cylinder Arrays.* 2001. Atlanta, GA, United States: American Society of Mechanical Engineers, New York, NY 10016-5990, United States.

3. Price, S.J., *A Review of Theoretical Models for Fluidelastic Instability of Cylinder Arrays in Cross-Flow.* Journal of Fluids and Structures, 1995. **9**(5): p. 463-518.

4. Pettigrew, M.J. and C.E. Taylor, *Two-Phase Flow-Induced Vibration: An Overview.* Journal of Pressure Vessel Technology, Transactions of the ASME, 1994. **116**(3): p. 233-253.

5. Khushnood, S., et al. *A Review of Heat Exchanger Tube Bundle Vibrations in Two-Phase Cross-Flow.* 2004. Tokyo, Japan: Elsevier Ltd.

6. Price, S.J. and M.P. Paidoussis, *Single-Flexible-Cylinder Analysis for the Fluidelastic Instability of an Array of Flexible Cylinders in Cross-Flow.* Journal of Fluids Engineering, Transactions of the ASME, 1986. **108**(2): p. 193-199.

7. Chen, S.S., *A General Theory for Dynamic Instability of Tube Arrays in Crossflow.* Fluids of Fluids and Structures, 1987. **1**: p. 35–53.

8. Roberts, B.W., *Low Frequency, Aeroelastic Vibrations in Cascade of Circular Cylinders.* Institution of Mechanical Engineers -- Mechanical Engineering Science -- Monograph. 1965: Institution of Mechanical Engineers, London, England. 29.

9. Roberts, B.W., *Low Frequency, Self-Excited Vibration in a Row of Circular Cylinders Mounted in an Airstream.* 1962, University of Cambridge: Cambridge, UK.

10. Connors, H.J., Jr., *Fluidelastic Vibration of Heat Exchanger Tube Arrays.* American Society of Mechanical Engineers (Paper), 1977(77-DET-90): p. 7.

11. Gorman, D.J., *Experimental Development of Design Criteria to Limit Liquid Cross-Flow-Induced Vibration in Nuclear Reactor Heat Exchange Equipment.* Nuclear Science and Engineering, 1976. **61**(3): p. 324-336.

12. Païdoussis, M.P. *Flow-Induced Vibrations in Nuclear Reactors and Heat Exchangers: Practical Experiences and State of Knowledge.* in *Practical Experiences with Flow-Induced Vibrations.* 1980. Berlin, Germany: Springer-Verlag.

13. Pettigrew, M.J. and C.E. Taylor, *Fluidelastic Instability of Heat Exchanger Tube Bundles. Review and Design Recommendations.* Journal of Pressure Vessel Technology, Transactions of the ASME, 1991. **113**(2): p. 242-256.

14. Price, S.J. and M.P. Paidoussis, *Improved Mathematical Model for the Stability of Cylinder Rows Subject to Cross-Flow.* Journal of Sound and Vibration, 1984. **97**(4): p. 615-640.

15. Price, S.J., M.P. Paidoussis, and N. Giannias. *Generalized Constrained-Mode Analysis for Cylinder Arrays in Cross-Flow.* 1988. Chicago, IL, USA: Publ by American Soc of Mechanical Engineers (ASME), New York, NY, USA.

16. Simpson, A. and J.W. Flower, *Improved Mathematical Model for the Aerodynamic Forces on Tandem Cylinders in Motion with Aeroelastic Applications.* Journal of Sound and Vibration, 1977. **51**(2): p. 183-217.

17. Granger, S. and M.P. Paidoussis, *Improvement to the Quasi-Steady Model with Application to Cross-Flow-Induced Vibration of Tube Arrays.* Journal of Fluid Mechanics, 1996. **320**: p. 163-184.

18. Dalton, C. and R.A. Helfinstine, *Potential Flow Past a Group of Circular Cylinders.* 1971. **93 Ser D**(4): p. 636-42.

19. Paidoussis, M.P., S.J. Price, and D. Mavriplis. *Semi-Potential Flow Theory for the Dynamics of Cylinder Arrays in Cross Flow.* 1984. New Orleans, LA, USA: ASME, New York, NY, USA.

20. Chen, S.S., S. Zhu, and J.A. Jendrzejczyk, *Fluid Damping and Fluid Stiffness of a Tube Row in Crossflow.* Journal of Pressure Vessel Technology, Transactions of the ASME, 1994. **116**(4): p. 370-383.

21. Tanaka, H. and S. Takahara, *Fluid Elastic Vibration of Tube Array in Cross Flow.* Journal of Sound and Vibration, 1981. **77**(1): p. 19-37.

22. Lever, J.H. and D.S. Weaver, *On the Stability of Heat Exchanger Tube Bundles, Part I: Modified Theoretical Model.* Journal of Sound and Vibration, 1986. **107**(3): p. 375-392.

23. Yetisir, M. and D.S. Weaver. *On an Unsteady Theory for Fluidelastic Instability of Heat Exchanger Tube Arrays.* 1988. Chicago, IL, USA: Publ by American Soc of Mechanical Engineers (ASME), New York, NY, USA.

24. Kassera, V. and K. Strohmeier, *Simulation of Tube Bundle Vibrations Induced by Cross-Flow.* Journal of Fluids and Structures, 1997. **11**(8): p. 909-928.

25. Schroeder, K. and H. Gelbe, *Two- and Three-Dimensional Cfd-Simulation of Flow-Induced Vibration Excitation in Tube Bundles.* Chemical Engineering and Processing, 1999. **38**(4-6): p. 621-629.

26. Pettigrew, M.J., J.H. Tromp, and J. Mastorakos, *Vibration of Tube Bundles Subjected to Two-Phase Cross-Flow.* Journal of Pressure Vessel Technology, Transactions of the ASME, 1985. **107**(4): p. 335-343.

27. Pettigrew, M.J., C.E. Taylor, and B.S. Kim, *Vibration of Tube Bundles in Two-Phase Cross-Flow. Part 1. Hydrodynamic Mass and Damping.* Journal of Pressure Vessel Technology, Transactions of the ASME, 1989. **111**(4): p. 466-477.

28. Pettigrew, M.J. and C.E. Taylor, *Damping of Heat Exchanger Tubes in Two-Phase Flow: Review and Design Guidelines.* Journal of Pressure Vessel Technology, Transactions of the ASME, 2004. **126**(4): p. 523-533.

29. Marn, J. and I. Catton, *On Stability Analysis of a Flexible Cylinder in an Array of Rigid Cylinders.* Journal of Fluids Engineering, Transactions of the ASME, 1992. **114**(1): p. 12-19.

30. Mureithi, N.W., et al. *Dynamics of an Inline Tube Array in Steam-Water Flow. Part Ii: Unsteady Fluid Forces.* 1996. Montreal, Can: ASME, New York, NY, USA.

31. Hirota, K., et al. *Dynamics of an Inline Tube Array in Steam-Water Flow. Part Iii: Fluidelastic Instability Tests and Comparison with Theory.* 1996. Montreal, Can: ASME, New York, NY, USA.

32. Pettigrew, M.J., et al., *Detailed Flow and Force Measurements in a Rotated Triangular Tube Bundle Subjected to Two-Phase Cross-Flow.* Journal of Fluids and Structures, 2005. **20**(4 SPEC ISS): p. 567-575.

33. Feenstra, P.A., D.S. Weaver, and R.L. Judd, *Improved Void Fraction Model for Two-Phase Cross-Flow in Horizontal Tube Bundles.* International Journal of Multiphase Flow, 2000. **26**(11): p. 1851-1873.

34. Price, S.J. and M.P. Paidoussis, *Fluidelastic Instability of an Infinite Double Row of Circular Cylinders Subject to a Uniform Cross-Flow.* Journal of Vibration, Acoustics, Stress, and Reliability in Design, 1983. **105**(1): p. 59-66.

35. Grant, I.D.R. and D. Chisholm, *Two-Phase Flow on the Shell-Side of a Segmentally Baffled Shell-and-Tube Heat Exchanger.* Journal of Heat Transfer, Transactions ASME, 1979. **101**(1): p. 38-42.

36. Ulbrich, R. and D. Mewes, *Vertical, Upward Gas-Liquid Two-Phase Flow across a Tube Bundle.* International Journal of Multiphase Flow, 1994. **20**(2): p. 249-272.

37. Violette, R., *Instabilité Fluidelastique D'un Faisceau De Tubes D'échangeurs De Chaleur Soumis À Un Écoulement Diphasique Transverse* in *Mechanical engineering*. 2005, École polytechnique de Montréal: Montréal.

38. Rogers, R.J., C. Taylor, and M.J. Pettigrew. *Fluid Effects on Multi-Span Heat-Exchanger Tube Variation.* 1984. San Antonio, TX, USA: ASME, New York, NY, USA.

APPENDIX A

Table A.1 Measured forces, flow rates and positions (uncorrected), using P-3500 and DCM160 ($\beta = 0\%$ and $U_\infty = 0.26$m/s) at different positions of central cylinder.

	Tube '1'		Tube '2'		Tube '3'		Tube '4'		Tube 'C'		Q_a	Q_w	y	x
	Drag (N)	Lift (N)	Drag (N)	Lift (N)	Drag (N)	Lift (N)	Drag (N)	Lift (N)	Drag (N)	Lift (N)	(Scfm)	(l/s)	(mm)	(mm)
Zero	0.00	0.00	-0.01	0.00	0.00	0.00	-	-	0.01	0.00	0.32	-0.01	-0.01	0.00
Buoyancy	2.16	0.03	2.18	-0.06	2.32	-0.01	-	-	2.48	0.00	-0.06	0.00	0.00	0.01
Normal tests	3.26	0.00	3.23	-0.17	3.14	-0.04	-	-	3.36	-0.08	-0.07	9.94	6.02	-0.04
	3.27	-0.01	3.26	-0.16	3.16	-0.05	-	-	3.37	-0.11	-0.04	9.97	5.02	-0.04
	3.26	-0.01	3.27	-0.16	3.17	-0.05	-	-	3.38	-0.08	-0.19	9.92	4.04	-0.05
	3.28	-0.01	3.27	-0.09	3.16	-0.02	-	-	3.38	-0.04	0.04	9.89	3.01	-0.05
	3.28	0.00	3.28	-0.10	3.18	-0.03	-	-	3.41	-0.04	-0.16	9.90	2.01	-0.05
	3.29	-0.01	3.30	-0.08	3.19	-0.01	-	-	3.41	-0.02	-0.18	9.93	1.03	-0.05
	3.27	-0.01	3.30	-0.10	3.20	-0.02	-	-	3.41	0.03	0.09	9.94	0.01	-0.05
	3.26	-0.02	3.28	-0.12	3.20	-0.01	-	-	3.41	0.07	-0.10	9.89	-1.01	-0.05
	3.26	-0.02	3.28	-0.09	3.18	0.01	-	-	3.40	0.11	-0.21	9.91	-2.01	-0.05
	3.27	-0.01	3.29	-0.10	3.18	0.01	-	-	3.41	0.12	-0.21	9.88	-3.03	-0.05
	3.27	-0.01	3.29	-0.07	3.15	-0.01	-	-	3.38	0.13	-0.15	9.83	-4.04	-0.04
	3.27	-0.06	3.28	-0.07	3.16	-0.02	-	-	3.40	0.17	-0.07	9.92	-5.03	-0.05
	3.27	-0.04	3.29	-0.07	3.15	-0.01	-	-	3.38	0.17	-0.17	9.91	-6.06	-0.04
	3.22	-0.02	3.35	-0.09	3.13	-0.05	-	-	3.60	0.05	-0.07	9.89	0.00	6.57
	3.23	-0.02	3.33	-0.08	3.13	-0.06	-	-	3.54	0.05	-0.20	9.89	0.01	5.48
	3.24	-0.03	3.32	-0.11	3.15	-0.05	-	-	3.52	0.03	-0.30	9.87	0.02	4.47
	3.25	-0.03	3.31	-0.09	3.15	-0.04	-	-	3.48	0.03	-0.17	9.87	0.00	3.30
	3.25	-0.01	3.32	-0.10	3.17	-0.05	-	-	3.46	0.03	-0.12	9.90	-0.01	2.21
	3.28	-0.02	3.29	-0.08	3.18	-0.01	-	-	3.42	0.03	-0.03	9.91	-0.01	1.12
	3.26	-0.03	3.27	-0.08	3.18	0.00	-	-	3.40	0.03	0.14	9.85	-0.02	0.03
	3.28	-0.03	3.27	-0.10	3.20	0.00	-	-	3.38	0.03	-0.06	9.89	-0.01	-1.12
	3.27	-0.05	3.26	-0.09	3.22	0.01	-	-	3.37	0.02	-0.21	9.85	0.00	-2.20
	3.25	-0.03	3.25	-0.09	3.21	0.01	-	-	3.35	0.03	-0.19	9.86	-0.01	-3.33
	3.26	-0.01	3.23	-0.09	3.24	0.04	-	-	3.34	0.02	-0.14	9.82	0.00	-4.42
	3.26	-0.03	3.24	-0.07	3.26	0.05	-	-	3.33	0.02	-0.14	9.88	0.00	-5.52
	3.28	-0.03	3.22	-0.09	3.29	0.08	-	-	3.34	0.02	-0.20	9.86	0.00	-6.61

Table A.1 Measured forces, flow rates and positions (uncorrected), using P-3500 and DCM160 ($\beta = 0\%$ and $U_\infty = 0.26$m/s) at different positions of central cylinder (continued).

	Tube '1'		Tube '2'		Tube '3'		Tube '4'		Tube 'C'		Q_a (Scfm)	Q_w (l/s)	y (mm)	x (mm)
	Drag (N)	Lift (N)	Drag (N)	Lift (N)	Drag (N)	Lift (N)	Drag (N)	Lift (N)	Drag (N)	Drag (N)				
Zero	0.00	0.00	0.00	0.00	-	-	0.00	0.00	0.00	0.00	0.24	0.01	0.00	0.00
Buoyancy	2.15	0.03	2.14	-0.05	-	-	2.29	-0.12	2.49	0.02	-0.05	0.00	0.00	-0.01
Normal Tests	3.26	0.03	3.24	-0.14	-	-	3.34	-0.07	3.39	-0.08	-0.15	9.94	6.03	0.07
	3.27	0.01	3.26	-0.12	-	-	3.32	-0.06	3.39	-0.09	-0.27	9.90	5.02	0.07
	3.28	0.00	3.26	-0.10	-	-	3.30	-0.06	3.41	-0.08	0.08	9.91	4.00	0.09
	3.28	-0.02	3.27	-0.10	-	-	3.29	-0.09	3.42	-0.07	0.14	9.91	3.01	0.09
	3.27	-0.01	3.28	-0.07	-	-	3.27	-0.14	3.42	-0.02	0.00	9.90	2.00	0.08
	3.27	-0.02	3.28	-0.06	-	-	3.26	-0.15	3.42	0.01	0.21	9.86	1.00	0.08
	3.27	-0.01	3.28	-0.06	-	-	3.27	-0.20	3.43	0.03	0.05	9.89	0.00	0.09
	3.27	-0.02	3.28	-0.08	-	-	3.26	-0.25	3.43	0.05	0.11	9.87	-1.03	0.08
	3.28	-0.04	3.28	-0.07	-	-	3.30	-0.29	3.43	0.10	0.10	9.87	-2.03	0.09
	3.28	-0.03	3.28	-0.05	-	-	3.29	-0.31	3.41	0.11	-0.42	9.85	-3.03	0.10
	3.27	-0.03	3.28	-0.05	-	-	3.31	-0.34	3.42	0.15	-0.30	9.85	-4.01	0.11
	3.26	-0.02	3.28	-0.05	-	-	3.32	-0.34	3.40	0.15	0.16	9.85	-5.05	0.10
	3.25	-0.04	3.29	-0.03	-	-	3.33	-0.33	3.38	0.16	-0.12	9.85	-6.04	0.11
	3.20	-0.03	3.33	-0.07	-	-	3.30	-0.23	3.59	0.03	-1.39	9.80	0.04	6.66
	3.23	-0.03	3.31	-0.05	-	-	3.29	-0.23	3.57	0.01	0.03	9.81	0.05	5.60
	3.24	-0.03	3.32	-0.06	-	-	3.29	-0.21	3.52	0.04	-0.09	9.85	0.06	4.51
	3.25	-0.01	3.30	-0.06	-	-	3.28	-0.23	3.49	0.02	-0.12	9.82	0.05	3.42
	3.25	-0.03	3.27	-0.06	-	-	3.27	-0.20	3.46	0.02	0.30	9.78	0.06	2.32
	3.26	-0.04	3.28	-0.05	-	-	3.26	-0.23	3.44	0.05	0.20	9.86	0.05	1.25
	3.27	-0.04	3.25	-0.06	-	-	3.25	-0.23	3.41	0.04	0.04	9.77	0.07	0.15
	3.28	-0.01	3.25	-0.05	-	-	3.26	-0.23	3.41	0.03	1.47	9.88	0.07	-1.00
	3.27	-0.03	3.26	-0.08	-	-	3.26	-0.24	3.40	0.03	-0.74	9.84	0.08	-2.09
	3.29	-0.01	3.25	-0.05	-	-	3.24	-0.19	3.37	0.03	-1.36	9.85	0.11	-3.18
	3.26	-0.01	3.22	-0.04	-	-	3.22	-0.22	3.36	0.02	0.05	9.79	0.09	-4.30
	3.29	-0.03	3.22	-0.05	-	-	3.23	-0.27	3.35	0.00	-0.14	9.84	0.09	-5.37
	3.30	-0.02	3.22	-0.04	-	-	3.21	-0.28	3.36	0.01	0.04	9.87	0.10	-6.50

Table A.2 Measured forces, flow rates and positions (uncorrected), using P-3500 and DCM160 ($\beta = 0\%$ and $U_\infty = 0.42$ m/s) at different positions of central cylinder.

	Tube '1'		Tube '2'		Tube '3'		Tube '4'		Tube 'C'		Q_a (Scfm)	Q_w (l/s)	y (mm)	x (mm)
	Drag (N)	Lift (N)	Drag (N)	Lift (N)	Drag (N)	Lift (N)	Drag (N)	Lift (N)	Drag (N)	Drag (N)				
Zero	0.00	0.00	-0.01	0.00	0.00	0.00	-	-	0.01	0.00	0.32	-0.01	-0.01	0.00
Buoyancy	2.16	0.03	2.18	-0.06	2.32	-0.01	-	-	2.48	0.00	-0.06	0.00	0.00	0.01
Normal Tests	4.74	-0.16	4.53	-0.31	4.45	-0.06	-	-	4.61	-0.24	-0.26	16.00	6.02	0.03
	4.70	-0.14	4.52	-0.24	4.48	-0.09	-	-	4.60	-0.26	0.28	15.87	5.02	0.02
	4.77	-0.15	4.57	-0.22	4.45	-0.06	-	-	4.62	-0.23	-0.70	15.87	4.03	0.00
	4.79	-0.10	4.63	-0.24	4.51	-0.09	-	-	4.67	-0.22	-0.29	15.97	3.02	0.01
	4.82	-0.08	4.69	-0.18	4.53	-0.11	-	-	4.70	-0.19	-0.25	16.01	2.04	0.01
	4.80	-0.12	4.69	-0.21	4.55	-0.05	-	-	4.70	-0.09	-0.20	15.97	1.03	0.01
	4.78	-0.05	4.69	-0.15	4.52	-0.03	-	-	4.70	0.04	-0.21	15.91	0.04	0.01
	4.77	-0.04	4.68	-0.14	4.50	-0.01	-	-	4.70	0.18	0.10	15.87	-1.02	0.00
	4.78	0.03	4.74	-0.17	4.52	-0.02	-	-	4.71	0.25	-0.19	15.97	-2.02	0.00
	4.74	0.00	4.68	-0.13	4.45	0.02	-	-	4.67	0.32	-0.11	15.81	-3.01	-0.01
	4.75	0.05	4.73	-0.08	4.46	-0.01	-	-	4.65	0.35	-0.15	15.92	-4.00	-0.01
	4.70	0.03	4.73	-0.08	4.42	-0.08	-	-	4.62	0.38	-0.21	15.92	-5.02	-0.02
	4.68	0.00	4.72	-0.09	4.41	-0.08	-	-	4.62	0.37	0.02	15.92	-6.04	-0.03
	4.78	-0.09	4.60	-0.07	4.77	0.20	-	-	4.50	0.03	0.02	15.94	0.01	-6.62
	4.81	-0.05	4.63	-0.08	4.74	0.16	-	-	4.53	0.00	0.07	16.03	0.01	-5.54
	4.78	-0.05	4.62	-0.09	4.72	0.09	-	-	4.53	0.01	-0.22	15.96	0.01	-4.44
	4.81	-0.02	4.68	-0.10	4.69	0.03	-	-	4.59	0.01	-0.08	16.02	-0.01	-3.34
	4.77	-0.07	4.67	-0.13	4.64	0.06	-	-	4.61	0.02	-0.88	15.92	0.00	-2.25
	4.80	-0.01	4.70	-0.14	4.59	-0.01	-	-	4.67	0.01	0.42	16.01	0.00	-1.16
	4.81	-0.03	4.71	-0.15	4.55	-0.02	-	-	4.72	0.07	-0.32	15.94	-0.01	-0.04
	4.75	-0.02	4.68	-0.18	4.46	-0.04	-	-	4.75	0.03	-0.31	15.85	-0.01	1.10
	4.76	-0.03	4.74	-0.24	4.44	-0.12	-	-	4.83	0.09	-0.45	15.95	-0.01	2.20
	4.72	-0.01	4.73	-0.18	4.41	-0.11	-	-	4.90	0.09	-0.21	15.97	0.00	3.28
	4.72	-0.03	4.76	-0.16	4.41	-0.10	-	-	5.00	0.10	-0.20	15.98	0.01	4.38
	4.69	-0.05	4.79	-0.22	4.39	-0.12	-	-	5.10	0.13	-0.15	16.00	0.00	5.47
	4.64	-0.05	4.77	-0.21	4.36	-0.16	-	-	5.19	0.09	-0.05	15.93	-0.01	6.59

Table A.2 Measured forces, flow rates and positions (uncorrected), using P-3500 and DCM160 ($\beta = 0\%$ and $U_\infty = 0.42$ m/s) at different positions of central cylinder (continued).

	Tube '1'		Tube '2'		Tube '3'		Tube '4'		Tube 'C'		Q_a (Scfm)	Q_w (l/s)	y (mm)	x (mm)
	Drag (N)	Lift (N)	Drag (N)	Lift (N)	Drag (N)	Lift (N)	Drag (N)	Lift (N)	Drag (N)	Drag (N)				
Zero	0.00	0.00	0.00	0.00	-	-	0.00	0.00	0.00	0.00	0.24	0.01	0.00	0.00
Buoyancy	2.15	0.03	2.14	-0.05	-	-	2.29	-0.12	2.49	0.02	-0.05	0.00	0.00	-0.01
Normal Tests	4.73	-0.13	4.50	-0.22	-	-	4.77	0.02	4.62	-0.24	-0.04	15.92	6.14	0.22
	4.75	-0.13	4.56	-0.23	-	-	4.74	0.02	4.67	-0.26	0.06	15.99	5.14	0.20
	4.74	-0.12	4.58	-0.21	-	-	4.67	-0.01	4.67	-0.30	0.05	15.81	4.14	0.21
	4.81	-0.09	4.65	-0.21	-	-	4.68	-0.06	4.72	-0.22	-0.08	15.97	3.14	0.21
	4.83	-0.08	4.65	-0.17	-	-	4.67	-0.14	4.73	-0.15	0.03	16.01	2.14	0.21
	4.83	-0.08	4.68	-0.14	-	-	4.64	-0.15	4.74	-0.06	0.07	15.92	1.15	0.21
	4.82	-0.06	4.69	-0.09	-	-	4.67	-0.27	4.74	0.03	0.02	15.92	0.16	0.21
	4.82	-0.01	4.69	-0.11	-	-	4.63	-0.32	4.73	0.15	0.06	15.82	-0.91	0.20
	4.83	-0.02	4.71	-0.08	-	-	4.69	-0.40	4.74	0.23	0.00	16.02	-1.93	0.18
	4.80	-0.02	4.73	-0.11	-	-	4.70	-0.43	4.74	0.28	-0.09	15.99	-2.94	0.17
	4.81	0.00	4.71	-0.02	-	-	4.68	-0.50	4.67	0.36	0.11	15.93	-3.92	0.17
	4.76	0.07	4.72	-0.05	-	-	4.73	-0.51	4.65	0.39	-0.11	15.93	-4.92	0.18
	4.76	0.03	4.77	-0.03	-	-	4.78	-0.50	4.65	0.36	0.11	15.99	-5.92	0.17
	4.83	-0.09	4.58	-0.01	-	-	4.52	-0.45	4.53	-0.01	-0.02	16.00	0.11	-6.50
	4.80	-0.05	4.58	-0.07	-	-	4.52	-0.31	4.55	0.01	-0.12	15.91	0.11	-5.39
	4.86	-0.08	4.64	-0.05	-	-	4.58	-0.27	4.58	0.00	0.20	16.00	0.10	-4.32
	4.82	-0.08	4.64	-0.06	-	-	4.60	-0.33	4.60	0.04	-0.12	16.01	0.12	-3.18
	4.86	-0.06	4.65	-0.07	-	-	4.60	-0.25	4.64	0.05	0.16	15.94	0.11	-2.08
	4.83	-0.06	4.66	-0.10	-	-	4.63	-0.25	4.68	0.03	0.01	15.95	0.12	-1.00
	4.83	-0.03	4.70	-0.15	-	-	4.64	-0.26	4.73	0.04	-0.03	15.98	0.11	0.10
	4.80	-0.05	4.69	-0.17	-	-	4.65	-0.27	4.78	0.05	0.10	15.87	0.12	1.26
	4.78	-0.02	4.76	-0.18	-	-	4.72	-0.31	4.90	0.05	0.15	15.97	0.11	2.35
	4.77	0.00	4.75	-0.20	-	-	4.69	-0.26	4.96	0.00	-0.11	15.93	0.11	3.44
	4.71	-0.07	4.74	-0.18	-	-	4.74	-0.27	5.00	0.06	-0.02	15.90	0.13	4.55
	4.69	-0.06	4.77	-0.18	-	-	4.74	-0.24	5.10	0.03	-0.15	15.90	0.12	5.66
	4.66	-0.04	4.78	-0.18	-	-	4.77	-0.24	5.19	0.04	0.00	15.88	0.13	6.76

Table A.3 Measured forces, flow rates and positions (uncorrected), using P-3500 and DCM160 ($\beta = 0\%$ and $U_\infty = 0.53$ m/s) at different positions of central cylinder.

	Tube '1'		Tube '2'		Tube '3'		Tube '4'		Tube 'C'		Q_a (Scfm)	Q_w (l/s)	y (mm)	x (mm)
	Drag (N)	Lift (N)	Drag (N)	Lift (N)	Drag (N)	Lift (N)	Drag (N)	Lift (N)	Drag (N)	Drag (N)				
Zero	0.00	0.00	-0.01	0.00	0.00	0.00	-	-	0.01	0.00	-	-0.01	-0.01	0.00
Buoyancy	2.16	0.03	2.18	-0.06	2.32	-0.01	-	-	2.48	0.00	-	0.00	0.00	0.01
Normal Tests	4.74	-0.16	4.53	-0.31	4.45	-0.06	-	-	4.61	-0.24	-	16.00	-6.02	0.03
	4.70	-0.14	4.52	-0.24	4.48	-0.09	-	-	4.60	-0.26	-	15.87	-5.02	0.02
	4.77	-0.15	4.57	-0.22	4.45	-0.06	-	-	4.62	-0.23	-	15.87	-4.03	0.00
	4.79	-0.10	4.63	-0.24	4.51	-0.09	-	-	4.67	-0.22	-	15.97	-3.02	0.01
	4.82	-0.08	4.69	-0.18	4.53	-0.11	-	-	4.70	-0.19	-	16.01	-2.04	0.01
	4.80	-0.12	4.69	-0.21	4.55	-0.05	-	-	4.70	-0.09	-	15.97	-1.03	0.01
	4.78	-0.05	4.69	-0.15	4.52	-0.03	-	-	4.70	0.04	-	15.91	-0.04	0.01
	4.77	-0.04	4.68	-0.14	4.50	-0.01	-	-	4.70	0.18	-	15.87	1.02	0.00
	4.78	0.03	4.74	-0.17	4.52	-0.02	-	-	4.71	0.25	-	15.97	2.02	0.00
	4.74	0.00	4.68	-0.13	4.45	0.02	-	-	4.67	0.32	-	15.81	3.01	-0.01
	4.75	0.05	4.73	-0.08	4.46	-0.01	-	-	4.65	0.35	-	15.92	4.00	-0.01
	4.70	0.03	4.73	-0.08	4.42	-0.08	-	-	4.62	0.38	-	15.92	5.02	-0.02
	4.68	0.00	4.72	-0.09	4.41	-0.08	-	-	4.62	0.37	-	15.92	6.04	-0.03
	4.78	-0.09	4.60	-0.07	4.77	0.20	-	-	4.50	0.03	-	15.94	-0.01	-6.62
	4.81	-0.05	4.63	-0.08	4.74	0.16	-	-	4.53	0.00	-	16.03	-0.01	-5.54
	4.78	-0.05	4.62	-0.09	4.72	0.09	-	-	4.53	0.01	-	15.96	-0.01	-4.44
	4.81	-0.02	4.68	-0.10	4.69	0.03	-	-	4.59	0.01	-	16.02	0.01	-3.34
	4.77	-0.07	4.67	-0.13	4.64	0.06	-	-	4.61	0.02	-	15.92	0.00	-2.25
	4.80	-0.01	4.70	-0.14	4.59	-0.01	-	-	4.67	0.01	-	16.01	0.00	-1.16
	4.81	-0.03	4.71	-0.15	4.55	-0.02	-	-	4.72	0.07	-	15.94	0.01	-0.04
	4.75	-0.02	4.68	-0.18	4.46	-0.04	-	-	4.75	0.03	-	15.85	0.01	1.10
	4.76	-0.03	4.74	-0.24	4.44	-0.12	-	-	4.83	0.09	-	15.95	0.01	2.20
	4.72	-0.01	4.73	-0.18	4.41	-0.11	-	-	4.90	0.09	-	15.97	0.00	3.28
	4.72	-0.03	4.76	-0.16	4.41	-0.10	-	-	5.00	0.10	-	15.98	-0.01	4.38
	4.69	-0.05	4.79	-0.22	4.39	-0.12	-	-	5.10	0.13	-	16.00	0.00	5.47
	4.64	-0.05	4.77	-0.21	4.36	-0.16	-	-	5.19	0.09	-	15.93	0.01	6.59

Table A.3 Measured forces, flow rates and positions (uncorrected), using P-3500 and DCM160 ($\beta = 0\%$ and $U_\infty = 0.53$ m/s) at different positions of central cylinder (continued).

	Tube '1'		Tube '2'		Tube '3'		Tube '4'		Tube 'C'		Q_a (Scfm)	Q_w (l/s)	y (mm)	x (mm)
	Drag (N)	Lift (N)	Drag (N)	Lift (N)	Drag (N)	Lift (N)	Drag (N)	Lift (N)	Drag (N)	Drag (N)				
Zero	0.00	0.00	0.00	0.00	-	-	0.00	0.00	0.00	0.00	-	0.01	0.00	0.00
Buoyancy	2.15	0.03	2.14	-0.05	-	-	2.29	-0.12	2.49	0.02	-	0.00	0.00	-0.01
Normal Tests	6.05	0.16	6.08	-0.12	-	-	6.06	-0.67	5.76	0.55	-	19.88	5.93	0.18
	6.06	0.14	6.07	-0.05	-	-	6.03	-0.65	5.78	0.59	-	19.93	4.95	0.19
	6.09	0.15	6.07	-0.07	-	-	5.97	-0.57	5.86	0.58	-	19.95	3.93	0.19
	6.22	0.04	6.11	-0.15	-	-	6.00	-0.51	5.95	0.55	-	20.02	2.93	0.19
	6.11	0.08	6.07	-0.14	-	-	5.96	-0.44	5.90	0.42	-	19.98	1.95	0.19
	6.17	0.04	6.02	-0.20	-	-	5.93	-0.41	5.91	0.26	-	19.93	0.92	0.19
	6.15	0.01	5.96	-0.20	-	-	5.91	-0.26	5.90	0.13	-	19.98	-0.15	0.19
	6.15	-0.09	5.94	-0.26	-	-	5.84	-0.20	5.88	-0.07	-	19.84	-1.16	0.20
	6.15	-0.11	5.87	-0.25	-	-	5.92	-0.19	5.89	-0.15	-	19.84	-2.16	0.20
	6.15	-0.20	5.86	-0.26	-	-	5.93	-0.08	5.84	-0.34	-	19.90	-3.16	0.20
	6.17	-0.23	5.86	-0.37	-	-	5.99	0.01	5.86	-0.39	-	19.97	-4.18	0.20
	6.05	-0.20	5.75	-0.29	-	-	5.95	0.08	5.75	-0.36	-	19.88	-5.15	0.20
	6.01	-0.32	5.70	-0.41	-	-	6.10	0.11	5.74	-0.36	-	19.99	-6.18	0.21
	5.97	-0.03	6.09	-0.26	-	-	6.14	-0.26	6.59	0.12	-	19.96	-0.19	6.81
	6.00	-0.04	6.11	-0.30	-	-	6.06	-0.32	6.46	0.12	-	19.95	-0.19	5.72
	5.98	-0.02	6.04	-0.34	-	-	6.01	-0.30	6.34	0.17	-	19.87	-0.19	4.64
	6.11	0.00	6.03	-0.24	-	-	5.98	-0.29	6.21	0.06	-	19.95	-0.18	3.55
	6.14	-0.03	6.06	-0.32	-	-	5.97	-0.30	6.16	0.10	-	19.93	-0.20	2.47
	6.14	0.02	6.01	-0.24	-	-	5.93	-0.31	6.01	0.14	-	19.93	-0.19	1.35
	6.22	-0.08	6.00	-0.21	-	-	5.91	-0.30	5.96	0.12	-	20.01	-0.19	0.28
	6.24	-0.08	6.04	-0.13	-	-	5.91	-0.30	5.88	0.06	-	20.07	-0.19	-0.88
	6.18	-0.06	5.94	-0.17	-	-	5.82	-0.29	5.74	0.06	-	19.89	-0.19	-1.95
	6.19	-0.08	5.94	-0.10	-	-	5.81	-0.29	5.70	0.09	-	19.99	-0.19	-3.05
	6.19	-0.06	5.93	-0.07	-	-	5.81	-0.31	5.68	0.05	-	20.02	-0.21	-4.16
	6.18	-0.04	5.93	0.04	-	-	5.74	-0.30	5.64	0.08	-	19.99	-0.19	-5.26
	6.09	-0.14	5.82	-0.03	-	-	5.65	-0.39	5.55	0.04	-	19.86	-0.19	-6.38

Table A.4 Measured forces, flow rates and positions (uncorrected), using P-3500 and DCM160 ($\beta = 0\%$ and $U_\infty = 0.61$ m/s) at different positions of central cylinder.

	Tube '1'		Tube '2'		Tube '3'		Tube '4'		Tube 'C'		Q_a (Scfm)	Q_w (l/s)	y (mm)	x (mm)
	Drag (N)	Lift (N)	Drag (N)	Lift (N)	Drag (N)	Lift (N)	Drag (N)	Lift (N)	Drag (N)	Drag (N)				
Zero	0.00	0.00	-0.01	0.00	0.00	0.00	-	-	0.01	0.00	-	-	-0.01	0.00
Buoyancy	2.16	0.03	2.18	-0.06	2.32	-0.01	-	-	2.48	0.00	-	-	0.00	0.01
Normal Tests	7.21	-0.41	6.82	-0.51	6.86	-0.08	-	-	6.83	-0.29	-	23.14	-6.01	0.06
	7.26	-0.43	6.88	-0.52	6.88	-0.11	-	-	6.83	-0.38	-	22.96	-5.04	0.04
	7.33	-0.37	6.98	-0.42	6.94	-0.11	-	-	6.94	-0.54	-	23.13	-4.07	0.04
	7.41	-0.23	7.11	-0.51	7.04	-0.10	-	-	6.99	-0.40	-	23.09	-3.07	0.04
	7.49	-0.17	7.20	-0.53	7.05	-0.14	-	-	7.08	-0.22	-	23.17	-2.04	0.03
	7.46	-0.08	7.24	-0.31	7.02	-0.04	-	-	7.07	0.00	-	23.13	-1.04	0.03
	7.49	-0.07	7.28	-0.35	7.03	-0.08	-	-	7.11	0.21	-	23.17	-0.06	0.04
	7.48	0.03	7.34	-0.35	7.00	-0.27	-	-	7.14	0.42	-	23.17	0.98	0.04
	7.45	0.03	7.37	-0.28	6.96	-0.11	-	-	7.09	0.52	-	23.14	2.00	0.03
	7.40	0.16	7.32	-0.22	6.81	-0.09	-	-	6.99	0.66	-	23.06	3.01	0.03
	7.32	0.11	7.41	-0.28	6.87	-0.06	-	-	6.98	0.78	-	23.09	4.00	0.04
	7.33	0.14	7.39	-0.11	6.74	-0.14	-	-	6.90	0.72	-	23.00	5.01	0.03
	7.28	0.16	7.44	-0.33	6.67	-0.14	-	-	6.84	0.75	-	23.08	6.02	0.03
	7.36	-0.11	7.12	-0.13	7.48	0.29	-	-	6.57	0.10	-	23.03	-0.03	-6.60
	7.41	-0.06	7.15	-0.12	7.40	0.27	-	-	6.64	0.08	-	23.12	-0.04	-5.51
	7.37	-0.14	7.08	-0.21	7.30	0.10	-	-	6.64	0.14	-	23.03	-0.02	-4.41
	7.46	-0.20	7.18	-0.29	7.24	0.07	-	-	6.78	0.14	-	23.18	-0.04	-3.32
	7.39	-0.07	7.16	-0.19	7.15	0.04	-	-	6.81	0.11	-	23.03	-0.03	-2.23
	7.46	-0.06	7.20	-0.28	7.07	-0.05	-	-	6.93	0.12	-	23.08	-0.03	-1.14
	7.45	-0.04	7.23	-0.28	6.97	-0.02	-	-	7.06	0.16	-	23.07	-0.02	-0.01
	7.47	-0.07	7.32	-0.35	6.92	-0.19	-	-	7.21	0.20	-	23.18	-0.02	1.13
	7.42	0.00	7.34	-0.41	6.87	-0.17	-	-	7.31	0.26	-	23.10	-0.04	2.22
	7.44	-0.06	7.38	-0.41	6.86	-0.21	-	-	7.47	0.20	-	23.17	-0.04	3.32
	7.41	-0.10	7.41	-0.41	6.66	-0.23	-	-	7.59	0.23	-	23.11	-0.04	4.40
	7.34	-0.07	7.38	-0.36	6.63	-0.18	-	-	7.77	0.21	-	23.11	-0.06	5.49
	7.25	-0.07	7.39	-0.43	6.60	-0.24	-	-	7.89	0.18	-	23.11	-0.04	6.62

Table A.4 Measured forces, flow rates and positions (uncorrected), using P-3500 and DCM160 ($\beta = 0\%$ and $U_\infty = 0.61$ m/s) at different positions of central cylinder (continued).

	Tube '1'		Tube '2'		Tube '3'		Tube '4'		Tube 'C'		Q_a (Scfm)	Q_w (l/s)	y (mm)	x (mm)
	Drag (N)	Lift (N)	Drag (N)	Lift (N)	Drag (N)	Lift (N)	Drag (N)	Lift (N)	Drag (N)	Drag (N)				
Zero	0.00	0.00	0.00	0.00	-	-	0.00	0.00	0.00	0.00	-	0.01	0.00	0.00
Buoyancy	2.15	0.03	2.14	-0.05	-	-	2.29	-0.12	2.49	0.02	-	0.00	0.00	-0.01
Normal Tests	7.58	-0.55	7.14	-0.57	-	-	7.67	0.31	7.16	-0.31	-	23.89	-6.23	0.28
	7.68	-0.44	7.22	-0.43	-	-	7.60	0.24	7.20	-0.47	-	23.90	-5.21	0.28
	7.68	-0.32	7.31	-0.46	-	-	7.52	0.14	7.24	-0.47	-	23.80	-4.22	0.28
	7.83	-0.26	7.43	-0.43	-	-	7.54	0.00	7.32	-0.44	-	23.89	-3.25	0.28
	7.70	-0.18	7.37	-0.31	-	-	7.36	-0.12	7.29	-0.24	-	23.65	-2.23	0.28
	7.83	-0.11	7.58	-0.35	-	-	7.44	-0.30	7.42	-0.02	-	23.93	-1.25	0.28
	7.71	-0.02	7.50	-0.36	-	-	7.34	-0.38	7.34	0.13	-	23.69	-0.22	0.28
	7.87	-0.05	7.67	-0.35	-	-	7.43	-0.44	7.46	0.38	-	23.92	0.83	0.28
	7.73	0.01	7.56	-0.18	-	-	7.39	-0.51	7.37	0.60	-	23.73	1.84	0.29
	7.79	0.03	7.73	-0.26	-	-	7.51	-0.58	7.42	0.74	-	23.87	2.86	0.28
	7.67	0.21	7.69	-0.13	-	-	7.42	-0.70	7.27	0.82	-	23.77	3.84	0.28
	7.67	0.10	7.72	-0.17	-	-	7.53	-0.71	7.24	0.88	-	23.84	4.86	0.28
	7.61	0.19	7.73	-0.12	-	-	7.62	-0.84	7.14	0.74	-	23.81	5.85	0.28
	7.65	-0.21	7.43	-0.17	-	-	7.13	-0.46	6.89	0.14	-	23.85	-0.18	-6.38
	7.69	-0.17	7.48	-0.14	-	-	7.18	-0.53	6.97	0.15	-	23.84	-0.18	-5.29
	7.65	-0.13	7.41	-0.17	-	-	7.18	-0.43	7.02	0.20	-	23.77	-0.19	-4.21
	7.68	-0.01	7.38	-0.18	-	-	7.21	-0.32	7.02	0.09	-	23.66	-0.19	-3.11
	7.83	-0.17	7.61	-0.24	-	-	7.31	-0.25	7.22	0.13	-	23.97	-0.19	-2.00
	7.71	-0.04	7.50	-0.35	-	-	7.30	-0.40	7.19	0.14	-	23.63	-0.19	-0.91
	7.79	-0.08	7.61	-0.37	-	-	7.46	-0.32	7.42	0.20	-	23.89	-0.18	0.23
	7.79	-0.12	7.61	-0.35	-	-	7.44	-0.42	7.48	0.22	-	23.88	-0.19	1.35
	7.74	-0.08	7.58	-0.35	-	-	7.55	-0.38	7.65	0.26	-	23.82	-0.19	2.44
	7.78	0.00	7.67	-0.25	-	-	7.60	-0.37	7.80	0.14	-	23.85	-0.18	3.53
	7.79	0.00	7.77	-0.36	-	-	7.73	-0.37	8.06	0.16	-	23.94	-0.20	4.64
	7.62	-0.03	7.70	-0.34	-	-	7.65	-0.30	8.10	0.26	-	23.80	-0.19	5.74
	7.56	-0.06	7.69	-0.33	-	-	7.67	-0.37	8.29	0.20	-	23.72	-0.20	6.86

Table A.5 Measured forces, flow rates and positions (uncorrected), using P-3500 and DCM160 ($\beta = 60\%$ and $U_\infty = 1.31$m/s) at different positions of central cylinder.

	Tube '1'		Tube '2'		Tube '3'		Tube '4'		Tube 'C'		Q_a (Scfm)	Q_w (l/s)	y (mm)	x (mm)
	Drag (N)	Lift (N)	Drag (N)	Lift (N)	Drag (N)	Lift (N)	Drag (N)	Lift (N)	Drag (N)	Drag (N)				
Zero	0.00	0.00	0.00	0.00	-	-	0.00	0.00	0.00	0.00	0.13	0.00	0.02	0.01
Buoyancy	2.20	-0.17	2.15	-0.17	-	-	2.11	0.01	2.51	-0.05	0.68	0.01	0.02	0.05
Normal Tests	12.70	-1.63	11.81	-0.32	-	-	10.67	-0.64	11.98	-1.20	63.28	19.58	6.10	0.08
	12.62	-1.70	11.85	-0.20	-	-	10.77	-0.59	11.89	-1.18	64.31	19.57	5.11	0.09
	12.24	-1.65	11.61	-0.15	-	-	10.72	-0.58	11.48	-1.10	63.37	19.56	4.12	0.09
	12.12	-1.55	11.51	-0.04	-	-	10.83	-0.52	11.20	-0.96	64.20	19.54	3.11	0.10
	11.96	-1.39	11.26	-0.03	-	-	10.82	-0.57	10.92	-0.77	63.36	19.52	2.12	0.10
	11.87	-0.96	11.05	-0.01	-	-	10.90	-0.52	10.69	-0.64	63.76	19.52	1.13	0.10
	11.92	-0.49	10.95	0.01	-	-	11.03	-0.47	10.67	-0.43	64.23	19.50	0.13	0.10
	11.84	-0.06	10.80	-0.10	-	-	11.12	-0.52	10.74	-0.18	63.49	19.50	-0.94	0.10
	12.01	0.30	10.84	-0.15	-	-	11.14	-0.53	11.02	-0.05	62.73	19.64	-1.95	0.10
	12.21	0.33	10.91	-0.18	-	-	11.24	-0.65	11.30	0.18	63.42	19.56	-2.92	0.11
	12.40	0.35	10.93	-0.12	-	-	11.14	-0.64	11.57	0.36	63.40	19.63	-3.95	0.11
	12.68	0.30	10.96	-0.10	-	-	10.99	-0.69	11.80	0.53	63.14	19.59	-4.94	0.12
	12.83	0.25	10.94	-0.01	-	-	10.78	-0.61	11.93	0.57	62.84	19.61	-5.91	0.13
	12.26	-0.49	10.30	-0.32	-	-	11.75	-0.40	10.62	-0.33	62.30	19.73	0.13	-6.47
	12.24	-0.40	10.36	-0.19	-	-	11.52	-0.28	10.58	-0.41	62.49	19.68	0.14	-5.38
	12.16	-0.44	10.49	-0.17	-	-	11.47	-0.31	10.58	-0.37	63.80	19.66	0.15	-4.29
	12.16	-0.54	10.66	-0.22	-	-	11.48	-0.48	10.64	-0.35	65.85	19.64	0.14	-3.19
	12.03	-0.35	10.66	-0.11	-	-	11.18	-0.40	10.56	-0.43	63.82	19.59	0.14	-2.10
	12.03	-0.47	10.82	-0.08	-	-	11.21	-0.50	10.64	-0.43	62.97	19.60	0.16	-0.98
	11.95	-0.55	10.98	-0.08	-	-	11.18	-0.61	10.72	-0.34	63.05	19.62	0.16	0.16
	11.90	-0.57	11.11	-0.06	-	-	11.17	-0.66	10.82	-0.34	62.89	19.69	0.15	1.23
	11.74	-0.58	11.11	-0.09	-	-	10.92	-0.76	10.80	-0.34	63.47	19.57	0.15	2.34
	11.69	-0.44	11.27	0.01	-	-	10.82	-0.66	10.95	-0.41	62.01	19.70	0.16	3.46
	11.60	-0.39	11.40	0.05	-	-	10.72	-0.65	11.10	-0.45	61.72	19.62	0.17	4.55
	11.43	-0.45	11.48	0.05	-	-	10.63	-0.71	11.17	-0.46	61.56	19.59	0.17	5.64
	11.50	-0.48	11.72	0.14	-	-	10.62	-0.69	11.47	-0.42	62.42	19.70	0.18	6.75

Table A.5 Measured forces, flow rates and positions (uncorrected), using P-3500 and DCM160 ($\beta = 60\%$ and $U_\infty = 1.31$m/s) at different positions of central cylinder (continued).

	Tube '1'		Tube '2'		Tube '3'		Tube '4'		Tube 'C'		Q_a (Scfm)	Q_w (l/s)	y (mm)	x (mm)
	Drag (N)	Lift (N)	Drag (N)	Lift (N)	Drag (N)	Lift (N)	Drag (N)	Lift (N)	Drag (N)	Drag (N)				
Zero	-0.01	0.00	-0.02	0.00	0.00	0.01	-	-	0.00	0.00	0.45	0.02	0.01	-6.55
Buoyancy	2.15	0.06	2.14	-0.04	2.29	-0.13	-	-	2.49	0.15	-1.18	-0.02	-0.01	-0.02
Normal Tests	12.57	1.31	11.64	-0.07	12.76	-0.52	-	-	11.90	1.54	61.84	19.54	6.03	0.00
	12.38	1.32	11.63	-0.04	12.70	-0.42	-	-	11.74	1.56	62.90	19.46	5.05	0.01
	12.26	1.31	11.51	0.17	12.59	-0.19	-	-	11.43	1.41	62.88	19.51	4.01	0.00
	12.13	1.09	11.44	0.09	12.62	-0.35	-	-	11.29	1.54	63.82	19.51	3.03	0.01
	11.93	0.88	11.18	0.19	12.40	-0.23	-	-	10.92	1.30	62.43	19.51	2.03	0.01
	12.00	0.70	11.09	0.18	12.51	-0.19	-	-	10.81	0.94	62.92	19.68	1.06	0.01
	11.90	0.56	10.90	0.19	12.47	-0.24	-	-	10.70	0.45	63.28	19.64	0.04	0.01
	11.92	0.27	10.83	0.07	12.58	-0.56	-	-	10.85	0.11	63.65	19.65	-0.99	0.02
	11.93	0.09	10.75	0.04	12.57	-0.42	-	-	11.01	-0.20	62.69	19.57	-2.00	0.02
	12.07	-0.11	10.76	0.10	12.63	-0.34	-	-	11.28	-0.40	62.26	19.65	-2.99	0.02
	12.28	-0.28	10.76	0.20	12.68	-0.17	-	-	11.49	-0.41	61.13	19.66	-4.03	0.02
	12.50	-0.52	10.79	0.13	12.78	-0.26	-	-	11.70	-0.29	61.30	19.48	-5.02	0.03
	12.84	-0.60	10.93	0.18	13.01	-0.15	-	-	12.04	-0.23	62.30	19.66	-6.01	0.02
	12.00	0.45	10.07	-0.07	11.74	-0.35	-	-	10.44	0.44	61.88	19.54	0.02	-6.59
	12.08	0.45	10.24	-0.02	11.96	-0.33	-	-	10.49	0.43	61.61	19.63	0.03	-5.49
	12.08	0.45	10.35	0.02	12.09	-0.31	-	-	10.51	0.42	61.92	19.64	0.03	-4.42
	11.98	0.49	10.43	0.07	12.09	-0.30	-	-	10.50	0.37	62.37	19.54	0.03	-3.31
	12.01	0.49	10.62	0.09	12.38	-0.28	-	-	10.63	0.37	63.62	19.62	0.03	-2.19
	12.02	0.51	10.77	0.17	12.45	-0.32	-	-	10.69	0.37	63.42	19.63	0.03	-1.10
	11.93	0.48	10.87	0.18	12.52	-0.32	-	-	10.74	0.41	62.98	19.64	0.04	0.02
	11.89	0.50	11.02	0.16	12.56	-0.34	-	-	10.83	0.45	63.86	19.64	0.03	1.12
	11.69	0.46	11.04	0.18	12.47	-0.35	-	-	10.84	0.45	63.04	19.51	0.03	2.23
	11.70	0.48	11.21	0.28	12.57	-0.31	-	-	11.00	0.38	63.41	19.52	0.04	3.34
	11.56	0.53	11.34	0.29	12.64	-0.23	-	-	11.15	0.36	63.30	19.59	0.05	4.41
	11.60	0.54	11.58	0.36	12.78	-0.26	-	-	11.37	0.44	63.24	19.63	0.04	5.51
	11.40	0.54	11.67	0.36	12.70	-0.25	-	-	11.47	0.40	63.61	19.55	0.05	6.62

Table A.6 Measured forces, flow rates and positions (uncorrected), using P-3500 and DCM160 ($\beta = 80\%$ and $U_\infty = 1.32$ m/s) at different positions of central cylinder.

	Tube '1'		Tube '2'		Tube '3'		Tube '4'		Tube 'C'		Q_a (Scfm)	Q_w (l/s)	y (mm)	x (mm)
	Drag (N)	Lift (N)	Drag (N)	Lift (N)	Drag (N)	Lift (N)	Drag (N)	Lift (N)	Drag (N)	Drag (N)				
Zero	0.00	0.00	-0.01	0.00	-	-	0.00	0.00	0.00	0.01	-0.17	0.02	0.01	0.01
Buoyancy	2.11	0.04	2.14	-0.03	-	-	2.29	0.04	2.46	0.02	-0.04	-0.01	0.04	0.03
Normal Tests	6.58	0.74	6.41	0.29	-	-	5.90	0.09	6.41	0.69	83.50	9.99	6.13	0.11
	6.58	0.70	6.35	0.36	-	-	5.86	0.17	6.39	0.66	84.95	9.95	5.14	0.12
	6.48	0.63	6.34	0.37	-	-	5.96	0.13	6.30	0.63	82.67	10.01	4.16	0.12
	6.41	0.48	6.16	0.28	-	-	5.94	0.13	6.24	0.52	86.65	9.96	3.12	0.12
	6.24	0.35	5.97	0.28	-	-	5.87	0.16	6.08	0.34	84.66	9.97	2.16	0.11
	6.28	0.25	6.01	0.19	-	-	6.07	0.05	6.12	0.21	84.58	10.00	1.14	0.11
	6.16	0.15	5.80	0.23	-	-	5.99	0.08	5.99	0.06	84.02	10.03	0.14	0.11
	6.24	0.09	5.79	0.22	-	-	5.98	0.12	6.00	-0.14	83.55	9.93	-0.87	0.12
	6.32	0.04	5.72	0.18	-	-	6.00	0.09	6.09	-0.34	83.15	10.01	-1.89	0.11
	6.43	-0.18	5.81	0.22	-	-	6.14	0.05	6.19	-0.47	83.75	9.98	-2.91	0.12
	6.45	-0.33	5.63	0.21	-	-	5.93	0.10	6.23	-0.50	84.24	9.91	-3.89	0.14
	6.60	-0.42	5.73	0.20	-	-	6.08	-0.01	6.29	-0.54	84.60	9.96	-4.93	0.14
	6.67	-0.46	5.73	0.29	-	-	5.96	0.05	6.32	-0.58	84.56	9.99	-5.92	0.14
	6.45	0.14	5.61	0.15	-	-	6.37	0.19	5.95	0.01	83.60	9.94	0.11	-6.45
	6.38	0.13	5.54	0.20	-	-	6.19	0.23	5.88	-0.02	84.39	9.94	0.11	-5.36
	6.44	0.11	5.65	0.18	-	-	6.23	0.20	5.98	0.02	81.84	9.93	0.11	-4.27
	6.34	0.12	5.68	0.22	-	-	6.12	0.18	5.96	0.06	84.57	9.98	0.12	-3.17
	6.32	0.13	5.69	0.18	-	-	6.08	0.15	5.99	-0.01	83.32	9.96	0.12	-2.05
	6.27	0.11	5.80	0.20	-	-	6.11	0.14	6.01	0.03	81.34	9.99	0.14	-0.98
	6.29	0.15	5.88	0.17	-	-	6.06	0.09	6.06	0.02	85.88	9.98	0.12	0.14
	6.13	0.14	5.79	0.15	-	-	5.89	0.11	6.05	-0.01	84.30	9.92	0.13	1.27
	6.18	0.08	6.01	0.25	-	-	5.98	0.12	6.17	0.05	85.81	9.94	0.13	2.35
	6.19	0.11	6.09	0.22	-	-	5.93	0.06	6.30	0.04	86.55	9.94	0.12	3.47
	6.10	0.13	6.06	0.25	-	-	5.79	0.07	6.30	0.00	87.28	9.88	0.14	4.55
	6.02	0.10	6.11	0.25	-	-	5.69	0.06	6.30	-0.02	85.41	9.93	0.13	5.65
	6.05	0.13	6.41	0.19	-	-	6.00	-0.02	6.51	0.03	86.02	9.97	0.14	6.74

Table A.6 Measured forces, flow rates and positions (uncorrected), using P-3500 and DCM160 ($\beta = 80\%$ and $U_\infty = 1.32$ m/s) at different positions of central cylinder (continued).

	Tube '1'		Tube '2'		Tube '3'		Tube '4'		Tube 'C'		Q_a (Scfm)	Q_w (l/s)	y (mm)	x (mm)
	Drag (N)	Lift (N)	Drag (N)	Lift (N)	Drag (N)	Lift (N)	Drag (N)	Lift (N)	Drag (N)	Drag (N)				
Zero	0.00	0.00	0.00	0.00	-0.01	0.00	-	-	-0.01	-0.01	-0.18	0.00	-0.01	0.01
Buoyancy	2.16	0.06	2.15	-0.03	2.25	-0.14	-	-	2.46	0.01	-0.42	0.12	0.00	0.00
Normal Tests	6.59	0.81	6.36	0.35	6.79	-0.50	-	-	6.36	0.67	84.43	10.00	6.01	-0.02
	6.50	0.71	6.33	0.38	6.73	-0.50	-	-	6.33	0.68	84.61	10.02	5.04	-0.03
	6.39	0.61	6.16	0.32	6.67	-0.41	-	-	6.21	0.61	84.74	10.01	4.06	-0.02
	6.30	0.47	6.12	0.29	6.69	-0.41	-	-	6.18	0.51	82.74	9.96	3.02	-0.02
	6.24	0.32	5.98	0.29	6.69	-0.45	-	-	6.11	0.44	85.78	9.93	2.06	-0.01
	6.18	0.22	5.90	0.23	6.62	-0.35	-	-	6.01	0.21	84.88	9.96	1.06	-0.02
	6.09	0.18	5.67	0.28	6.49	-0.29	-	-	5.97	0.04	84.63	9.89	0.05	-0.02
	6.22	0.05	5.82	0.18	6.67	-0.35	-	-	6.02	-0.08	84.42	9.98	-0.97	-0.02
	6.32	-0.03	5.71	0.21	6.61	-0.24	-	-	6.07	-0.31	84.39	9.97	-1.99	-0.01
	6.30	-0.14	5.72	0.26	6.58	-0.19	-	-	6.09	-0.45	84.83	9.94	-2.99	-0.02
	6.40	-0.28	5.66	0.21	6.63	-0.20	-	-	6.17	-0.49	84.29	9.97	-4.00	-0.01
	6.53	-0.33	5.67	0.30	6.63	-0.08	-	-	6.25	-0.57	84.77	9.87	-5.01	-0.01
	6.70	-0.47	5.69	0.25	6.75	-0.10	-	-	6.31	-0.60	84.53	9.98	-6.02	-0.01
	6.40	0.12	5.53	0.14	6.33	-0.36	-	-	5.86	0.07	85.31	9.91	0.04	-6.59
	6.40	0.13	5.59	0.17	6.33	-0.35	-	-	5.87	0.01	85.26	9.90	0.04	-5.51
	6.29	0.12	5.53	0.18	6.40	-0.34	-	-	5.87	0.02	84.65	9.86	0.04	-4.41
	6.36	0.18	5.72	0.15	6.59	-0.44	-	-	5.93	0.11	85.23	10.00	0.06	-3.31
	6.41	0.36	5.80	0.18	6.62	-0.35	-	-	6.00	0.03	85.21	9.98	0.04	-2.20
	6.28	0.12	5.78	0.20	6.58	-0.45	-	-	5.98	0.08	84.47	10.00	0.06	-1.09
	6.24	0.19	5.83	0.20	6.59	-0.35	-	-	6.00	-0.03	84.80	9.99	0.06	0.04
	6.20	0.11	5.88	0.25	6.65	-0.41	-	-	6.05	0.05	84.63	9.94	0.06	1.15
	6.10	0.16	5.94	0.24	6.63	-0.41	-	-	6.03	0.01	84.79	9.99	0.06	2.27
	6.11	0.12	6.00	0.25	6.68	-0.43	-	-	6.16	0.04	84.49	9.93	0.07	3.34
	6.03	0.13	6.03	0.21	6.73	-0.43	-	-	6.20	0.05	84.65	9.92	0.08	4.46
	5.99	0.16	6.11	0.29	6.75	-0.41	-	-	6.29	0.03	84.43	9.98	0.06	5.52
	5.99	0.14	6.23	0.27	6.83	-0.40	-	-	6.41	0.02	84.10	9.99	0.07	6.64

APPENDIX B

Table B.1 Measured forces, flow rates and positions (uncorrected), using 2110A and DCM160 ($\beta = 0\%$ and $U_\infty = 0.15$ m/s) at different positions of central cylinder.

	Tube '1'		Tube '2'		Tube '3'		Tube '4'		Tube 'C'		Q_a (Scfm)	Q_w (l/s)	y (mm)	x (mm)
	Drag (N)	Lift (N)	Drag (N)	Lift (N)	Drag (N)	Lift (N)	Drag (N)	Lift (N)	Drag (N)	Drag (N)				
Zero	-0.01	0.00	-0.03	0.00	-0.02	-0.01	-0.04	0.00	0.00	0.00	-0.16	0.00	-0.01	-0.01
Buoyancy	2.14	-0.09	2.12	0.02	2.15	-0.02	2.10	0.06	2.44	0.28	-0.15	0.03	0.04	-0.03
Normal tests	2.78	-0.15	2.73	0.06	2.49	-0.08	2.75	-0.01	2.75	0.33	0.01	5.85	-5.53	0.01
	2.80	-0.15	2.73	0.06	2.50	-0.08	2.76	-0.01	2.75	0.32	-0.25	5.92	-4.66	-0.02
	2.79	-0.14	2.74	0.05	2.53	-0.08	2.76	0.00	2.76	0.32	-0.11	5.87	-3.70	-0.01
	2.80	-0.14	2.75	0.05	2.52	-0.09	2.74	-0.01	2.75	0.33	-0.12	5.85	-2.78	-0.01
	2.80	-0.12	2.75	0.05	2.53	-0.08	2.74	0.01	2.76	0.32	-0.19	5.89	-1.89	-0.01
	2.79	-0.11	2.75	0.05	2.54	-0.07	2.73	0.02	2.76	0.34	-0.27	5.85	-0.93	0.00
	2.79	-0.12	2.74	0.03	2.55	-0.10	2.73	0.07	2.77	0.35	0.04	5.87	0.04	-0.01
	2.79	-0.12	2.74	0.03	2.54	-0.10	2.72	0.10	2.77	0.35	-0.15	5.88	0.91	-0.01
	2.78	-0.13	2.74	0.04	2.52	-0.11	2.72	0.11	2.76	0.34	-0.09	5.87	1.88	-0.01
	2.79	-0.11	2.75	0.03	2.52	-0.12	2.75	0.11	2.76	0.35	0.16	5.85	2.81	-0.02
	2.79	-0.12	2.74	0.02	2.50	-0.12	2.75	0.11	2.76	0.36	0.15	5.83	3.83	0.00
	2.80	-0.10	2.73	0.00	2.50	-0.14	2.76	0.13	2.75	0.36	0.09	5.83	4.69	0.00
	2.79	-0.09	2.74	0.00	2.49	-0.13	2.75	0.13	2.75	0.36	-0.08	5.84	5.59	0.00
	2.81	-0.12	2.71	0.02	2.58	-0.05	2.71	0.04	2.74	0.33	-0.24	5.81	0.02	-5.68
	2.80	-0.11	2.72	0.02	2.57	-0.05	2.71	0.02	2.74	0.34	0.03	5.78	0.01	-4.75
	2.80	-0.13	2.73	0.01	2.56	-0.06	2.70	0.03	2.74	0.33	-0.12	5.81	0.04	-3.80
	2.80	-0.12	2.71	0.01	2.53	-0.07	2.72	0.04	2.74	0.33	-0.03	5.83	0.04	-2.86
	2.79	-0.12	2.72	0.02	2.53	-0.08	2.73	0.05	2.75	0.34	-0.14	5.84	0.03	-1.90
	2.79	-0.12	2.73	0.02	2.53	-0.08	2.73	0.05	2.75	0.33	-0.05	5.83	0.07	-0.96
	2.80	-0.11	2.74	0.02	2.51	-0.09	2.73	0.03	2.75	0.33	0.07	5.81	0.09	0.00
	2.79	-0.12	2.74	0.02	2.51	-0.11	2.74	0.05	2.76	0.34	-0.15	5.86	0.05	0.94
	2.78	-0.13	2.75	0.03	2.51	-0.10	2.74	0.04	2.77	0.33	-0.01	5.84	0.03	1.88
	2.78	-0.12	2.74	0.03	2.52	-0.10	2.74	0.05	2.78	0.33	-0.21	5.82	0.09	2.86
	2.78	-0.13	2.74	0.04	2.52	-0.10	2.74	0.05	2.79	0.32	0.01	5.85	0.06	3.76
	2.76	-0.12	2.75	0.03	2.51	-0.12	2.75	0.03	2.80	0.31	-0.18	5.85	0.04	4.70
	2.76	-0.11	2.75	0.03	2.52	-0.12	2.74	0.03	2.82	0.30	0.00	5.78	0.03	5.64

Table B.2 Measured forces, flow rates and positions (uncorrected), using 2110A and DCM160 ($\beta = 0\%$ and $U_\infty = 0.63$ m/s) at different positions of central cylinder.

	Tube '1'		Tube '2'		Tube '3'		Tube '4'		Tube 'C'		Q_a (Scfm)	Q_w (l/s)	y (mm)	x (mm)
	Drag (N)	Lift (N)	Drag (N)	Lift (N)	Drag (N)	Lift (N)	Drag (N)	Lift (N)	Drag (N)	Drag (N)				
Zero	0.01	-0.01	0.00	0.00	-0.02	0.00	-0.01	-0.01	0.00	0.00	-0.38	-0.04	0.02	-0.02
Buoyancy	2.39	-0.10	2.23	-0.01	2.22	-0.12	2.17	0.03	2.40	0.28	0.45	0.16	0.02	0.06
Normal tests	7.79	0.04	7.86	0.02	6.55	-0.75	7.70	-0.50	6.74	0.07	0.12	23.74	-5.54	0.07
	7.81	0.03	7.83	-0.13	6.56	-0.81	7.63	-0.44	6.83	-0.01	0.32	23.75	-4.63	0.06
	7.91	-0.01	7.81	-0.03	6.59	-0.74	7.59	-0.41	6.90	-0.01	0.23	23.72	-3.64	0.09
	7.85	-0.12	7.76	-0.14	6.62	-0.81	7.60	-0.24	6.96	0.16	0.17	23.74	-2.73	0.09
	7.85	-0.12	7.76	-0.18	6.63	-0.76	7.58	-0.21	7.02	0.31	-0.02	23.75	-1.83	0.10
	7.88	-0.18	7.70	-0.21	6.66	-0.80	7.51	-0.04	7.04	0.40	0.08	23.72	-0.87	0.10
	7.81	-0.27	7.67	-0.34	6.66	-0.82	7.52	0.00	7.10	0.60	0.32	23.70	0.07	0.11
	7.84	-0.40	7.61	-0.25	6.67	-0.83	7.55	0.14	7.14	0.85	0.05	23.70	1.04	0.11
	7.75	-0.43	7.52	-0.29	6.65	-0.83	7.55	0.20	7.12	0.96	0.33	23.72	1.99	0.13
	7.74	-0.47	7.46	-0.31	6.61	-0.89	7.61	0.43	7.08	1.03	0.31	23.75	2.90	0.14
	7.68	-0.52	7.44	-0.34	6.57	-0.85	7.67	0.44	7.05	1.09	0.36	23.71	3.80	0.12
	7.65	-0.62	7.36	-0.33	6.60	-0.86	7.75	0.56	7.02	0.99	0.25	23.77	4.76	0.14
	7.52	-0.64	7.26	-0.40	6.56	-0.82	7.78	0.56	6.94	0.84	0.35	23.73	5.69	0.13
	7.80	-0.19	7.50	-0.02	7.21	-0.44	7.24	0.02	6.59	0.76	0.20	23.69	0.16	-5.45
	7.77	-0.20	7.53	-0.11	7.13	-0.54	7.30	0.01	6.60	0.79	0.18	23.70	0.18	-4.54
	7.80	-0.22	7.58	-0.15	7.11	-0.60	7.35	-0.08	6.71	0.71	0.12	23.70	0.12	-3.61
	7.82	-0.25	7.59	-0.16	6.95	-0.62	7.36	-0.02	6.77	0.72	0.27	23.69	0.16	-2.67
	7.84	-0.23	7.67	-0.29	6.89	-0.72	7.45	-0.01	6.87	0.63	0.34	23.74	0.20	-1.73
	7.79	-0.20	7.66	-0.32	6.75	-0.82	7.43	0.00	6.95	0.61	0.38	23.70	0.14	-0.77
	7.82	-0.20	7.66	-0.35	6.68	-0.82	7.51	-0.04	7.13	0.56	0.34	23.72	0.14	0.22
	7.76	-0.17	7.71	-0.39	6.61	-0.94	7.57	0.01	7.28	0.54	0.25	23.71	0.18	1.13
	7.80	-0.21	7.76	-0.36	6.50	-0.94	7.61	0.03	7.40	0.52	0.38	23.77	0.19	2.10
	7.72	-0.24	7.74	-0.37	6.40	-0.97	7.65	-0.02	7.53	0.46	0.08	23.71	0.18	3.06
	7.67	-0.27	7.78	-0.35	6.33	-1.03	7.67	-0.02	7.67	0.26	0.38	23.70	0.18	4.01
	7.55	-0.30	7.78	-0.44	6.22	-1.11	7.75	-0.03	7.80	0.11	0.49	23.71	0.22	4.91
	7.44	-0.25	7.83	-0.38	6.15	-1.13	7.74	-0.07	7.96	-0.13	0.14	23.69	0.24	5.88

Table B.3 Measured forces, flow rates and positions (uncorrected), using 2110A and DCM160 ($\beta = 21\%$ and $U_\infty = 0.62$ m/s) at different positions of central cylinder.

	Tube '1'		Tube '2'		Tube '3'		Tube '4'		Tube 'C'		Q_a	Q_w	y	x
	Drag (N)	Lift (N)	Drag (N)	Lift (N)	Drag (N)	Lift (N)	Drag (N)	Lift (N)	Drag (N)	Lift (N)	(Scfm)	(l/s)	(mm)	(mm)
Zero	0.00	0.00	0.01	0.00	0.01	0.01	0.00	0.01	0.00	0.00	-0.10	-0.14	-0.08	0.03
Buoyancy	2.36	-0.07	2.34	-0.07	2.29	-0.10	2.17	0.06	2.47	0.26	-0.02	-0.17	-0.10	0.03
Normal tests	7.16	-0.23	6.67	0.14	5.85	-0.31	6.61	-0.17	6.31	0.36	10.36	18.58	-5.63	0.03
	7.17	-0.21	6.65	0.16	5.87	-0.31	6.59	-0.10	6.30	0.39	10.49	18.54	-4.70	0.04
	7.21	-0.20	6.67	0.11	5.90	-0.33	6.55	-0.09	6.26	0.39	10.60	18.49	-3.81	0.03
	7.26	-0.18	6.68	0.17	5.97	-0.31	6.54	0.02	6.26	0.47	10.72	18.51	-2.94	0.03
	7.25	-0.18	6.59	0.11	5.97	-0.33	6.49	0.12	6.24	0.49	10.59	18.46	-1.95	0.02
	7.19	-0.15	6.58	0.09	6.01	-0.33	6.50	0.25	6.22	0.60	10.66	18.43	-1.02	0.03
	7.13	-0.14	6.50	0.10	5.94	-0.37	6.45	0.32	6.19	0.71	10.14	18.42	-0.04	0.03
	7.10	-0.15	6.52	0.08	5.96	-0.35	6.48	0.37	6.23	0.75	10.10	18.46	0.91	0.02
	7.06	-0.19	6.49	0.17	5.87	-0.36	6.47	0.45	6.23	0.77	10.13	18.37	1.80	0.03
	7.08	-0.20	6.51	0.12	5.82	-0.40	6.52	0.60	6.30	0.80	10.19	18.38	2.72	0.02
	7.10	-0.23	6.47	0.19	5.78	-0.35	6.58	0.61	6.32	0.80	10.13	18.42	3.67	0.04
	7.08	-0.22	6.41	0.08	5.74	-0.38	6.63	0.62	6.33	0.81	10.12	18.39	4.61	0.03
	7.09	-0.23	6.39	0.03	5.67	-0.38	6.66	0.58	6.33	0.73	9.81	18.39	5.49	0.02
	7.27	-0.19	6.20	0.10	6.35	-0.23	6.24	0.36	5.92	0.79	9.86	18.37	-0.02	-5.65
	7.24	-0.18	6.20	0.08	6.24	-0.27	6.28	0.37	5.94	0.83	9.65	18.37	-0.05	-4.69
	7.18	-0.16	6.25	0.07	6.21	-0.29	6.30	0.32	5.96	0.79	9.47	18.37	-0.03	-3.70
	7.20	-0.16	6.34	0.09	6.17	-0.29	6.35	0.33	6.00	0.77	10.00	18.34	-0.02	-2.85
	7.19	-0.18	6.39	0.10	6.07	-0.32	6.39	0.32	6.06	0.75	10.24	18.42	-0.07	-1.87
	7.19	-0.14	6.47	0.12	6.04	-0.32	6.43	0.31	6.14	0.73	10.31	18.37	-0.04	-0.95
	7.14	-0.14	6.51	0.13	5.97	-0.37	6.45	0.29	6.18	0.70	10.38	18.39	-0.04	0.04
	7.07	-0.15	6.53	0.11	5.85	-0.40	6.48	0.33	6.26	0.70	10.29	18.40	-0.05	1.00
	7.04	-0.15	6.62	0.08	5.86	-0.38	6.49	0.28	6.37	0.66	10.41	18.34	-0.04	1.91
	6.99	-0.14	6.67	0.12	5.80	-0.40	6.55	0.30	6.45	0.55	10.41	18.38	-0.05	2.86
	6.94	-0.13	6.73	0.11	5.74	-0.41	6.57	0.29	6.55	0.48	10.53	18.40	-0.06	3.79
	6.88	-0.18	6.78	0.15	5.68	-0.44	6.56	0.26	6.67	0.43	10.25	18.36	-0.05	4.73
	6.83	-0.22	6.80	0.14	5.63	-0.46	6.58	0.26	6.77	0.37	10.35	18.37	-0.06	5.70

Table B.4 Measured forces, flow rates and positions (uncorrected), using 2110A and DCM160 ($\beta = 30\%$ and $U_\infty = 0.62$ m/s) at different positions of central cylinder.

	Tube '1'		Tube '2'		Tube '3'		Tube '4'		Tube 'C'		Q_a	Q_w	y	x
	Drag (N)	Lift (N)	Drag (N)	Lift (N)	Drag (N)	Lift (N)	Drag (N)	Lift (N)	Drag (N)	Lift (N)	(Scfm)	(l/s)	(mm)	(mm)
Zero	0.01	0.02	0.00	-0.04	-0.03	0.04	-0.04	-0.03	0.08	-0.01	-0.05	0.03	0.08	0.02
Buoyancy	2.33	-0.02	2.30	-0.06	2.23	-0.06	2.06	0.04	2.36	0.25	-0.04	0.03	0.03	0.01
Normal tests	6.44	-0.14	5.94	0.11	5.20	-0.18	5.85	-0.11	5.80	0.38	14.67	16.55	-5.60	0.01
	6.43	-0.13	5.96	0.13	5.25	-0.20	5.81	-0.11	5.72	0.38	14.93	16.55	-4.59	-0.01
	6.39	-0.13	5.92	0.12	5.27	-0.19	5.75	-0.09	5.65	0.42	14.66	16.53	-3.67	-0.01
	6.39	-0.10	5.91	0.12	5.32	-0.21	5.72	-0.06	5.60	0.44	14.51	16.52	-2.82	-0.01
	6.38	-0.05	5.86	0.11	5.31	-0.20	5.68	0.06	5.56	0.48	14.58	16.46	-1.87	-0.01
	6.40	-0.03	5.83	0.11	5.32	-0.22	5.68	0.17	5.56	0.55	14.77	16.49	-0.92	-0.02
	6.37	-0.04	5.87	0.10	5.34	-0.23	5.70	0.24	5.58	0.57	14.93	16.47	0.05	-0.03
	6.40	-0.03	5.87	0.12	5.30	-0.24	5.72	0.30	5.62	0.63	15.04	16.46	0.97	-0.02
	6.33	-0.02	5.91	0.14	5.26	-0.22	5.72	0.39	5.69	0.65	15.12	16.44	1.86	-0.02
	6.35	-0.04	5.91	0.13	5.23	-0.22	5.77	0.46	5.78	0.70	15.22	16.40	2.82	-0.01
	6.41	-0.05	5.94	0.11	5.18	-0.20	5.81	0.47	5.85	0.71	15.33	16.41	3.73	-0.01
	6.46	-0.05	5.89	0.07	5.13	-0.19	5.89	0.45	5.90	0.69	15.36	16.41	4.67	-0.02
	6.49	-0.08	5.89	0.00	5.08	-0.16	5.94	0.40	5.98	0.64	15.59	16.41	5.61	-0.01
	6.55	-0.10	5.57	0.07	5.62	-0.14	5.49	0.27	5.41	0.63	14.85	16.42	0.02	-5.62
	6.54	-0.08	5.60	0.09	5.56	-0.15	5.55	0.30	5.41	0.64	14.91	16.40	-0.01	-4.68
	6.49	-0.06	5.61	0.12	5.51	-0.18	5.56	0.29	5.41	0.64	15.06	16.40	-0.01	-3.71
	6.49	-0.06	5.70	0.11	5.46	-0.20	5.61	0.27	5.44	0.62	15.09	16.42	-0.07	-2.82
	6.45	-0.03	5.77	0.10	5.42	-0.19	5.63	0.28	5.48	0.61	14.79	16.38	0.11	-1.86
	6.48	-0.04	5.81	0.10	5.39	-0.22	5.71	0.26	5.56	0.63	15.10	16.53	0.06	-0.90
	6.42	-0.05	5.92	0.09	5.37	-0.23	5.72	0.24	5.62	0.59	14.88	16.49	0.02	0.06
	6.36	-0.02	5.91	0.10	5.32	-0.24	5.75	0.23	5.66	0.57	14.67	16.56	0.04	0.99
	6.36	-0.04	5.97	0.13	5.24	-0.24	5.79	0.27	5.74	0.55	15.84	16.52	0.08	1.99
	6.28	-0.02	6.07	0.10	5.22	-0.27	5.80	0.22	5.83	0.52	15.56	16.48	0.02	2.95
	6.23	-0.04	6.10	0.13	5.17	-0.28	5.82	0.21	5.88	0.46	15.37	16.52	0.03	3.82
	6.17	-0.04	6.18	0.12	5.12	-0.30	5.84	0.22	5.96	0.44	15.38	16.53	0.06	4.78
	6.13	-0.04	6.25	0.12	5.12	-0.30	5.87	0.21	6.07	0.38	15.40	16.50	0.04	5.72

Table B.5 Measured forces, flow rates and positions (uncorrected), using 2110A and DCM160 ($\beta = 31\%$ and $U_\infty = 0.75$ m/s) at different positions of central cylinder.

	Tube '1'		Tube '2'		Tube '3'		Tube '4'		Tube 'C'		Q_a (Scfm)	Q_w (l/s)	y (mm)	x (mm)
	Drag (N)	Lift (N)	Drag (N)	Lift (N)	Drag (N)	Lift (N)	Drag (N)	Lift (N)	Drag (N)	Drag (N)				
Zero	-0.01	0.00	-0.01	0.01	-0.01	0.00	-0.01	0.00	0.00	0.00	0.02	-0.01	-0.05	0.02
Buoyancy	2.33	-0.10	2.31	-0.06	2.24	-0.11	2.13	0.04	2.40	0.25	0.03	0.00	-0.05	0.04
Normal tests	8.44	-0.17	7.73	0.23	6.67	-0.24	7.40	-0.08	7.35	0.49	18.14	19.73	-5.60	0.03
	8.39	-0.18	7.63	0.23	6.66	-0.21	7.30	-0.10	7.24	0.52	18.49	19.75	-4.70	0.00
	8.43	-0.15	7.65	0.26	6.75	-0.23	7.27	-0.07	7.16	0.57	18.59	19.76	-3.80	0.02
	8.41	-0.10	7.61	0.22	6.80	-0.22	7.23	-0.01	7.08	0.61	18.82	19.79	-2.83	0.01
	8.42	-0.05	7.62	0.21	6.80	-0.25	7.21	0.16	7.03	0.66	18.92	19.71	-1.93	0.00
	8.45	-0.03	7.53	0.22	6.79	-0.24	7.20	0.33	7.03	0.73	19.05	19.64	-0.96	0.00
	8.44	-0.01	7.61	0.25	6.79	-0.25	7.23	0.40	7.04	0.75	19.11	19.67	0.01	-0.01
	8.38	0.03	7.58	0.26	6.71	-0.27	7.20	0.47	7.06	0.80	18.49	19.65	0.91	0.00
	8.41	0.06	7.61	0.30	6.67	-0.24	7.27	0.62	7.20	0.80	18.62	19.67	1.82	0.00
	8.42	0.05	7.64	0.30	6.60	-0.27	7.32	0.68	7.30	0.83	18.66	19.65	2.79	0.00
	8.46	0.04	7.61	0.21	6.53	-0.19	7.39	0.68	7.40	0.82	18.78	19.67	3.74	0.01
	8.52	0.00	7.61	0.14	6.46	-0.17	7.44	0.65	7.49	0.80	18.88	19.64	4.62	0.00
	8.55	-0.07	7.58	0.04	6.39	-0.16	7.54	0.56	7.62	0.73	18.72	19.65	5.58	0.00
	8.72	-0.08	7.20	0.23	7.27	-0.11	6.92	0.50	6.82	0.87	17.85	19.78	-0.02	-5.63
	8.69	-0.06	7.30	0.19	7.22	-0.16	7.00	0.44	6.85	0.85	18.16	19.80	-0.02	-4.69
	8.63	-0.04	7.35	0.21	7.13	-0.20	7.02	0.42	6.84	0.84	17.90	19.78	0.00	-3.74
	8.62	-0.01	7.36	0.20	7.06	-0.17	7.11	0.47	6.90	0.84	18.93	19.77	-0.02	-2.81
	8.58	0.02	7.50	0.22	7.01	-0.23	7.15	0.43	6.95	0.82	18.13	19.81	0.06	-1.84
	8.50	-0.01	7.53	0.21	6.88	-0.27	7.17	0.39	7.00	0.80	18.10	19.78	0.02	-0.92
	8.44	0.01	7.60	0.21	6.81	-0.29	7.21	0.40	7.06	0.77	18.03	19.81	0.05	0.05
	8.40	0.01	7.70	0.22	6.77	-0.30	7.25	0.40	7.16	0.75	17.98	19.78	0.02	0.97
	8.32	0.04	7.73	0.24	6.66	-0.30	7.28	0.38	7.24	0.72	17.93	19.79	0.04	1.95
	8.25	0.02	7.83	0.24	6.62	-0.31	7.30	0.38	7.32	0.66	17.86	19.79	0.04	2.89
	8.17	0.04	7.90	0.22	6.55	-0.34	7.33	0.36	7.47	0.65	18.00	19.75	0.08	3.89
	8.11	0.02	7.95	0.23	6.48	-0.37	7.34	0.33	7.59	0.62	17.97	19.77	0.07	4.78
	8.06	0.03	8.05	0.25	6.43	-0.36	7.37	0.34	7.75	0.54	18.02	19.76	0.04	5.74

Table B.6 Measured forces, flow rates and positions (uncorrected), using 2110A and DCM160 ($\beta = 40\%$ and $U_\infty = 0.44$ m/s) at different positions of central cylinder.

	Tube '1'		Tube '2'		Tube '3'		Tube '4'		Tube 'C'		Q_a (Scfm)	Q_w (l/s)	y (mm)	x (mm)
	Drag (N)	Lift (N)	Drag (N)	Lift (N)	Drag (N)	Lift (N)	Drag (N)	Lift (N)	Drag (N)	Drag (N)				
Zero	-0.02	0.01	-0.01	0.00	0.00	0.02	-0.01	0.00	0.00	0.00	-0.03	0.05	0.02	0.00
Buoyancy	2.33	-0.04	2.32	-0.02	2.25	-0.06	2.05	0.10	2.44	0.24	-0.02	-0.01	-0.02	-0.02
Normal tests	3.80	-0.21	3.53	0.00	3.24	-0.18	3.76	-0.02	3.85	0.49	14.39	9.93	-5.62	-0.07
	3.80	-0.20	3.52	0.02	3.26	-0.19	3.76	-0.01	3.83	0.47	14.34	9.90	-4.71	-0.07
	3.77	-0.21	3.49	0.03	3.25	-0.18	3.71	-0.03	3.78	0.44	14.43	9.86	-3.76	-0.07
	3.70	-0.24	3.47	0.04	3.25	-0.17	3.67	-0.01	3.73	0.39	14.42	9.78	-2.85	-0.09
	3.72	-0.22	3.47	0.03	3.26	-0.17	3.65	0.04	3.72	0.35	14.04	9.81	-1.92	-0.09
	3.79	-0.23	3.50	0.03	3.32	-0.19	3.72	0.10	3.78	0.35	14.54	9.98	-1.02	-0.08
	3.76	-0.23	3.50	0.04	3.29	-0.18	3.68	0.16	3.76	0.34	14.28	9.93	-0.01	-0.09
	3.77	-0.24	3.48	0.06	3.27	-0.21	3.71	0.26	3.79	0.34	14.06	9.94	0.89	-0.09
	3.74	-0.24	3.45	0.04	3.22	-0.22	3.70	0.29	3.78	0.32	13.92	9.90	1.83	-0.10
	3.80	-0.23	3.47	0.03	3.20	-0.23	3.76	0.29	3.82	0.29	13.90	9.88	2.73	-0.10
	3.82	-0.21	3.48	0.02	3.19	-0.24	3.76	0.28	3.85	0.28	14.15	9.86	3.65	-0.10
	3.82	-0.22	3.46	-0.02	3.16	-0.27	3.79	0.26	3.85	0.22	14.29	9.86	4.61	-0.09
	3.84	-0.22	3.45	-0.02	3.14	-0.28	3.82	0.24	3.86	0.20	14.58	9.89	5.57	-0.08
	3.88	-0.27	3.38	0.02	3.43	-0.12	3.66	0.12	3.71	0.37	14.41	10.05	-0.01	-5.69
	3.88	-0.28	3.42	0.02	3.42	-0.15	3.66	0.15	3.75	0.37	14.34	9.99	-0.01	-4.77
	3.84	-0.26	3.43	0.03	3.39	-0.15	3.67	0.16	3.73	0.36	14.43	9.99	-0.05	-3.81
	3.84	-0.28	3.42	0.05	3.34	-0.18	3.69	0.15	3.72	0.35	14.41	10.04	-0.05	-2.89
	3.82	-0.27	3.45	0.05	3.33	-0.18	3.70	0.13	3.75	0.34	14.54	9.99	-0.03	-1.93
	3.81	-0.28	3.47	0.03	3.32	-0.19	3.72	0.13	3.76	0.32	14.63	9.97	-0.08	-1.02
	3.77	-0.27	3.46	0.04	3.28	-0.21	3.71	0.15	3.77	0.31	14.45	9.90	-0.08	-0.06
	3.79	-0.24	3.53	0.05	3.31	-0.22	3.75	0.13	3.83	0.32	14.62	10.01	-0.03	0.90
	3.76	-0.27	3.52	0.04	3.25	-0.23	3.76	0.15	3.85	0.31	14.33	10.05	-0.02	1.82
	3.72	-0.26	3.54	0.07	3.25	-0.22	3.75	0.14	3.87	0.31	14.05	10.00	-0.05	2.79
	3.67	-0.27	3.54	0.06	3.20	-0.23	3.72	0.14	3.87	0.28	13.90	9.96	-0.04	3.73
	3.63	-0.26	3.56	0.06	3.22	-0.24	3.75	0.15	3.91	0.29	13.69	9.98	-0.06	4.67
	3.59	-0.25	3.56	0.07	3.18	-0.26	3.75	0.15	3.93	0.26	13.84	10.00	-0.07	5.61

Table B.7 Measured forces, flow rates and positions (uncorrected), using 2110A and DCM160 ($\beta = 41\%$ and $U_\infty = 0.31$ m/s) at different positions of central cylinder.

	Tube '1'		Tube '2'		Tube '3'		Tube '4'		Tube 'C'		Q_a (Scfm)	Q_w (l/s)	y (mm)	x (mm)
	Drag (N)	Lift (N)	Drag (N)	Lift (N)	Drag (N)	Lift (N)	Drag (N)	Lift (N)	Drag (N)	Drag (N)				
Zero	-0.01	0.00	0.00	-0.01	0.00	0.01	0.00	0.00	0.00	0.00	-0.04	-0.01	0.00	0.02
Buoyancy	2.44	-0.15	2.30	-0.01	2.28	-0.11	2.15	0.05	2.48	0.27	-0.07	-0.01	0.02	0.06
Normal tests	3.07	-0.23	2.87	0.01	2.74	-0.21	3.12	-0.03	3.10	0.43	10.58	7.00	-5.51	0.10
	3.06	-0.23	2.90	0.01	2.77	-0.23	3.11	-0.01	3.10	0.42	10.72	7.02	-4.62	0.10
	3.07	-0.24	2.87	0.01	2.74	-0.23	3.12	-0.02	3.08	0.40	10.16	6.98	-3.70	0.09
	3.06	-0.23	2.88	0.01	2.76	-0.24	3.10	-0.02	3.07	0.39	10.22	6.97	-2.71	0.10
	3.04	-0.25	2.88	0.02	2.76	-0.23	3.09	0.02	3.05	0.36	10.21	6.97	-1.81	0.10
	3.03	-0.24	2.88	0.01	2.76	-0.23	3.06	0.04	3.06	0.36	10.26	6.95	-0.89	0.10
	3.03	-0.23	2.88	0.02	2.76	-0.23	3.06	0.09	3.06	0.34	10.28	6.91	0.02	0.10
	3.05	-0.23	2.90	0.02	2.76	-0.23	3.06	0.13	3.07	0.32	10.31	6.95	1.04	0.11
	3.04	-0.24	2.88	0.01	2.72	-0.24	3.08	0.14	3.07	0.30	10.32	6.94	1.94	0.13
	3.06	-0.25	2.88	0.02	2.71	-0.27	3.12	0.16	3.07	0.26	10.28	6.92	2.89	0.11
	3.04	-0.23	2.90	0.03	2.72	-0.25	3.10	0.18	3.06	0.27	9.94	6.92	3.82	0.12
	3.05	-0.23	2.86	0.00	2.67	-0.29	3.12	0.15	3.09	0.24	9.78	6.88	4.74	0.11
	3.07	-0.22	2.88	-0.03	2.67	-0.30	3.13	0.15	3.11	0.24	9.70	6.83	5.66	0.11
	3.16	-0.26	2.84	0.00	2.83	-0.20	3.06	0.11	3.04	0.34	9.97	7.05	0.10	-5.55
	3.17	-0.28	2.86	-0.01	2.84	-0.21	3.10	0.06	3.05	0.34	10.10	7.09	0.08	-4.61
	3.14	-0.25	2.87	-0.03	2.83	-0.21	3.08	0.10	3.05	0.34	10.27	7.07	0.06	-3.66
	3.14	-0.24	2.92	-0.02	2.85	-0.23	3.09	0.09	3.06	0.35	10.41	7.04	0.04	-2.72
	3.12	-0.25	2.88	0.01	2.80	-0.23	3.08	0.10	3.05	0.34	10.49	7.04	0.04	-1.83
	3.09	-0.24	2.91	0.00	2.80	-0.26	3.10	0.10	3.08	0.35	10.49	7.06	0.05	-0.86
	3.08	-0.26	2.89	-0.01	2.79	-0.26	3.09	0.07	3.07	0.34	10.66	7.06	0.09	0.13
	3.07	-0.25	2.92	0.01	2.79	-0.26	3.10	0.07	3.09	0.32	10.65	7.04	0.03	1.07
	3.06	-0.26	2.95	0.01	2.79	-0.28	3.12	0.08	3.12	0.32	10.67	7.10	0.05	2.00
	3.06	-0.23	2.95	0.03	2.78	-0.29	3.14	0.08	3.14	0.31	10.66	7.04	0.05	2.94
	3.04	-0.21	2.97	0.01	2.79	-0.29	3.13	0.08	3.15	0.30	10.67	7.08	0.07	3.87
	3.03	-0.25	2.93	0.01	2.74	-0.29	3.14	0.06	3.18	0.25	10.76	7.03	0.05	4.83
	3.02	-0.26	2.94	0.04	2.73	-0.30	3.14	0.07	3.21	0.24	10.72	7.07	0.04	5.77

Table B.8 Measured forces, flow rates and positions (uncorrected), using 2110A and DCM160 ($\beta = 51\%$ and $U_\infty = 0.62$ m/s) at different positions of central cylinder.

	Tube '1'		Tube '2'		Tube '3'		Tube '4'		Tube 'C'		Q_a (Scfm)	Q_w (l/s)	y (mm)	x (mm)
	Drag (N)	Lift (N)	Drag (N)	Lift (N)	Drag (N)	Lift (N)	Drag (N)	Lift (N)	Drag (N)	Drag (N)				
Zero	0.00	-0.01	0.00	-0.01	0.00	0.00	0.00	0.00	0.00	0.00	0.01	-0.02	-0.03	0.01
Buoyancy	2.25	-0.11	2.28	0.05	2.25	-0.07	2.16	0.10	2.50	0.25	0.05	-0.06	-0.01	0.01
Normal Tests	5.01	-0.27	4.65	0.04	4.33	-0.31	4.90	-0.02	4.83	0.65	25.81	11.68	-5.59	0.08
	4.97	-0.23	4.55	0.07	4.23	-0.27	4.83	-0.01	4.80	0.63	25.59	11.66	-4.63	0.08
	4.95	-0.25	4.53	0.05	4.27	-0.29	4.79	-0.03	4.73	0.59	25.28	11.62	-3.69	0.07
	4.89	-0.23	4.50	0.07	4.27	-0.25	4.73	-0.04	4.63	0.53	25.15	11.61	-2.75	0.04
	4.91	-0.23	4.50	0.07	4.30	-0.25	4.73	0.01	4.61	0.49	25.11	11.64	-1.87	0.04
	4.86	-0.20	4.39	0.08	4.19	-0.27	4.68	0.12	4.58	0.46	25.07	11.61	-0.92	0.08
	4.83	-0.18	4.43	0.07	4.20	-0.28	4.69	0.20	4.60	0.41	25.00	11.58	0.05	0.07
	4.85	-0.17	4.44	0.06	4.16	-0.28	4.70	0.32	4.65	0.39	24.94	11.59	1.01	0.08
	4.90	-0.17	4.44	0.07	4.11	-0.27	4.74	0.33	4.69	0.35	24.81	11.57	1.91	0.10
	4.92	-0.18	4.42	0.07	4.03	-0.29	4.76	0.33	4.73	0.31	24.95	11.57	2.82	0.07
	5.05	-0.18	4.66	0.05	4.17	-0.32	4.90	0.28	4.88	0.22	25.04	11.69	3.77	0.09
	5.08	-0.18	4.63	0.02	4.13	-0.33	4.92	0.26	4.92	0.19	25.28	11.68	4.70	0.10
	5.15	-0.20	4.69	-0.03	4.14	-0.37	4.99	0.20	4.98	0.13	26.21	11.69	5.66	0.10
	5.08	-0.24	4.38	0.04	4.52	-0.23	4.63	0.23	4.54	0.42	25.66	11.66	0.07	-5.58
	5.04	-0.23	4.33	0.02	4.40	-0.24	4.61	0.23	4.52	0.42	25.57	11.62	0.08	-4.66
	5.00	-0.23	4.39	0.03	4.41	-0.25	4.64	0.23	4.54	0.43	25.53	11.62	0.09	-3.72
	4.98	-0.23	4.37	0.04	4.32	-0.28	4.66	0.19	4.53	0.41	25.53	11.65	0.05	-2.77
	4.96	-0.20	4.35	0.05	4.25	-0.30	4.66	0.19	4.55	0.41	24.73	11.66	0.11	-1.80
	4.90	-0.22	4.42	0.06	4.24	-0.32	4.68	0.20	4.56	0.41	24.62	11.68	0.06	-0.87
	4.96	-0.19	4.49	0.09	4.24	-0.33	4.76	0.21	4.66	0.41	25.84	11.68	0.08	0.11
	4.85	-0.17	4.46	0.09	4.14	-0.34	4.73	0.20	4.66	0.42	24.98	11.65	0.06	1.06
	4.81	-0.18	4.51	0.09	4.14	-0.37	4.73	0.18	4.68	0.39	24.76	11.64	0.06	1.98
	4.79	-0.17	4.50	0.10	4.10	-0.36	4.77	0.21	4.73	0.38	24.69	11.65	0.06	2.92
	4.74	-0.18	4.60	0.09	4.11	-0.40	4.77	0.17	4.76	0.36	24.54	11.62	0.15	3.88
	4.71	-0.18	4.57	0.10	4.03	-0.41	4.78	0.18	4.82	0.37	24.79	11.62	0.09	4.81
	4.66	-0.19	4.68	0.10	4.08	-0.41	4.79	0.18	4.87	0.27	24.75	11.61	0.10	5.78

Table B.9 Measured forces, flow rates and positions (uncorrected), using 2110A and DCM160 ($\beta = 50\%$ and $U_\infty = 0.79$ m/s) at different positions of central cylinder.

	Tube '1'		Tube '2'		Tube '3'		Tube '4'		Tube 'C'		Q_a (Scfm)	Q_w (l/s)	y (mm)	x (mm)
	Drag (N)	Lift (N)	Drag (N)	Lift (N)	Drag (N)	Lift (N)	Drag (N)	Lift (N)	Drag (N)	Drag (N)				
Zero	-0.01	-0.02	0.00	-0.01	-0.01	0.00	0.01	-0.01	0.00	0.00	-0.23	0.04	-0.01	0.00
Buoyancy	2.24	-0.22	2.19	0.01	2.14	-0.07	2.11	0.03	2.48	0.26	-0.17	0.03	0.08	0.02
Normal Tests	6.76	-0.68	6.17	0.07	5.55	-0.46	6.69	-0.14	6.26	0.83	31.62	14.85	-5.50	0.02
	6.68	-0.70	6.10	0.06	5.56	-0.47	6.64	-0.17	6.16	0.80	31.00	14.84	-4.60	0.02
	6.69	-0.70	6.13	0.07	5.61	-0.48	6.65	-0.15	6.10	0.77	31.47	14.90	-3.68	0.03
	6.63	-0.69	6.07	0.04	5.64	-0.46	6.62	-0.13	5.99	0.72	31.97	14.86	-2.70	0.02
	6.67	-0.66	6.13	0.06	5.70	-0.48	6.61	-0.09	5.94	0.64	32.17	14.94	-1.82	0.09
	6.66	-0.64	6.11	0.09	5.69	-0.49	6.60	0.02	5.88	0.51	31.99	14.87	-0.82	0.09
	6.71	-0.60	6.15	0.12	5.66	-0.49	6.64	0.16	5.92	0.40	31.98	14.90	0.15	0.11
	6.74	-0.52	6.18	0.11	5.60	-0.50	6.65	0.30	6.02	0.32	31.94	14.91	1.04	0.11
	6.70	-0.57	6.22	0.09	5.53	-0.53	6.68	0.31	6.08	0.21	31.97	14.90	2.01	0.13
	6.79	-0.51	6.30	0.07	5.52	-0.55	6.75	0.28	6.20	0.15	31.71	14.94	2.97	0.15
	6.83	-0.45	6.29	0.05	5.44	-0.56	6.82	0.29	6.30	0.16	31.49	14.95	3.90	0.16
	6.86	-0.48	6.29	0.01	5.40	-0.57	6.87	0.22	6.40	0.14	31.39	14.90	4.86	0.16
	6.96	-0.49	6.36	-0.06	5.41	-0.60	6.99	0.14	6.52	0.14	32.33	14.95	5.83	0.17
	6.92	-0.65	5.81	0.09	5.92	-0.40	6.37	0.24	5.78	0.44	31.43	14.95	0.26	-5.48
	6.93	-0.65	5.90	0.05	5.92	-0.45	6.45	0.15	5.80	0.43	32.07	14.80	0.26	-4.53
	6.92	-0.61	5.95	0.07	5.85	-0.47	6.48	0.21	5.80	0.44	32.01	14.90	0.24	-3.62
	6.85	-0.58	6.01	0.08	5.82	-0.50	6.53	0.20	5.84	0.43	31.92	14.85	0.27	-2.66
	6.81	-0.60	6.02	0.11	5.74	-0.47	6.57	0.17	5.87	0.42	31.82	14.91	0.25	-1.73
	6.76	-0.60	6.09	0.09	5.71	-0.55	6.60	0.15	5.89	0.39	31.83	14.85	0.19	-0.78
	6.71	-0.57	6.13	0.13	5.64	-0.56	6.61	0.13	5.89	0.41	31.71	14.92	0.27	0.21
	6.66	-0.57	6.18	0.12	5.58	-0.58	6.64	0.17	5.95	0.39	31.62	14.87	0.30	1.15
	6.60	-0.56	6.24	0.15	5.54	-0.59	6.67	0.13	6.00	0.36	31.55	14.86	0.29	2.11
	6.52	-0.54	6.27	0.15	5.50	-0.64	6.67	0.13	6.03	0.31	31.61	14.82	0.30	3.05
	6.51	-0.53	6.34	0.15	5.47	-0.65	6.71	0.11	6.13	0.32	31.51	14.81	0.31	3.99
	6.44	-0.52	6.38	0.16	5.41	-0.65	6.73	0.13	6.19	0.30	31.70	14.82	0.31	4.93
	6.42	-0.55	6.49	0.18	5.45	-0.68	6.82	0.11	6.33	0.23	32.60	14.88	0.28	5.90

Table B.10 Measured forces, flow rates and positions (uncorrected), using 2110A and DCM160 ($\beta = 60\%$ and $U_\infty = 0.83$ m/s) at different positions of central cylinder.

	Tube '1'		Tube '2'		Tube '3'		Tube '4'		Tube 'C'		Q_a (Scfm)	Q_w (l/s)	y (mm)	x (mm)
	Drag (N)	Lift (N)	Drag (N)	Lift (N)	Drag (N)	Lift (N)	Drag (N)	Lift (N)	Drag (N)	Drag (N)				
Zero	-0.01	0.00	-0.02	-0.01	-0.03	-0.02	-0.03	0.00	0.00	0.00	-0.04	0.02	-0.01	0.01
Buoyancy	2.12	-0.17	2.13	0.00	1.95	-0.22	2.06	-0.01	2.52	0.27	-0.06	0.03	0.04	0.02
Normal tests	5.81	-0.47	5.56	-0.07	5.18	-0.56	5.79	-0.14	5.74	0.86	40.39	12.40	-5.54	0.03
	5.81	-0.46	5.64	-0.10	5.27	-0.57	5.80	-0.20	5.74	0.83	40.30	12.56	-4.63	0.03
	5.77	-0.42	5.62	-0.10	5.28	-0.54	5.76	-0.22	5.65	0.76	39.59	12.51	-3.70	0.02
	5.70	-0.40	5.57	-0.12	5.25	-0.50	5.67	-0.25	5.54	0.68	39.72	12.42	-2.75	0.02
	5.74	-0.34	5.61	-0.12	5.30	-0.53	5.72	-0.23	5.54	0.61	39.77	12.57	-1.82	0.03
	5.68	-0.32	5.57	-0.12	5.23	-0.52	5.62	-0.20	5.46	0.46	39.13	12.50	-0.93	0.00
	5.77	-0.28	5.67	-0.10	5.27	-0.55	5.68	-0.11	5.52	0.35	39.93	12.49	0.06	0.02
	5.77	-0.27	5.71	-0.10	5.23	-0.57	5.70	-0.04	5.55	0.20	40.44	12.51	0.96	0.06
	5.73	-0.24	5.73	-0.07	5.16	-0.54	5.71	-0.07	5.59	0.12	39.81	12.48	2.02	0.07
	5.78	-0.18	5.76	-0.09	5.11	-0.57	5.74	-0.07	5.65	0.07	40.35	12.38	2.92	0.07
	5.84	-0.15	5.84	-0.08	5.08	-0.56	5.81	-0.10	5.76	0.01	39.35	12.50	3.78	0.10
	5.97	-0.12	5.90	-0.16	5.08	-0.59	5.88	-0.16	5.89	0.02	39.97	12.59	4.76	0.10
	6.04	-0.09	5.95	-0.18	5.08	-0.60	5.95	-0.24	5.99	0.01	39.90	12.58	5.69	0.09
	5.98	-0.30	5.46	-0.14	5.53	-0.47	5.48	-0.10	5.41	0.31	39.78	12.55	0.10	-5.55
	5.97	-0.30	5.49	-0.16	5.48	-0.48	5.53	-0.10	5.41	0.33	39.61	12.61	0.04	-4.66
	5.94	-0.31	5.55	-0.15	5.46	-0.50	5.58	-0.15	5.43	0.30	39.99	12.50	0.10	-3.72
	5.92	-0.28	5.58	-0.12	5.40	-0.51	5.61	-0.08	5.45	0.35	39.91	12.53	0.12	-2.78
	5.86	-0.26	5.61	-0.13	5.34	-0.54	5.63	-0.06	5.46	0.33	39.60	12.53	0.11	-1.81
	5.80	-0.28	5.66	-0.14	5.34	-0.57	5.66	-0.10	5.49	0.30	40.55	12.55	0.13	-0.91
	5.76	-0.26	5.67	-0.13	5.25	-0.58	5.70	-0.12	5.53	0.32	40.88	12.53	0.12	0.07
	5.70	-0.28	5.75	-0.10	5.25	-0.59	5.69	-0.14	5.54	0.29	39.85	12.52	0.12	1.05
	5.63	-0.28	5.75	-0.10	5.17	-0.60	5.72	-0.13	5.59	0.29	39.63	12.47	0.16	1.98
	5.58	-0.27	5.78	-0.12	5.12	-0.64	5.72	-0.12	5.62	0.28	40.15	12.41	0.15	2.94
	5.57	-0.27	5.88	-0.12	5.15	-0.65	5.80	-0.13	5.72	0.24	40.07	12.52	0.12	3.87
	5.54	-0.26	5.92	-0.11	5.10	-0.65	5.83	-0.15	5.78	0.23	40.07	12.54	0.13	4.82
	5.49	-0.26	5.95	-0.05	5.03	-0.64	5.82	-0.14	5.86	0.23	39.86	12.50	0.16	5.74

Table B.11 Measured forces, flow rates and positions (uncorrected), using 2110A and DCM160 ($\beta = 61\%$ and $U_\infty = 1.05$ m/s) at different positions of central cylinder.

	Tube '1'		Tube '2'		Tube '3'		Tube '4'		Tube 'C'		Q_a (Scfm)	Q_w (l/s)	y (mm)	x (mm)
	Drag (N)	Lift (N)	Drag (N)	Lift (N)	Drag (N)	Lift (N)	Drag (N)	Lift (N)	Drag (N)	Drag (N)				
Zero	-0.03	0.00	-0.05	0.01	-0.01	-0.01	-0.02	-0.04	0.00	0.00	0.01	0.02	-0.07	-0.01
Buoyancy	2.07	0.00	2.21	0.03	2.20	-0.06	2.07	0.01	2.49	0.28	0.25	0.02	-0.06	-0.01
Normal tests	8.20	-0.63	7.70	-0.15	7.30	-0.76	8.27	-0.04	7.93	1.19	51.32	15.45	-5.65	-0.02
	8.12	-0.62	7.69	-0.20	7.37	-0.75	8.22	-0.15	7.79	1.11	51.15	15.54	-4.78	-0.02
	8.09	-0.51	7.71	-0.19	7.43	-0.70	8.20	-0.17	7.70	1.06	51.38	15.50	-3.84	-0.01
	7.97	-0.46	7.65	-0.21	7.41	-0.71	8.07	-0.24	7.49	0.92	50.68	15.52	-2.92	-0.01
	7.89	-0.35	7.58	-0.18	7.31	-0.66	7.97	-0.21	7.36	0.82	50.39	15.50	-1.96	-0.02
	8.01	-0.28	7.72	-0.16	7.41	-0.70	8.06	-0.19	7.39	0.62	51.62	15.45	-1.04	-0.01
	8.11	-0.19	7.86	-0.17	7.43	-0.72	8.13	-0.04	7.47	0.32	51.12	15.57	-0.13	0.00
	8.04	-0.15	7.88	-0.13	7.28	-0.70	8.07	0.04	7.45	0.13	50.67	15.56	0.83	0.00
	8.11	-0.06	8.00	-0.16	7.25	-0.71	8.16	0.04	7.58	0.02	50.98	15.56	1.77	0.01
	8.20	0.03	8.13	-0.21	7.23	-0.76	8.28	-0.01	7.76	-0.07	52.01	15.56	2.65	0.00
	8.32	0.14	8.19	-0.16	7.15	-0.65	8.32	-0.07	7.90	-0.09	51.93	15.53	3.63	0.01
	8.44	0.21	8.27	-0.21	7.12	-0.68	8.40	-0.14	8.04	-0.07	51.88	15.53	4.58	0.01
	8.49	0.22	8.25	-0.34	7.04	-0.75	8.45	-0.17	8.13	0.00	51.64	15.50	5.48	0.01
	8.35	-0.18	7.42	-0.18	7.71	-0.48	7.72	0.04	7.26	0.38	50.84	15.53	-0.08	-5.66
	8.27	-0.22	7.46	-0.24	7.64	-0.59	7.75	-0.01	7.22	0.34	50.76	15.51	-0.05	-4.74
	8.18	-0.19	7.50	-0.26	7.58	-0.65	7.81	0.00	7.21	0.35	50.20	15.44	-0.11	-3.81
	8.15	-0.20	7.54	-0.21	7.47	-0.65	7.83	0.00	7.22	0.33	49.87	15.53	-0.06	-2.86
	8.13	-0.24	7.65	-0.19	7.48	-0.67	7.94	-0.05	7.30	0.31	50.76	15.49	-0.13	-1.90
	8.05	-0.21	7.69	-0.18	7.39	-0.68	7.94	-0.07	7.28	0.29	50.60	15.49	-0.07	-0.99
	7.95	-0.18	7.67	-0.16	7.23	-0.69	7.92	0.00	7.32	0.32	49.63	15.48	-0.09	-0.01
	7.96	-0.17	7.83	-0.17	7.29	-0.76	8.06	-0.07	7.44	0.29	50.26	15.47	-0.07	0.96
	7.76	-0.20	7.77	-0.16	7.11	-0.75	7.97	-0.06	7.40	0.27	49.58	15.39	-0.09	1.88
	7.85	-0.16	8.00	-0.11	7.20	-0.79	8.17	-0.03	7.60	0.26	51.01	15.50	-0.08	2.83
	7.79	-0.15	8.09	-0.12	7.18	-0.82	8.24	-0.05	7.72	0.26	51.76	15.40	-0.10	3.77
	7.62	-0.16	8.05	-0.11	7.00	-0.82	8.13	-0.05	7.74	0.26	50.55	15.44	-0.06	4.74
	7.55	-0.15	8.08	-0.05	6.91	-0.82	8.10	-0.02	7.80	0.23	49.67	15.48	-0.10	5.67

Table B.12 Measured forces, flow rates and positions (uncorrected), using 2110A and DCM160 ($\beta = 70\%$ and $U_\infty = 0.90$ m/s) at different positions of central cylinder.

	Tube '1'		Tube '2'		Tube '3'		Tube '4'		Tube 'C'		Q_a (Scfm)	Q_w (l/s)	y (mm)	x (mm)
	Drag (N)	Lift (N)	Drag (N)	Lift (N)	Drag (N)	Lift (N)	Drag (N)	Lift (N)	Drag (N)	Drag (N)				
Zero	0.00	0.00	-0.01	0.01	0.00	0.00	-0.01	0.00	0.00	0.00	0.08	0.03	0.05	0.01
Buoyancy	2.28	-0.05	2.19	-0.01	2.22	-0.06	2.12	0.08	2.44	0.27	0.10	-0.01	0.01	-0.03
Normal tests	5.20	-0.37	4.84	0.04	4.57	-0.22	5.16	0.09	5.17	0.84	51.75	10.15	-5.52	-0.04
	5.13	-0.34	4.83	0.03	4.59	-0.19	5.14	0.08	5.13	0.81	50.95	10.06	-4.61	-0.06
	5.07	-0.27	4.79	0.03	4.56	-0.20	5.07	0.06	5.06	0.75	50.78	10.08	-3.69	-0.06
	5.01	-0.24	4.75	0.01	4.53	-0.16	5.02	0.02	4.97	0.67	49.99	10.03	-2.74	-0.03
	5.01	-0.23	4.79	0.02	4.56	-0.17	5.02	0.02	4.96	0.56	49.61	10.11	-1.86	-0.02
	5.00	-0.18	4.86	0.02	4.60	-0.18	5.01	0.00	4.94	0.45	50.97	10.06	-0.96	-0.04
	5.03	-0.17	4.85	0.04	4.56	-0.18	5.00	0.06	4.95	0.35	50.52	10.04	0.01	-0.03
	5.03	-0.14	4.87	0.04	4.52	-0.19	5.00	0.11	4.98	0.25	49.94	10.00	0.93	-0.01
	5.03	-0.13	4.92	0.06	4.48	-0.18	5.01	0.10	5.00	0.14	49.60	10.03	1.89	-0.01
	5.08	-0.08	4.98	0.08	4.46	-0.17	5.04	0.09	5.05	0.09	50.48	10.03	2.84	-0.01
	5.16	-0.03	5.06	0.06	4.46	-0.17	5.10	0.04	5.15	0.04	51.35	10.01	3.70	-0.02
	5.16	-0.01	4.97	0.07	4.33	-0.19	5.05	0.07	5.13	0.05	49.87	10.02	4.67	-0.02
	5.26	0.01	5.07	0.06	4.36	-0.17	5.12	0.02	5.23	0.04	50.87	9.97	5.63	-0.01
	5.18	-0.17	4.62	0.02	4.73	-0.08	4.81	0.07	4.81	0.32	50.81	10.00	0.07	-5.66
	5.16	-0.16	4.64	0.01	4.69	-0.10	4.84	0.10	4.82	0.33	49.86	9.99	0.05	-4.75
	5.14	-0.12	4.64	0.01	4.62	-0.11	4.85	0.08	4.84	0.36	49.72	10.00	0.06	-3.80
	5.14	-0.12	4.73	0.06	4.63	-0.10	4.90	0.10	4.85	0.36	49.99	9.95	0.06	-2.88
	5.12	-0.14	4.78	0.06	4.61	-0.12	4.96	0.06	4.88	0.32	50.88	10.00	0.03	-1.92
	5.11	-0.14	4.87	0.05	4.63	-0.15	5.00	0.06	4.92	0.31	52.48	9.98	0.07	-0.98
	5.04	-0.12	4.90	0.08	4.58	-0.15	5.04	0.08	4.96	0.32	51.77	10.01	0.05	0.00
	5.03	-0.12	4.89	0.08	4.52	-0.16	5.06	0.10	5.01	0.33	51.26	9.97	0.06	0.93
	4.99	-0.13	4.95	0.06	4.52	-0.20	5.10	0.09	5.03	0.32	51.44	9.97	0.03	1.87
	4.88	-0.11	4.93	0.08	4.44	-0.18	5.03	0.08	5.01	0.32	49.89	9.96	0.00	2.80
	4.79	-0.12	4.92	0.09	4.36	-0.20	4.98	0.06	5.00	0.30	49.87	9.85	0.03	3.74
	4.84	-0.13	5.02	0.09	4.38	-0.23	5.10	0.09	5.15	0.32	51.57	9.98	-0.02	4.70
	4.77	-0.13	5.08	0.12	4.38	-0.24	5.11	0.06	5.17	0.28	51.00	9.94	0.04	5.62

Table B.13 Measured forces, flow rates and positions (uncorrected), using 2110A and DCM160 ($\beta = 71\%$ and $U_\infty = 1.07$ m/s) at different positions of central cylinder.

	Tube '1'		Tube '2'		Tube '3'		Tube '4'		Tube 'C'		Q_a (Scfm)	Q_w (l/s)	y (mm)	x (mm)
	Drag (N)	Lift (N)	Drag (N)	Lift (N)	Drag (N)	Lift (N)	Drag (N)	Lift (N)	Drag (N)	Drag (N)				
Zero	-0.01	0.00	-0.01	-0.01	0.00	-0.01	-0.02	0.00	0.00	0.00	-0.04	0.01	0.03	0.00
Buoyancy	2.31	-0.04	2.35	-0.01	2.26	-0.07	2.08	0.09	2.51	0.28	-0.28	0.01	0.00	0.01
Normal tests	6.69	-0.73	6.36	0.08	6.09	-0.46	6.91	0.00	6.42	1.09	59.45	12.12	-5.59	-0.02
	6.58	-0.72	6.25	0.16	6.05	-0.47	6.88	0.01	6.28	1.03	59.53	11.93	-4.66	-0.03
	6.54	-0.61	6.30	0.17	6.13	-0.44	6.91	0.06	6.30	1.00	60.94	11.87	-3.73	0.05
	6.47	-0.52	6.30	0.13	6.14	-0.49	6.88	0.01	6.19	0.87	61.79	11.80	-2.76	0.05
	6.44	-0.45	6.31	0.15	6.13	-0.46	6.82	-0.04	6.11	0.72	60.77	11.84	-1.87	0.03
	6.41	-0.37	6.30	0.14	6.07	-0.45	6.78	-0.05	6.04	0.54	60.25	11.78	-0.91	0.01
	6.41	-0.29	6.30	0.14	6.00	-0.45	6.71	-0.02	6.01	0.36	59.88	11.75	0.06	0.00
	6.52	-0.25	6.50	0.20	6.05	-0.42	6.84	-0.04	6.11	0.16	62.42	11.76	0.99	0.02
	6.45	-0.20	6.48	0.20	5.92	-0.41	6.74	-0.08	6.09	0.05	60.19	11.72	1.93	0.03
	6.55	-0.08	6.58	0.20	5.88	-0.42	6.79	-0.09	6.22	-0.05	61.65	11.75	2.87	0.04
	6.58	0.00	6.57	0.23	5.76	-0.41	6.77	-0.08	6.27	-0.06	59.13	11.70	3.79	0.05
	6.64	0.07	6.57	0.26	5.68	-0.38	6.76	-0.10	6.31	-0.05	59.55	11.69	4.72	0.06
	6.86	0.11	6.73	0.19	5.76	-0.44	6.94	-0.19	6.50	-0.07	61.32	11.70	5.64	0.05
	6.61	-0.34	6.02	0.15	6.20	-0.31	6.40	-0.03	5.83	0.32	60.44	11.74	0.09	-5.60
	6.58	-0.33	6.06	0.15	6.20	-0.35	6.48	-0.05	5.83	0.33	59.20	11.72	0.04	-4.69
	6.62	-0.31	6.15	0.18	6.19	-0.34	6.59	-0.04	5.91	0.35	60.50	11.73	0.06	-3.75
	6.60	-0.29	6.22	0.15	6.18	-0.39	6.70	-0.04	5.97	0.35	62.28	11.69	0.09	-2.81
	6.48	-0.29	6.18	0.16	6.00	-0.39	6.57	-0.02	5.92	0.33	60.10	11.75	0.08	-1.85
	6.42	-0.30	6.22	0.19	5.98	-0.39	6.64	-0.01	5.94	0.32	60.72	11.71	0.01	-0.92
	6.44	-0.28	6.35	0.19	6.03	-0.43	6.74	-0.03	6.03	0.34	61.17	11.73	0.07	0.05
	6.29	-0.31	6.24	0.20	5.81	-0.42	6.64	-0.02	5.99	0.29	61.02	11.62	0.05	1.02
	6.25	-0.30	6.38	0.20	5.89	-0.46	6.73	-0.04	6.07	0.30	59.49	11.73	0.05	1.94
	6.24	-0.29	6.42	0.21	5.79	-0.46	6.76	-0.01	6.15	0.29	59.83	11.74	0.08	2.89
	6.15	-0.31	6.44	0.19	5.74	-0.50	6.74	-0.05	6.17	0.29	59.43	11.73	0.08	3.82
	6.13	-0.25	6.56	0.21	5.76	-0.52	6.85	0.00	6.31	0.32	60.74	11.70	0.09	4.77
	6.09	-0.24	6.59	0.25	5.67	-0.50	6.84	0.03	6.39	0.34	60.02	11.66	0.08	5.73

Table B.14 Measured forces, flow rates and positions (uncorrected), using 2110A and DCM160 ($\beta = 80\%$ and $U_\infty = 1.31$ m/s) at different positions of central cylinder.

	Tube '1'		Tube '2'		Tube '3'		Tube '4'		Tube 'C'		Q_a (Scfm)	Q_w (l/s)	y (mm)	x (mm)
	Drag (N)	Lift (N)	Drag (N)	Lift (N)	Drag (N)	Lift (N)	Drag (N)	Lift (N)	Drag (N)	Drag (N)				
Zero	-0.03	0.00	-0.01	-0.01	-0.02	0.01	-0.01	0.01	0.00	0.00	-0.06	-0.01	0.04	0.01
Buoyancy	2.20	-0.10	2.35	0.03	2.24	-0.09	2.10	0.06	2.44	0.27	-0.13	0.03	0.05	0.00
Normal tests	6.16	-0.78	5.58	0.23	5.45	-0.32	6.08	0.20	5.91	0.99	81.28	9.73	-5.58	0.01
	6.22	-0.77	5.69	0.17	5.62	-0.35	6.20	0.21	5.95	0.97	85.09	9.64	-4.69	0.01
	6.14	-0.65	5.72	0.14	5.66	-0.37	6.21	0.21	5.88	0.89	85.22	9.64	-3.72	-0.02
	6.06	-0.56	5.70	0.16	5.64	-0.37	6.18	0.16	5.81	0.81	85.63	9.62	-2.82	-0.02
	6.06	-0.46	5.75	0.16	5.66	-0.33	6.18	0.09	5.78	0.65	85.79	9.65	-1.87	0.03
	5.99	-0.34	5.76	0.16	5.62	-0.30	6.12	0.08	5.72	0.52	84.83	9.61	-0.94	0.02
	5.88	-0.30	5.71	0.17	5.52	-0.29	6.02	0.01	5.63	0.32	83.23	9.55	0.03	0.01
	6.03	-0.20	5.84	0.21	5.53	-0.27	6.09	0.00	5.74	0.19	81.43	9.72	0.93	0.01
	6.06	-0.10	5.92	0.23	5.48	-0.23	6.09	-0.01	5.76	0.08	82.32	9.72	1.90	0.02
	6.24	0.01	6.17	0.26	5.56	-0.24	6.23	-0.07	5.94	-0.03	84.83	9.74	2.78	0.02
	6.33	0.12	6.22	0.27	5.51	-0.24	6.24	-0.11	5.99	-0.09	84.73	9.74	3.83	0.02
	6.45	0.19	6.29	0.30	5.48	-0.25	6.29	-0.16	6.07	-0.13	84.90	9.72	4.67	0.03
	6.53	0.23	6.34	0.29	5.44	-0.26	6.31	-0.16	6.11	-0.14	85.38	9.67	5.62	0.03
	6.30	-0.30	5.62	0.15	5.92	-0.17	5.94	0.00	5.64	0.31	83.70	9.73	0.07	-5.63
	6.23	-0.28	5.64	0.13	5.86	-0.22	6.00	0.02	5.62	0.33	84.12	9.72	0.05	-4.69
	6.22	-0.31	5.66	0.12	5.80	-0.22	6.02	-0.01	5.64	0.30	83.15	9.73	0.04	-3.76
	6.12	-0.27	5.66	0.18	5.70	-0.22	5.99	0.01	5.61	0.31	81.93	9.75	0.04	-2.80
	6.10	-0.27	5.77	0.15	5.74	-0.28	6.09	-0.03	5.66	0.30	83.59	9.73	0.05	-1.86
	6.15	-0.27	5.82	0.18	5.69	-0.27	6.17	0.00	5.74	0.33	84.86	9.73	0.02	-0.92
	6.02	-0.27	5.85	0.16	5.66	-0.30	6.20	0.01	5.74	0.33	84.18	9.69	0.03	0.06
	5.99	-0.25	5.89	0.16	5.61	-0.33	6.23	0.01	5.79	0.34	85.30	9.65	0.04	0.96
	5.94	-0.25	5.91	0.17	5.51	-0.32	6.21	0.01	5.82	0.33	83.73	9.67	0.04	1.93
	5.90	-0.25	6.01	0.21	5.53	-0.32	6.25	0.02	5.86	0.32	84.63	9.70	0.07	2.90
	5.91	-0.22	6.13	0.24	5.50	-0.33	6.33	0.03	5.97	0.32	84.95	9.70	0.04	3.83
	5.83	-0.23	6.13	0.24	5.43	-0.35	6.34	0.02	6.02	0.33	84.56	9.74	0.05	4.74
	5.81	-0.20	6.22	0.24	5.44	-0.36	6.39	0.03	6.13	0.35	84.82	9.70	0.03	5.70

Table B.15 Measured forces, flow rates and positions (uncorrected), using 2110A and DCM160 ($\beta = 80\%$ and $U_\infty = 1.58$ m/s) at different positions of central cylinder.

	Tube '1'		Tube '2'		Tube '3'		Tube '4'		Tube 'C'		Q_a (Scfm)	Q_w (l/s)	y (mm)	x (mm)
	Drag (N)	Lift (N)	Drag (N)	Lift (N)	Drag (N)	Lift (N)	Drag (N)	Lift (N)	Drag (N)	Drag (N)				
Zero	-0.04	0.01	-0.03	0.02	-0.02	0.00	-0.02	0.01	0.00	0.00	-0.25	-0.01	0.05	0.02
Buoyancy	2.18	-0.03	2.20	0.02	2.26	-0.05	2.08	0.08	2.49	0.27	-0.22	-0.01	0.07	0.03
Normal tests	8.66	-1.27	7.66	0.25	7.91	-0.61	9.19	0.37	8.09	1.52	102.85	11.68	-5.51	0.02
	8.54	-1.21	7.66	0.24	7.94	-0.60	9.15	0.35	8.03	1.48	103.99	11.68	-4.54	0.03
	8.30	-1.03	7.58	0.19	7.85	-0.60	9.00	0.30	7.80	1.33	102.02	11.60	-3.65	0.01
	8.21	-0.83	7.60	0.16	7.86	-0.63	8.99	0.24	7.70	1.18	102.34	11.61	-2.70	0.04
	8.04	-0.63	7.54	0.19	7.70	-0.56	8.86	0.19	7.55	0.97	99.93	11.63	-1.82	0.03
	7.97	-0.43	7.55	0.16	7.66	-0.58	8.78	0.15	7.47	0.75	98.28	11.60	-0.82	0.02
	8.05	-0.29	7.70	0.21	7.65	-0.55	8.83	0.09	7.50	0.48	100.48	11.64	0.08	0.09
	8.18	-0.12	7.89	0.23	7.69	-0.54	8.96	0.05	7.61	0.26	101.65	11.57	1.02	0.09
	8.36	0.08	8.20	0.28	7.79	-0.54	9.10	-0.12	7.76	0.00	102.79	11.72	1.98	0.10
	8.43	0.25	8.27	0.35	7.65	-0.50	9.04	-0.11	7.80	-0.10	102.71	11.63	2.87	0.11
	8.62	0.39	8.43	0.38	7.63	-0.52	9.10	-0.19	7.95	-0.19	102.52	11.68	3.90	0.11
	8.69	0.47	8.45	0.42	7.45	-0.49	9.05	-0.21	7.95	-0.25	101.95	11.61	4.80	0.13
	8.86	0.54	8.55	0.37	7.42	-0.58	9.16	-0.25	8.08	-0.30	100.83	11.72	5.73	0.14
	8.51	-0.33	7.52	0.10	8.28	-0.48	8.79	0.07	7.50	0.46	102.92	11.68	0.14	-5.54
	8.42	-0.28	7.51	0.15	8.08	-0.44	8.73	0.09	7.42	0.45	102.02	11.65	0.15	-4.61
	8.40	-0.27	7.60	0.15	8.06	-0.47	8.84	0.06	7.46	0.45	102.11	11.71	0.17	-3.68
	8.26	-0.31	7.70	0.15	8.00	-0.52	8.90	0.06	7.47	0.44	101.35	11.70	0.20	-2.73
	8.09	-0.33	7.63	0.18	7.81	-0.53	8.80	0.05	7.39	0.43	97.76	11.72	0.21	-1.77
	8.10	-0.28	7.77	0.18	7.84	-0.56	8.96	0.08	7.51	0.43	101.32	11.65	0.20	-0.85
	8.10	-0.29	7.85	0.20	7.77	-0.58	9.03	0.06	7.61	0.44	102.51	11.65	0.19	0.13
	8.03	-0.26	7.92	0.23	7.72	-0.57	9.08	0.12	7.69	0.45	102.85	11.64	0.14	1.07
	7.92	-0.29	7.95	0.21	7.61	-0.62	9.04	0.05	7.69	0.43	101.36	11.66	0.16	2.02
	7.87	-0.28	8.01	0.24	7.55	-0.61	9.09	0.07	7.78	0.45	102.08	11.63	0.19	2.98
	7.83	-0.26	8.09	0.24	7.51	-0.65	9.14	0.06	7.87	0.44	102.16	11.64	0.14	3.92
	7.75	-0.28	8.17	0.24	7.47	-0.71	9.20	0.04	7.99	0.41	103.36	11.67	0.16	4.85
	7.69	-0.24	8.21	0.26	7.41	-0.70	9.22	0.06	8.08	0.43	102.76	11.65	0.25	5.78

Table B.16 Measured forces, flow rates and positions (uncorrected), using 2110A and DCM160 ($\beta = 90\%$ and $U_\infty = 1.35$ m/s) at different positions of central cylinder.

	Tube '1'		Tube '2'		Tube '3'		Tube '4'		Tube 'C'		Q_a (Scfm)	Q_w (l/s)	y (mm)	x (mm)
	Drag (N)	Lift (N)	Drag (N)	Lift (N)	Drag (N)	Lift (N)	Drag (N)	Lift (N)	Drag (N)	Drag (N)				
Zero	0.00	0.02	0.01	-0.01	-0.01	0.00	-0.03	0.00	0.00	0.00	0.23	-0.09	0.00	0.04
Buoyancy	2.33	-0.03	2.35	0.00	2.27	-0.02	2.09	0.07	2.45	0.29	-0.30	-0.04	-0.05	0.04
Normal tests	3.25	-0.23	3.19	0.04	3.17	-0.11	3.30	0.13	3.40	0.71	98.03	4.77	-5.64	0.02
	3.24	-0.19	3.17	0.05	3.14	-0.10	3.31	0.13	3.37	0.69	98.31	4.77	-4.67	0.05
	3.29	-0.19	3.28	0.05	3.24	-0.09	3.38	0.11	3.40	0.65	96.73	4.91	-3.76	0.07
	3.24	-0.15	3.24	0.05	3.20	-0.09	3.35	0.10	3.37	0.60	95.44	4.87	-2.81	0.06
	3.21	-0.09	3.21	0.02	3.17	-0.09	3.32	0.10	3.31	0.56	95.20	4.88	-1.88	0.06
	3.21	-0.11	3.24	0.03	3.20	-0.09	3.36	0.07	3.32	0.49	95.01	4.87	-0.99	0.08
	3.22	-0.07	3.29	0.07	3.21	-0.07	3.37	0.08	3.35	0.45	95.33	4.88	0.00	0.07
	3.28	-0.06	3.36	0.07	3.24	-0.06	3.40	0.06	3.36	0.39	97.38	4.91	0.90	0.07
	3.31	-0.03	3.40	0.08	3.21	-0.06	3.42	0.02	3.35	0.32	98.36	4.88	1.83	0.06
	3.35	0.02	3.45	0.08	3.22	-0.06	3.43	0.02	3.41	0.29	98.70	4.91	2.73	0.07
	3.37	0.04	3.46	0.10	3.19	-0.05	3.42	0.02	3.41	0.26	99.40	4.89	3.69	0.07
	3.37	0.05	3.46	0.07	3.17	-0.08	3.43	0.00	3.42	0.21	99.00	4.85	4.63	0.05
	3.45	0.07	3.50	0.10	3.17	-0.06	3.44	-0.01	3.45	0.20	97.70	4.89	5.56	0.05
	3.38	-0.09	3.15	0.02	3.35	-0.04	3.26	0.06	3.35	0.41	96.09	4.88	0.00	-5.62
	3.40	-0.08	3.17	0.04	3.32	-0.07	3.31	0.07	3.35	0.43	97.41	4.87	-0.07	-4.69
	3.35	-0.10	3.19	0.03	3.30	-0.08	3.31	0.07	3.33	0.43	98.87	4.86	-0.03	-3.74
	3.33	-0.08	3.20	0.05	3.27	-0.05	3.31	0.06	3.32	0.42	98.53	4.84	-0.11	-2.81
	3.33	-0.10	3.25	0.04	3.28	-0.07	3.39	0.08	3.34	0.44	99.84	4.90	-0.05	-1.89
	3.28	-0.09	3.23	0.05	3.22	-0.07	3.39	0.08	3.31	0.44	97.65	4.86	-0.06	-0.93
	3.26	-0.08	3.28	0.05	3.20	-0.09	3.39	0.06	3.30	0.45	95.27	4.83	-0.08	0.04
	3.22	-0.11	3.27	0.06	3.18	-0.10	3.41	0.07	3.31	0.43	96.64	4.83	-0.06	0.98
	3.22	-0.11	3.31	0.07	3.16	-0.11	3.42	0.08	3.34	0.42	96.57	4.83	-0.05	1.93
	3.19	-0.11	3.36	0.07	3.15	-0.13	3.47	0.06	3.37	0.41	98.14	4.85	-0.05	2.85
	3.15	-0.09	3.33	0.07	3.10	-0.13	3.44	0.06	3.35	0.42	97.07	4.82	-0.07	3.78
	3.16	-0.11	3.38	0.08	3.11	-0.12	3.50	0.09	3.40	0.43	98.26	4.86	-0.06	4.70
	3.11	-0.10	3.43	0.09	3.08	-0.15	3.51	0.09	3.44	0.41	98.62	4.85	-0.05	5.67

Table B.17 Measured forces, flow rates and positions (uncorrected), using 2110A and DCM160 ($\beta = 90\%$ and $U_\infty = 1.62$ m/s) at different positions of central cylinder.

	Tube '1'		Tube '2'		Tube '3'		Tube '4'		Tube 'C'		Q_a (Scfm)	Q_w (l/s)	y (mm)	x (mm)
	Drag (N)	Lift (N)	Drag (N)	Lift (N)	Drag (N)	Lift (N)	Drag (N)	Lift (N)	Drag (N)	Drag (N)				
Zero	0.00	0.00	-0.01	0.01	-0.01	0.00	0.00	0.00	0.00	0.00	-0.25	-0.01	0.07	-0.05
Buoyancy	2.30	-0.05	2.15	0.07	2.22	-0.07	2.12	0.13	2.36	0.28	-0.22	-0.02	0.01	-0.06
Normal tests	4.26	-0.40	3.96	0.15	3.93	-0.16	4.26	0.30	3.97	0.80	113.75	5.94	-5.56	-0.09
	4.32	-0.37	4.03	0.15	4.04	-0.19	4.36	0.28	4.03	0.76	117.22	5.96	-4.61	-0.08
	4.23	-0.31	3.97	0.15	3.97	-0.17	4.29	0.27	3.94	0.70	117.62	5.92	-3.65	-0.06
	4.18	-0.26	3.97	0.14	3.95	-0.16	4.27	0.23	3.88	0.62	117.01	5.91	-2.72	-0.04
	4.18	-0.22	4.00	0.14	3.97	-0.13	4.31	0.22	3.87	0.55	115.59	5.92	-1.79	-0.04
	4.16	-0.16	4.01	0.15	3.95	-0.15	4.31	0.17	3.84	0.45	117.51	5.93	-0.90	-0.04
	4.17	-0.13	4.06	0.13	3.95	-0.14	4.32	0.16	3.83	0.36	117.02	5.92	0.04	-0.04
	4.20	-0.05	4.12	0.16	3.96	-0.12	4.35	0.17	3.88	0.30	118.24	5.93	1.01	-0.04
	4.27	-0.04	4.15	0.16	3.92	-0.10	4.33	0.08	3.89	0.20	117.46	5.87	1.92	-0.05
	4.28	0.04	4.22	0.17	3.91	-0.10	4.33	0.08	3.92	0.14	118.03	5.92	2.82	-0.04
	4.28	0.09	4.26	0.15	3.85	-0.09	4.26	0.08	3.89	0.12	115.38	5.82	3.76	-0.05
	4.37	0.12	4.33	0.18	3.83	-0.10	4.32	0.07	3.95	0.08	115.02	5.88	4.70	-0.05
	4.48	0.15	4.39	0.23	3.83	-0.10	4.36	0.03	3.99	0.01	118.34	5.84	5.66	-0.08
	4.36	-0.15	3.92	0.10	4.15	-0.12	4.21	0.12	3.85	0.32	118.33	5.90	0.06	-5.71
	4.34	-0.11	3.94	0.12	4.13	-0.11	4.21	0.19	3.84	0.36	117.35	5.84	0.04	-5.10
	4.29	-0.14	3.95	0.13	4.05	-0.11	4.20	0.15	3.79	0.34	115.95	5.84	0.04	-3.88
	4.21	-0.12	3.94	0.10	4.00	-0.12	4.21	0.18	3.78	0.37	115.10	5.84	0.10	-2.93
	4.23	-0.12	4.00	0.15	3.97	-0.13	4.26	0.18	3.81	0.36	115.47	5.85	0.05	-1.97
	4.22	-0.12	4.06	0.15	3.96	-0.13	4.30	0.17	3.83	0.36	118.15	5.85	0.09	-1.05
	4.22	-0.11	4.14	0.15	3.97	-0.13	4.36	0.17	3.90	0.38	118.28	5.84	0.07	-0.06
	4.17	-0.11	4.11	0.15	3.93	-0.16	4.38	0.18	3.89	0.38	117.76	5.84	0.06	0.87
	4.13	-0.15	4.15	0.15	3.88	-0.16	4.39	0.17	3.91	0.35	118.74	5.86	0.07	1.80
	4.09	-0.13	4.19	0.12	3.86	-0.18	4.39	0.18	3.93	0.37	118.67	5.85	0.03	2.76
	4.03	-0.14	4.19	0.15	3.79	-0.17	4.39	0.16	3.93	0.35	117.35	5.83	-0.02	3.70
	3.99	-0.15	4.17	0.14	3.74	-0.19	4.38	0.16	3.96	0.36	115.10	5.88	0.03	4.64
	3.97	-0.15	4.23	0.13	3.73	-0.19	4.43	0.19	4.03	0.36	115.56	5.89	0.02	5.57

Table B.18 Measured forces, flow rates and positions (uncorrected), using 2110A and DCM160 ($\beta = 95\%$ and $U_\infty = 2.65$ m/s) at different positions of central cylinder.

	Tube '1'		Tube '2'		Tube '3'		Tube '4'		Tube 'C'		Q_a (Scfm)	Q_w (l/s)	y (mm)	x (mm)
	Drag (N)	Lift (N)	Drag (N)	Lift (N)	Drag (N)	Lift (N)	Drag (N)	Lift (N)	Drag (N)	Drag (N)				
Zero	0.00	-0.01	0.00	-0.01	0.00	0.00	0.01	-0.01	0.00	0.00	0.53	-0.04	-0.06	0.00
Buoyancy	2.36	-0.11	2.31	0.03	2.30	-0.08	2.23	0.07	2.53	0.28	0.21	0.01	-0.03	0.00
Normal tests	4.41	-0.56	4.11	0.11	4.47	-0.20	4.85	0.20	4.45	0.85	201.87	4.87	-5.68	-0.01
	4.33	-0.54	4.10	0.09	4.45	-0.21	4.88	0.15	4.43	0.76	202.04	4.91	-4.78	0.00
	4.29	-0.46	4.09	0.11	4.45	-0.20	4.87	0.14	4.37	0.70	202.08	4.86	-3.83	0.01
	4.26	-0.43	4.12	0.10	4.45	-0.19	4.87	0.12	4.35	0.61	201.74	4.93	-2.94	-0.03
	4.25	-0.35	4.16	0.10	4.46	-0.19	4.73	0.08	4.31	0.53	201.33	4.92	-2.03	-0.01
	4.23	-0.24	4.22	0.09	4.45	-0.20	4.52	0.06	4.28	0.47	201.68	4.88	-1.07	0.03
	4.28	-0.20	4.28	0.07	4.48	-0.21	4.57	0.01	4.33	0.37	204.53	4.88	-0.11	0.02
	4.31	-0.16	4.32	0.09	4.45	-0.20	4.58	-0.02	4.33	0.28	204.93	4.87	0.81	0.02
	4.35	-0.09	4.33	0.08	4.39	-0.20	4.50	-0.06	4.29	0.21	201.75	4.85	1.75	0.02
	4.44	0.01	4.43	0.12	4.40	-0.18	4.53	-0.08	4.34	0.14	201.00	4.86	2.66	0.02
	4.45	0.05	4.48	0.16	4.36	-0.16	4.49	-0.08	4.35	0.09	200.24	4.87	3.59	0.01
	4.58	0.04	4.56	0.19	4.35	-0.16	4.54	-0.12	4.39	-0.03	203.69	4.83	4.53	0.00
	4.63	0.09	4.62	0.24	4.33	-0.16	4.54	-0.13	4.41	-0.09	202.96	4.86	5.48	0.01
	4.47	-0.24	4.05	0.08	4.65	-0.18	4.37	0.01	4.20	0.36	201.69	4.88	-0.12	-5.67
	4.61	-0.29	4.10	0.10	4.65	-0.20	4.46	0.01	4.21	0.36	205.15	4.85	-0.13	-4.74
	4.52	-0.25	4.05	0.10	4.44	-0.18	4.37	0.00	4.15	0.36	197.97	4.85	-0.16	-3.80
	4.53	-0.26	4.12	0.09	4.43	-0.19	4.45	0.03	4.18	0.39	200.71	4.85	-0.18	-2.88
	4.50	-0.27	4.13	0.11	4.38	-0.21	4.46	0.03	4.18	0.38	199.80	4.83	-0.16	-1.93
	4.45	-0.29	4.18	0.10	4.37	-0.22	4.51	0.00	4.21	0.36	202.31	4.86	-0.16	-1.00
	4.47	-0.31	4.24	0.11	4.35	-0.22	4.58	0.00	4.28	0.36	204.54	4.82	-0.18	-0.03
	4.43	-0.29	4.27	0.12	4.31	-0.22	4.60	0.02	4.30	0.37	204.12	4.85	-0.14	0.92
	4.37	-0.31	4.27	0.10	4.25	-0.24	4.59	0.01	4.31	0.35	202.32	4.82	-0.19	1.86
	4.28	-0.30	4.25	0.11	4.16	-0.26	4.57	0.02	4.30	0.36	201.93	4.76	-0.16	2.80
	4.30	-0.31	4.33	0.11	4.17	-0.24	4.62	0.00	4.38	0.36	200.64	4.78	-0.17	3.74
	4.22	-0.30	4.31	0.12	4.08	-0.24	4.59	0.02	4.41	0.37	200.08	4.79	-0.19	4.68
	4.23	-0.30	4.38	0.12	4.09	-0.27	4.66	0.03	4.50	0.39	201.50	4.82	-0.18	5.62

Table B.19 Measured forces, flow rates and positions (uncorrected), using 2110A and DCM160 ($\beta = 95\%$ and $U_\infty = 2.91$ m/s) at different positions of central cylinder.

	Tube '1'		Tube '2'		Tube '3'		Tube '4'		Tube 'C'		Q_a (Scfm)	Q_w (l/s)	y (mm)	x (mm)
	Drag (N)	Lift (N)	Drag (N)	Lift (N)	Drag (N)	Lift (N)	Drag (N)	Lift (N)	Drag (N)	Drag (N)				
Zero	-0.01	-0.02	-0.02	-0.01	-0.02	0.00	0.01	-0.01	0.00	0.00	-0.39	0.03	0.04	-0.01
Buoyancy	2.34	-0.10	2.23	0.02	2.27	-0.08	2.13	0.06	2.49	0.28	-0.60	0.04	0.08	-0.01
Normal tests	5.49	-0.78	4.94	0.13	5.25	-0.44	6.02	0.24	5.20	1.01	222.54	5.61	-5.56	-0.02
	5.41	-0.77	4.92	0.13	5.20	-0.44	6.00	0.23	5.14	0.91	219.97	5.62	-4.62	0.01
	5.33	-0.75	4.90	0.11	5.20	-0.45	5.99	0.23	5.08	0.80	218.60	5.61	-3.70	0.00
	5.30	-0.68	4.93	0.12	5.22	-0.45	6.06	0.18	5.04	0.66	221.14	5.59	-2.78	-0.04
	5.24	-0.61	4.95	0.11	5.21	-0.47	6.06	0.14	5.01	0.56	222.27	5.59	-1.85	0.01
	5.26	-0.50	5.01	0.12	5.24	-0.46	6.11	0.13	4.99	0.46	221.08	5.60	-0.90	0.01
	5.25	-0.42	5.01	0.13	5.17	-0.44	6.06	0.07	4.94	0.34	219.79	5.63	0.03	0.02
	5.22	-0.30	5.01	0.15	5.09	-0.42	6.00	0.05	4.90	0.25	215.65	5.59	0.91	0.02
	5.39	-0.23	5.17	0.16	5.15	-0.42	6.08	-0.01	4.98	0.12	220.86	5.63	1.98	0.01
	5.43	-0.12	5.24	0.22	5.09	-0.39	6.05	-0.01	4.99	0.05	218.15	5.61	2.83	0.04
	5.52	-0.06	5.29	0.23	5.03	-0.39	6.02	-0.06	5.00	-0.07	220.08	5.58	3.80	0.04
	5.69	0.00	5.50	0.29	5.11	-0.39	6.17	-0.12	5.11	-0.20	226.39	5.55	4.73	0.03
	5.75	0.06	5.57	0.35	5.04	-0.40	6.14	-0.11	5.12	-0.27	223.84	5.58	5.63	0.01
	5.45	-0.44	4.78	0.14	5.44	-0.42	5.89	0.08	4.82	0.31	220.92	5.57	0.06	-5.67
	5.37	-0.43	4.76	0.16	5.34	-0.42	5.85	0.09	4.77	0.33	217.99	5.59	0.08	-4.74
	5.42	-0.43	4.87	0.16	5.39	-0.43	5.98	0.09	4.84	0.34	222.28	5.54	0.03	-3.80
	5.39	-0.46	4.89	0.15	5.35	-0.45	6.06	0.07	4.86	0.32	225.58	5.56	0.02	-2.87
	5.35	-0.47	4.91	0.14	5.24	-0.46	6.04	0.08	4.85	0.31	219.59	5.56	0.05	-1.93
	5.29	-0.43	4.93	0.16	5.18	-0.45	6.03	0.09	4.85	0.35	219.03	5.58	0.04	-0.98
	5.29	-0.45	4.98	0.15	5.14	-0.47	6.11	0.09	4.91	0.33	219.79	5.60	0.00	-0.01
	5.19	-0.45	4.98	0.16	5.04	-0.49	6.08	0.10	4.90	0.34	217.89	5.55	0.04	0.93
	5.17	-0.46	5.03	0.16	5.02	-0.49	6.13	0.09	4.96	0.35	219.72	5.55	0.05	1.89
	5.21	-0.46	5.16	0.16	5.07	-0.50	6.27	0.09	5.11	0.35	225.75	5.55	0.02	2.78
	5.13	-0.47	5.14	0.13	4.97	-0.53	6.24	0.07	5.14	0.33	226.10	5.55	-0.03	3.74
	5.08	-0.49	5.18	0.16	4.92	-0.53	6.23	0.07	5.20	0.34	220.97	5.58	0.01	4.71
	5.03	-0.46	5.24	0.16	4.91	-0.54	6.26	0.11	5.29	0.38	222.49	5.58	-0.01	5.62

APPENDIX C

5.1.1 Subroutines

The program is written using separate modules related through the flow diagram given in Appendix C. The separate modules intended to ease the understanding the program are as follows:

ADDEDMASS: Finds the added mass per unit length using equations (2.31) and (2.32).
CALCCONS: Forms the structural mass, structural damping and total mass matrices.
CALCEIG: Calculates the state-space equation eigenvalues.
CALCVAR: Introduction of phase angles, drag coefficient and formation of fluid stiffness and fluid damping matrices.
STATESOLVE: Forms state-space equations and calls CALCEIG to find the eigenvalues.
MAIN: Reads the array and flow parameters, force coefficient variations versus local coordinates, reading the structural damping and changing the velocity to find and recording the critical frequency and velocity.

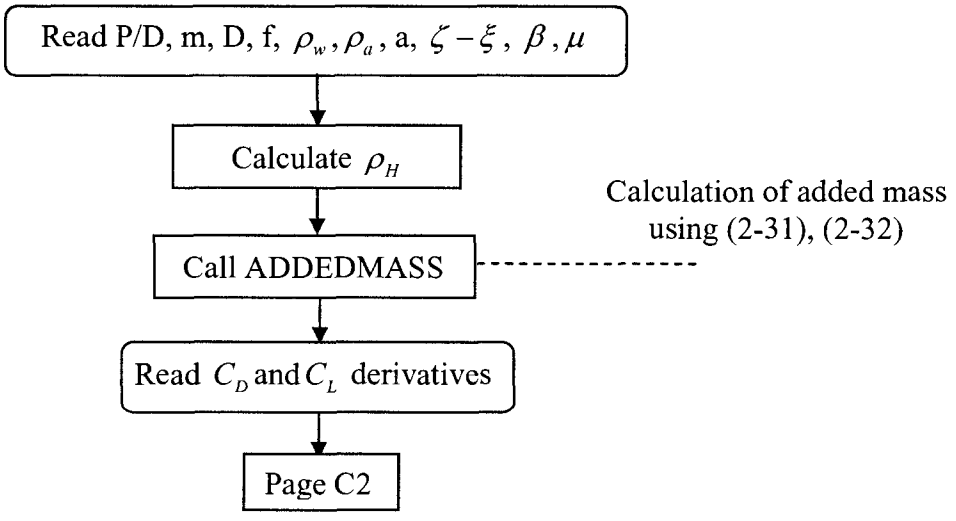

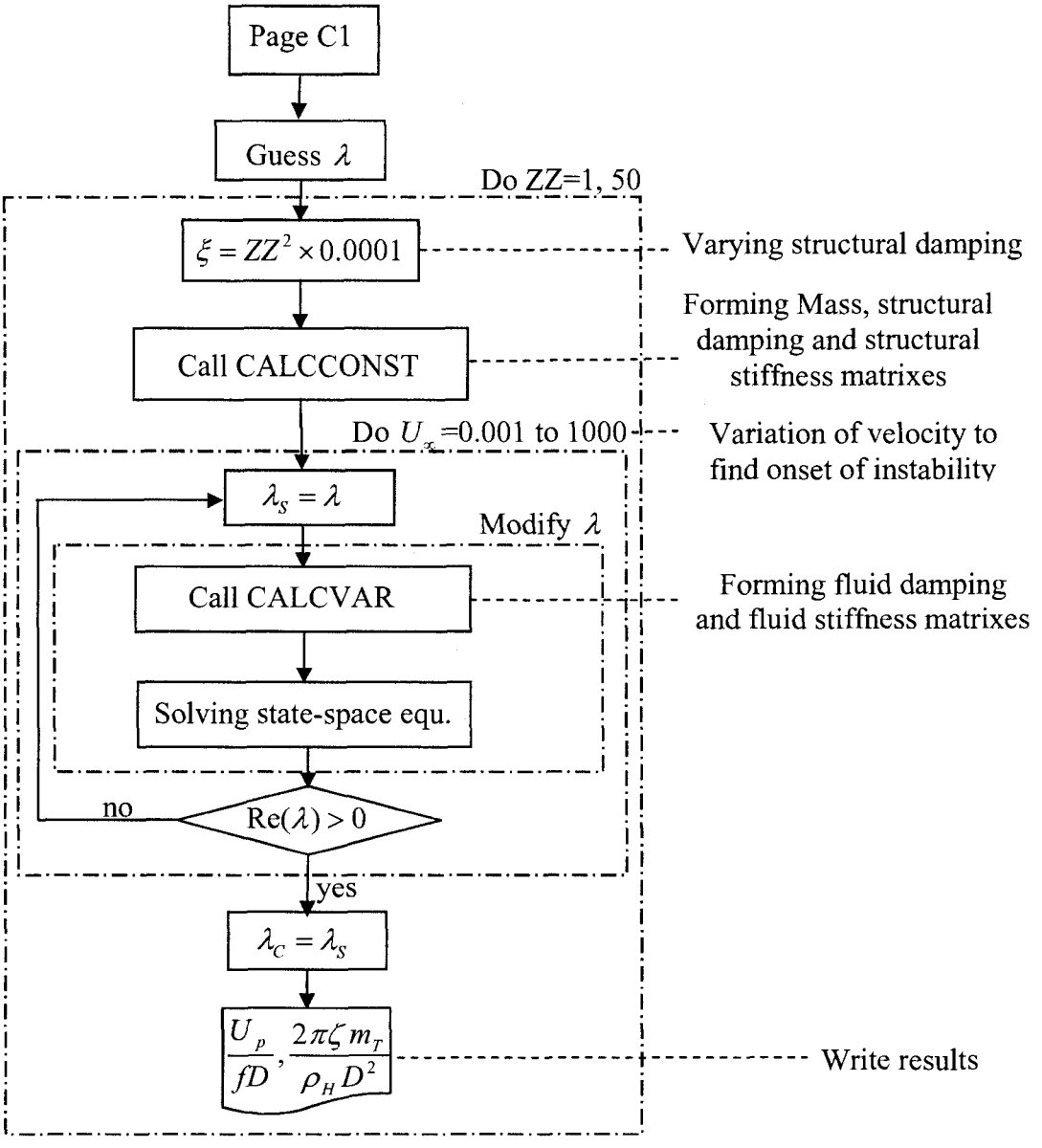
Page C1
Guess λ
Do ZZ=1, 50
$\xi = ZZ^2 \times 0.0001$
Varying structural damping
Call CALCCONST
Forming Mass, structural damping and structural stiffness matrixes
Do U_∞=0.001 to 1000
Variation of velocity to find onset of instability
$\lambda_S = \lambda$
Modify λ
Call CALCVAR
Forming fluid damping and fluid stiffness matrixes
Solving state-space equ.
no
$\mathrm{Re}(\lambda) > 0$
yes
$\lambda_C = \lambda_S$
$\frac{U_p}{fD}, \frac{2\pi\zeta m_T}{\rho_H D^2}$
Write results